Collider Physics II: Measuring the Mass of the W Boson

Ashutosh Kotwal
Duke University

TIFR
September 23, 2023

Detecting New Physics through Precision Measurements

- Willis Lamb (Nobel Prize 1955) measured the difference between energies of $^2S_{1/2}$ and $^2P_{1/2}$ states of hydrogen atom

  - 4 micro electron volts difference compared to few electron volts binding energy

  - States should be degenerate in energy according to tree-level calculation

- Harbinger of vacuum fluctuations to be calculated by Feynman diagrams containing quantum loops

  - Modern quantum field theory of electrodynamics followed (Nobel Prize 1965 for Schwinger, Feynman, Tomonaga)
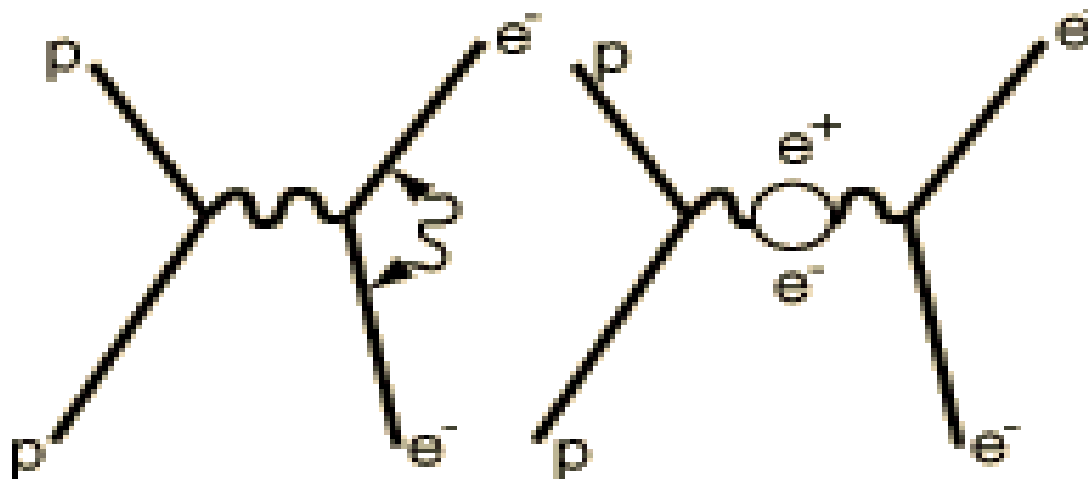
Parameters of Electro-Weak Interactions

- Gauge symmetries related to the electromagnetic and weak forces in the standard model, extension of QED

    - U(1) gauge group with gauge coupling g

    - SU(2) gauge group with gauge coupling g'

- And gauge symmetry-breaking via vacuum expectation value of Higgs field $v \neq 0$

- Another interesting phenomenon in nature: the U(1) generator and the neutral generator of SU(2) get mixed (linear combination) to yield the observed gauge bosons

    - Photon for electromagnetism

    - Z boson as one of the three gauge bosons of weak interaction

- Linear combination is given by Weinberg mixing angle ϑ_W

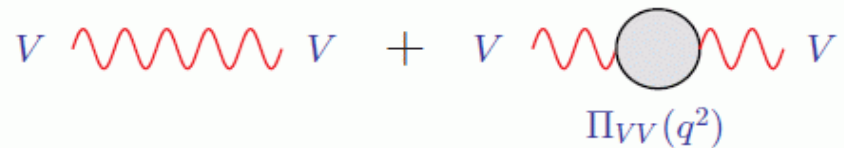# Parameters of Electro-Weak Interactions

At tree level, all of the observables can be expressed in terms of *three parameters* of the SM Lagrangian: $v,\ g,\ g'$ or, equivalently, $v,\ e,\ s \equiv \sin\theta_W$ (also $c \equiv \cos\theta_W$)

$$\alpha = \frac{e^2}{4\pi}, \qquad G_F = \frac{1}{2\sqrt{2}v^2}, \qquad m_Z = \frac{e\,v}{\sqrt{2}sc}, \qquad m_W = \frac{e\,v}{\sqrt{2}s}, \qquad s_{\text{eff}}^2 = s^2,$$
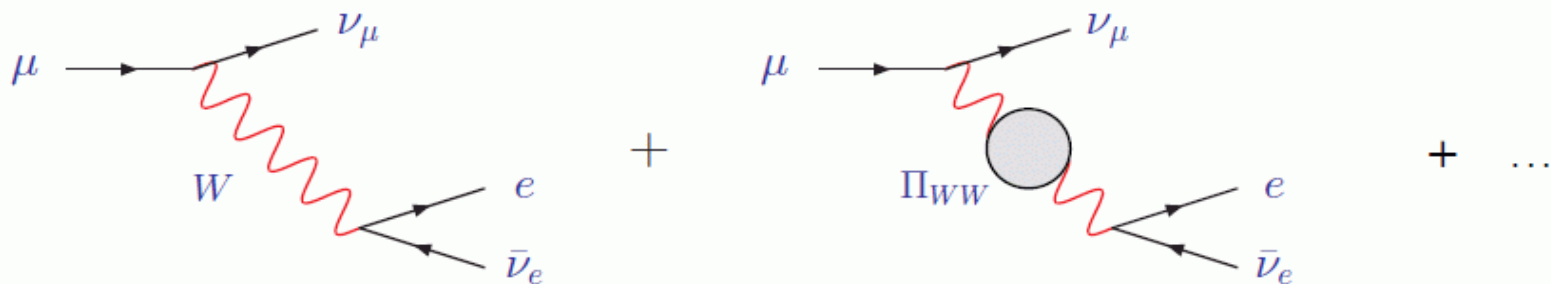
Radiative corrections to the relations between physical observables and Lagrangian params:

$$m_Z^2 = \frac{e^2v^2}{2\,s^2c^2} + \Pi_{ZZ}(m_Z^2)$$

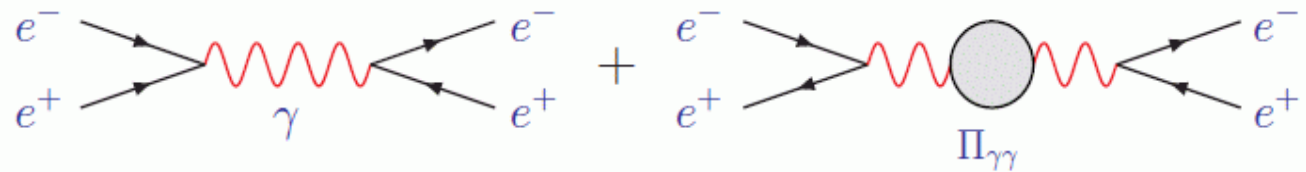$$m_W^2 = \frac{e^2v^2}{2\,s^2} + \Pi_{WW}(m_W^2)$$

$$\Pi_{VV}(q^2)$$

$$G_F = \frac{1}{2\sqrt{2}v^2}\left[1 - \frac{\Pi_{WW}(0)}{m_W^2} + \delta_{\text{VB}}\right]$$

Radiative Corrections to Electromagnetic Coupling

$$\alpha = \frac{e^2}{4\pi}\left[1 + \lim_{q^2 \to 0} \frac{\Pi_{\gamma\gamma}(q^2)}{q^2}\right]$$

this one is tricky: the hadronic contribution to $\Pi'_{\gamma\gamma}(0)$ cannot be computed perturbatively

We can however trade it for another experimental observable: $\quad R_{\text{had}}(q^2) = \dfrac{\sigma_{\text{had}}(q^2)}{\sigma_{\ell^+\ell^-}(q^2)}$

$$\alpha(m_Z) = \frac{e^2}{4\pi}\left[1 + \frac{\Pi_{\gamma\gamma}(m_Z)}{m_Z^2}\right] = \frac{\alpha}{1 - \Delta\alpha(m_Z)}$$

$$\Delta\alpha(m_Z) = \underbrace{\Delta\alpha_\ell(m_Z) + \Delta\alpha_{\text{top}}(m_Z)}_{\text{calculable}} + \Delta\alpha_{\text{had}}^{(5)}(m_Z)$$

$$\Delta\alpha_{\text{had}}^{(5)}(m_Z) = -\frac{m_Z^2}{3\pi}\int_{4m_\pi^2}^{\infty} \frac{R_{\text{had}}(q^2)\,dq^2}{q^2\,(q^2 - m_Z^2)} = 0.02758 \pm 0.00035$$

(This hadronic contribution is one of the biggest sources of uncertainty in EW studies)

Radiative Corrections to W Boson Mass

All these corrections can be combined into relations among physical observables, e.g.:

$$m_W^2 = m_Z^2 \left[\frac{1}{2} + \frac{1}{2}\sqrt{1 - \frac{2\sqrt{2}\,\pi\alpha}{G_F\, m_Z^2}\,(1 + \Delta r)} \right]$$

Δr can be parametrized in terms of two universal corrections and a remainder:

$$\Delta r = \Delta\alpha(m_Z) - \frac{c^2}{s^2}\Delta\rho + \Delta r_{\text{rem}}$$

The leading corrections depend quadratically on m_t but only logarithmically on m_H:

$$\Delta\rho = \frac{\Pi_{ZZ}(0)}{m_Z^2} - \frac{\Pi_{WW}(0)}{m_W^2} \approx \frac{3\,\alpha}{16\pi c^2}\left(\frac{m_t^2}{s^2 m_Z^2} + \log\frac{m_H^2}{m_W^2} + \dots \right)$$

$$\frac{\delta m_W^2}{m_W^2} \approx \frac{c^2}{c^2 - s^2}\Delta\rho\,, \qquad \delta\sin^2\theta_{\text{eff}} \approx -\frac{c^2 s^2}{c^2 - s^2}\Delta\rho$$

Motivation for Precision Measurements

- The electroweak gauge sector of the standard model is constrained by three precisely known parameters

    - $\alpha_{EM} (M_Z) = 1 / 127.918(18)$

    - $G_F = 1.16637 (1) \times 10^{-5} \, GeV^{-2}$

    $M_Z = 91.1876 (21) \, GeV$

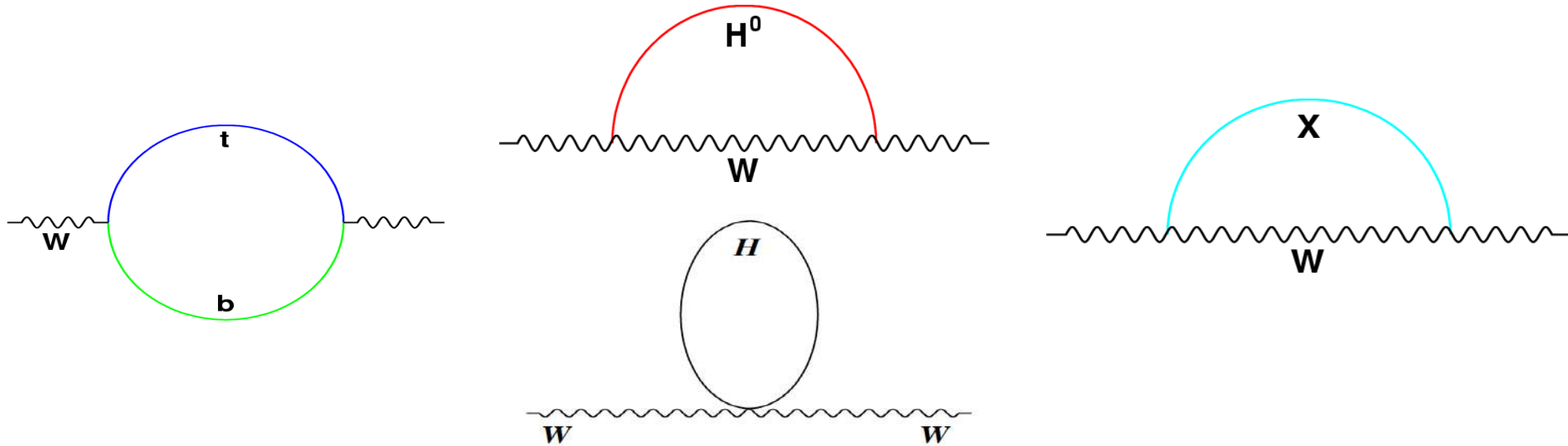- At tree-level, these parameters are related to other electroweak observables, *e.g.* M_W

    - $M_W^2 = \pi\alpha_{\pm\int} / \sqrt{2}G_F \sin^2\vartheta_W$

        - Where ϑ_W is the Weinberg mixing angle, defined by

        $\cos \vartheta_W = M_W/M_Z$

Motivation for Precision Measurements
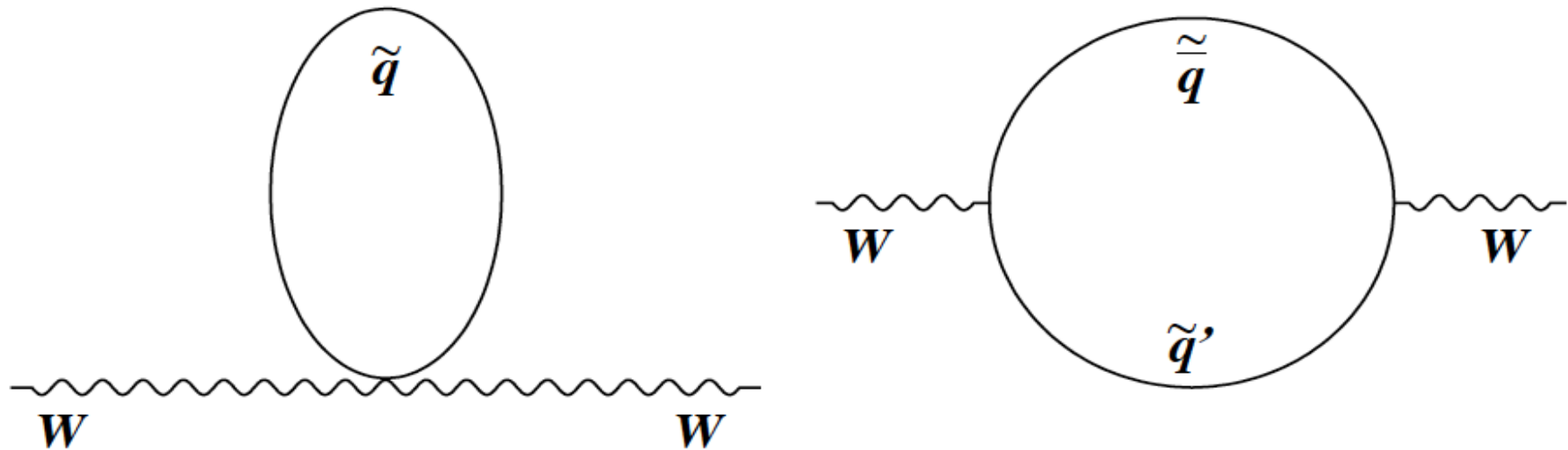
- Radiative corrections due to heavy quark and Higgs loops and exotica

Motivate the introduction of the ρ parameter: $M_W^2 = \rho \, [M_W(tree)]^2$
with the predictions $\Delta\rho = (\rho - 1) \, \gamma \, \int_{top}^2$ and $\Delta\rho \, \gamma \, \ln M_H$

- In conjunction with M_{top} and the Higgs boson mass, the W boson mass stringently tests the SM
  - A discrepancy with SM prediction will point to new physics !

# Contributions from Supersymmetric Particles

- Radiative correction depends on mass splitting (Δm^2) between squarks in SU(2) doublet

- After folding in limits on SUSY particles from direct searches, SUSY loops can still contribute 10's of MeV to M_W

1998 Status of M_W vs M_{top}
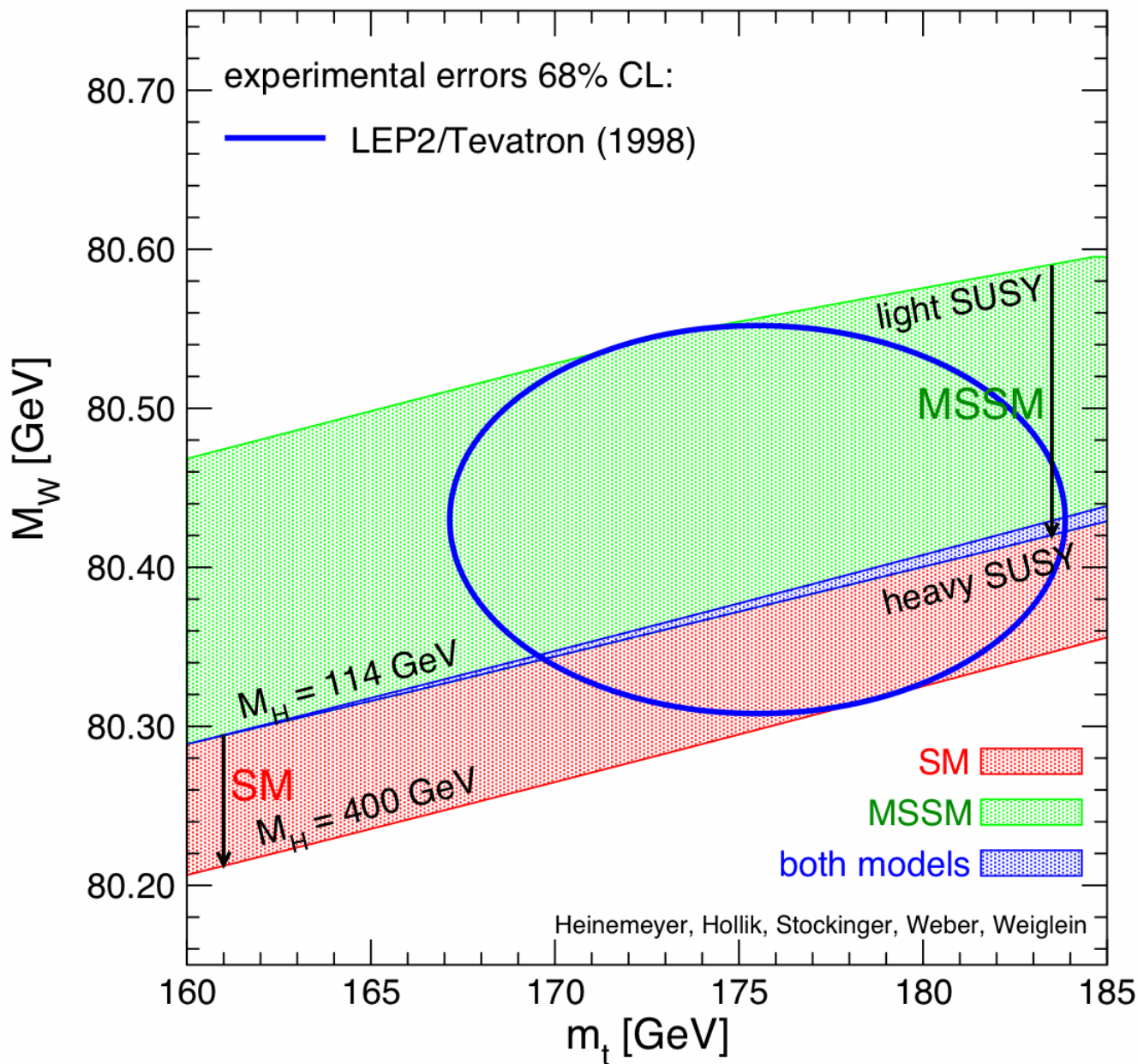
Motivation

- Generic parameterization of new physics contributing to W and Z boson self-energies through radiative corrections in propagators

  - *S, T, U* parameters (Peskin & Takeuchi, Marciano & Rosner, Kennedy & Langacker, Kennedy & Lynn)
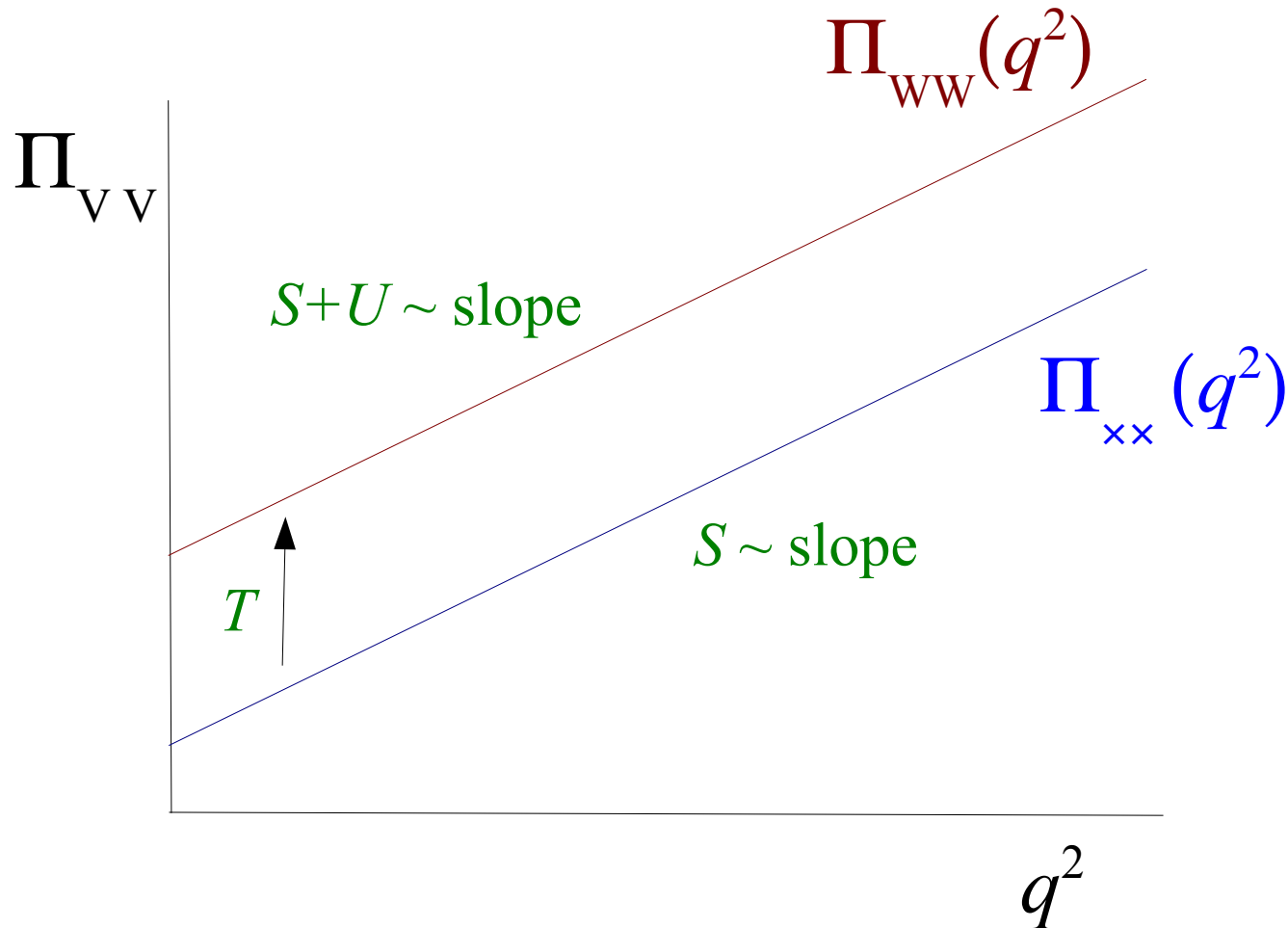
Motivation

- Generic parameterization of new physics contributing to W and Z boson self-energies: *S, T, U* parameters (Peskin & Takeuchi)
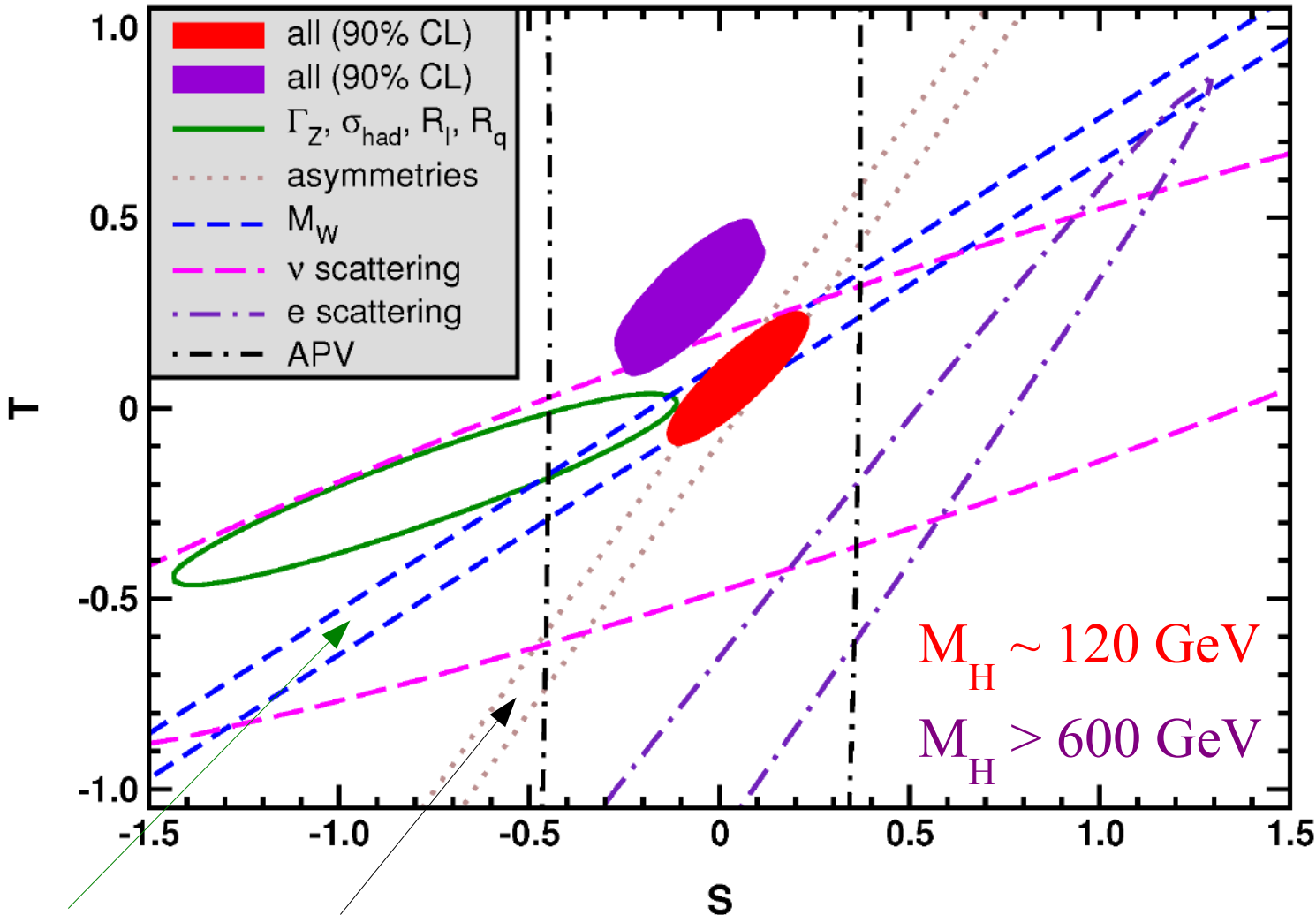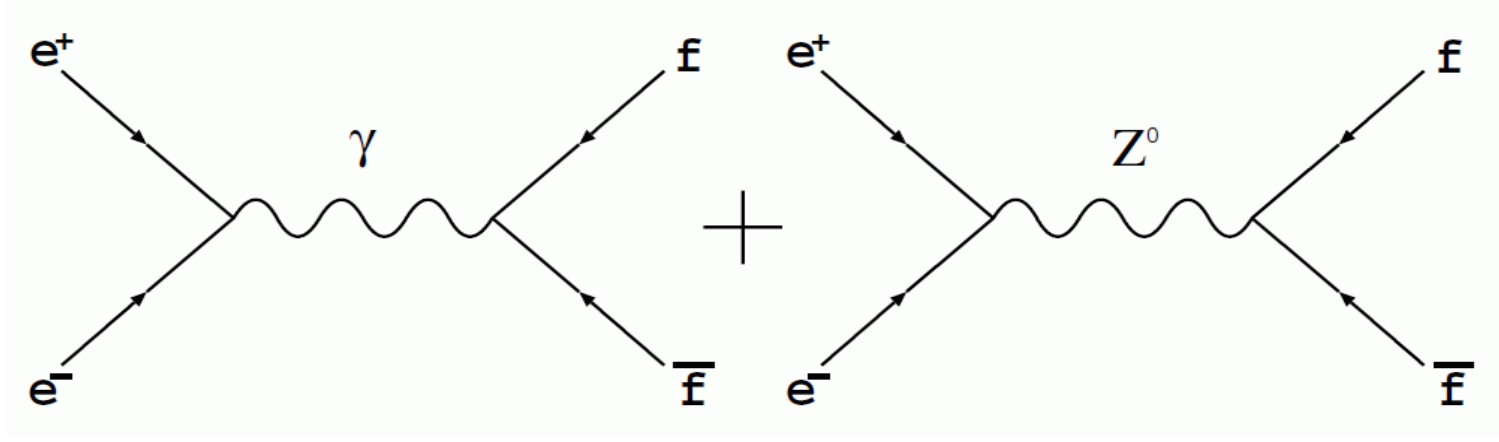

Additionally, M_W is the only measurement which constrains *U*

$M_H \sim 120$ GeV

$M_H > 600$ GeV

(from P. Langacker, 2012)

M_W and Asymmetries are the most powerful observables in this parameterization

A_{FB} and A_{LR} Observables

- Asymmetries definable in electron-positron scattering sensitive to Weinberg mixing angle ϑ_W

- Higgs and Supersymmetry also contribute radiative corrections to ϑ_W via quantum loops

- A_{FB} is the angular (forward – backward) asymmetry of the final state

- A_{LR} is the asymmetry in the total scattering probability for different polarizations of the initial state
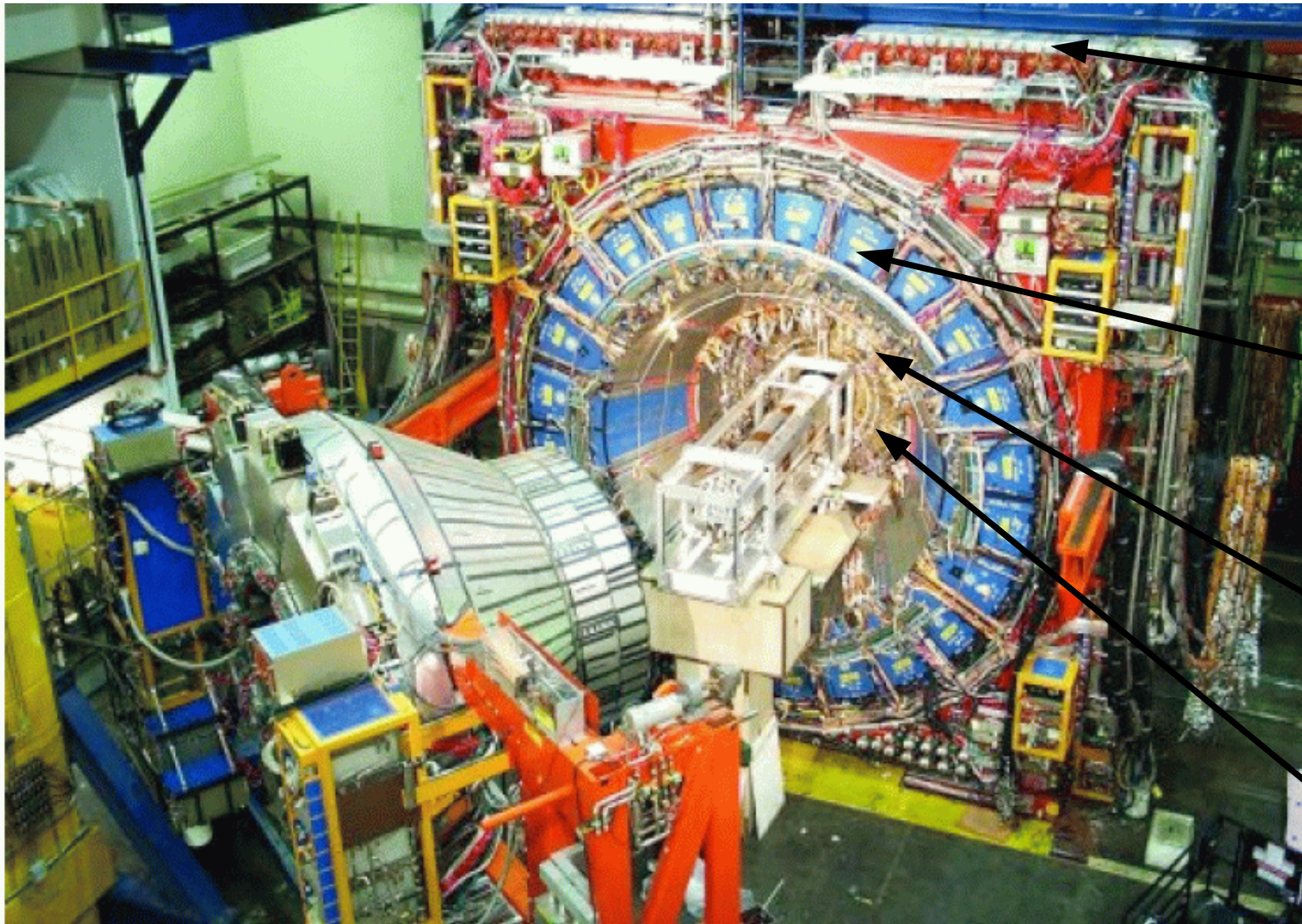
D0 Detector at Fermilab

η = 0

η = 1

η = 2

η = 3

Muon Scintillators

Muon Chambers

Shielding

Calorimeter

Toroid
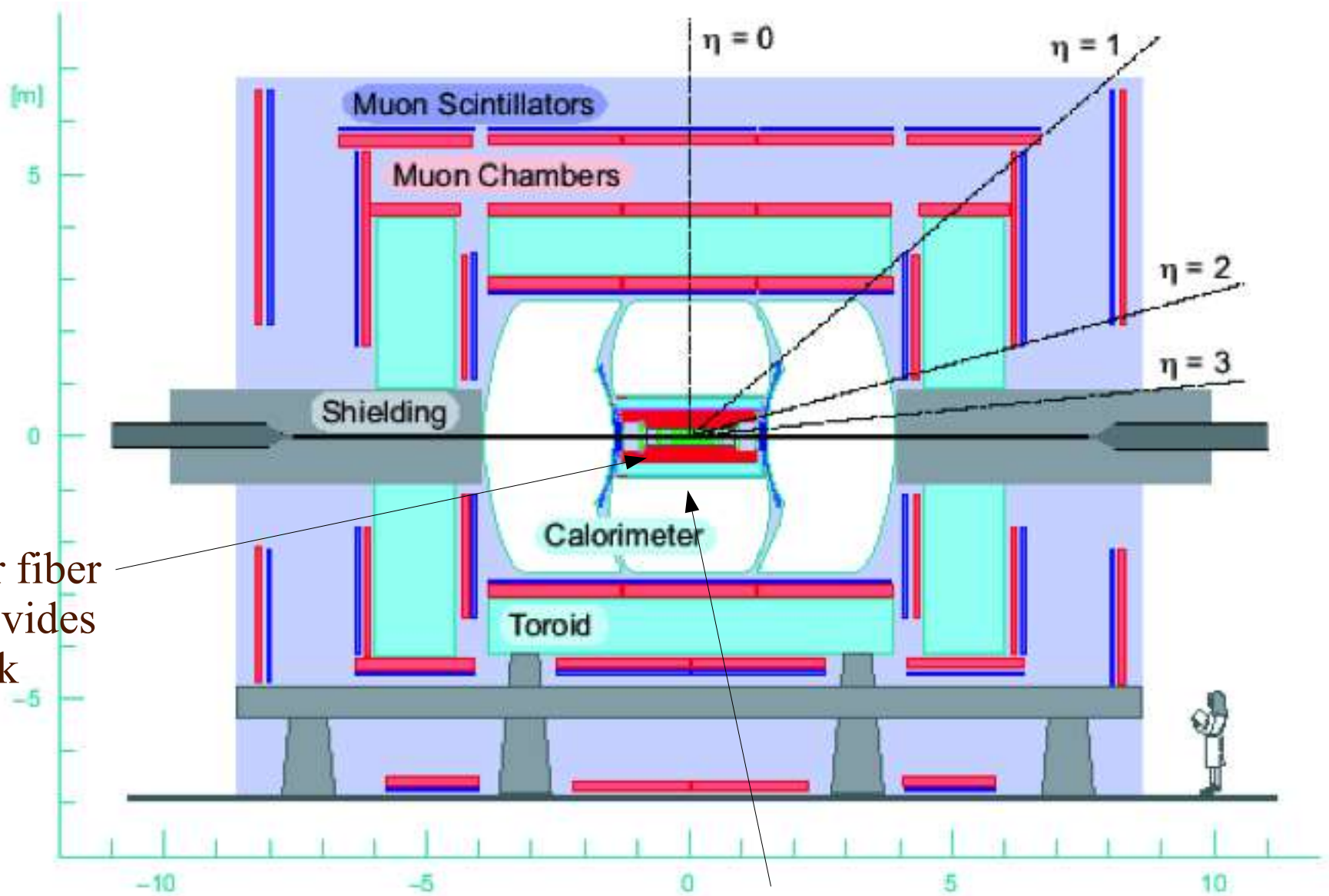
Scintillator fiber tracker provides lepton track direction

Electromagnetic Calorimeter measures electron energy
Hadronic calorimeters measure recoil particles

Collider Detector at Fermilab (CDF)

Muon detector

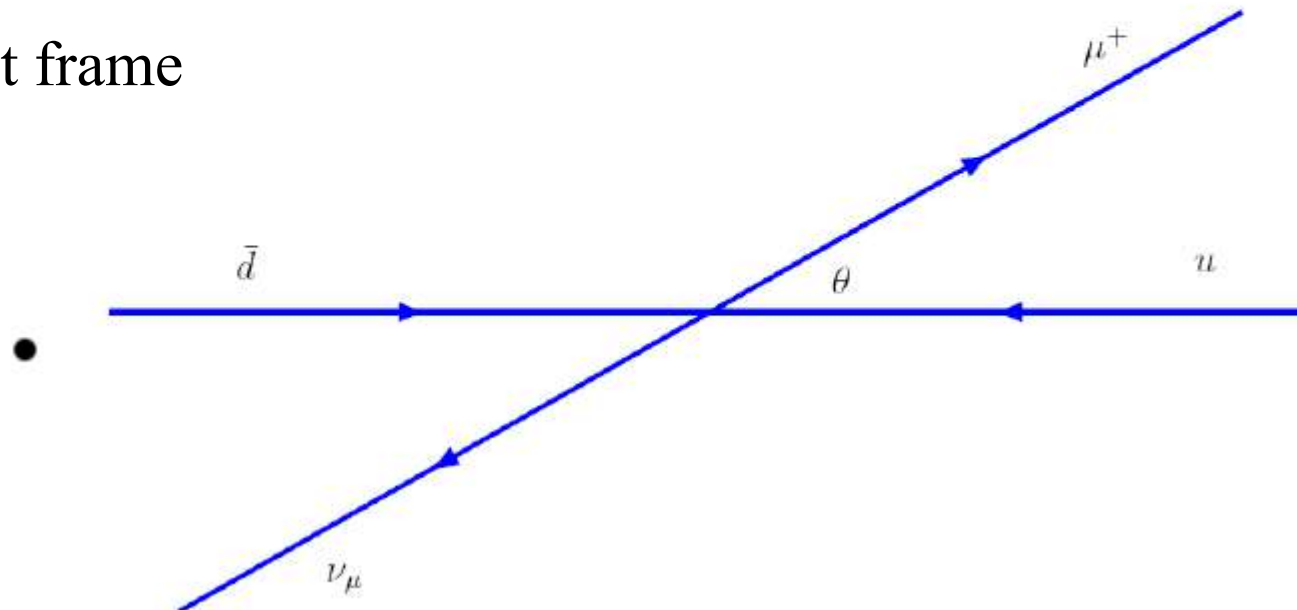Central hadronic calorimeter

Central EM calorimeter

Central outer tracker (COT)

W mass measurement – decay kinematics

- Main complication: invariant mass cannot be reconstructed from 2-body leptonic decay mode

    - Because neutrino is not detectable directly

- Exploit the "Jacobian edge" in lepton transverse momentum spectrum

$$\frac{d\sigma}{d\cos\hat\theta} = \sigma_0(\hat{s})\left[\frac{1}{2}(1+\cos\hat\theta)^2 + \frac{1}{2}(1-\cos\hat\theta)^2\right]$$

$$= \sigma_0(\hat{s})(1+\cos^2\hat\theta)$$

W boson rest frame

W mass measurement – decay kinematics

- Main complication: invariant mass cannot be reconstructed from 2-body leptonic decay mode

    - Because neutrino is not detectable directly

- Exploit the "Jacobian edge" in lepton transverse momentum spectrum

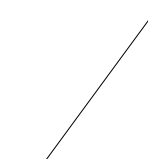$$\frac{d\sigma}{dp_T} = \frac{d\sigma}{d((m_W/2)\sin\hat\theta)}$$

$$= \frac{2}{m_W}\frac{d\sigma}{d\sin\hat\theta}$$

$$= \frac{2}{m_W}\frac{d\sigma}{d\cos\hat\theta}\left|\frac{d\cos\hat\theta}{d\sin\hat\theta}\right|$$

$$= \frac{2}{m_W}\sigma_0(\hat s)(1+\cos^2\theta)|\tan\hat\theta|$$

$$= \sigma_0(\hat s)\frac{4p_T}{m_W^2}(2-4p_T^2/m_W^2)\left(\frac{1}{\sqrt{1-4p_T^2/m_W^2}}\right)$$

Invariant under longitudinal boost
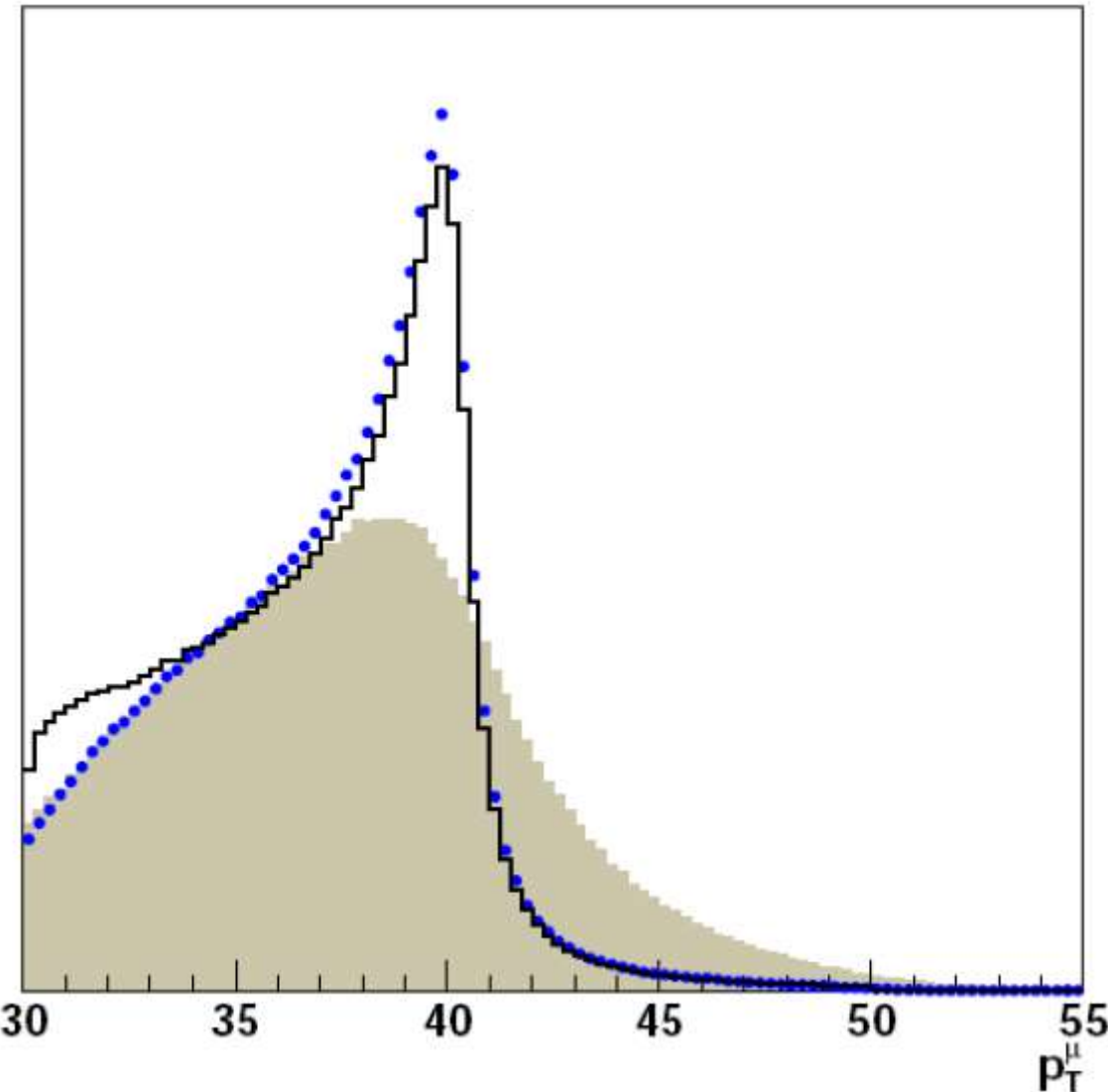
W mass measurement – decay kinematics

- Main complication: invariant mass cannot be reconstructed from 2-body leptonic decay mode

    - Because neutrino is not detectable directly

- Exploit the "Jacobian edge" in lepton transverse momentum spectrum

We can transfer $\frac{d\sigma}{dp_T}$ to $\frac{d\sigma}{dm_T}$ by using $m_T = 2p_T$:

$$\frac{d\sigma}{dm_T} = \frac{1}{2}\frac{d\sigma}{dp_T}$$

$$= \sigma_0(\hat{s})\frac{m_T}{m_W}\left(2 - \frac{m_T^2}{m_W^2}\right)\left(\frac{1}{\sqrt{1 - m_T^2/m_W^2}}\right)$$

W mass measurement – decay kinematics

- Lepton transverse momentum not invariant under transverse boost

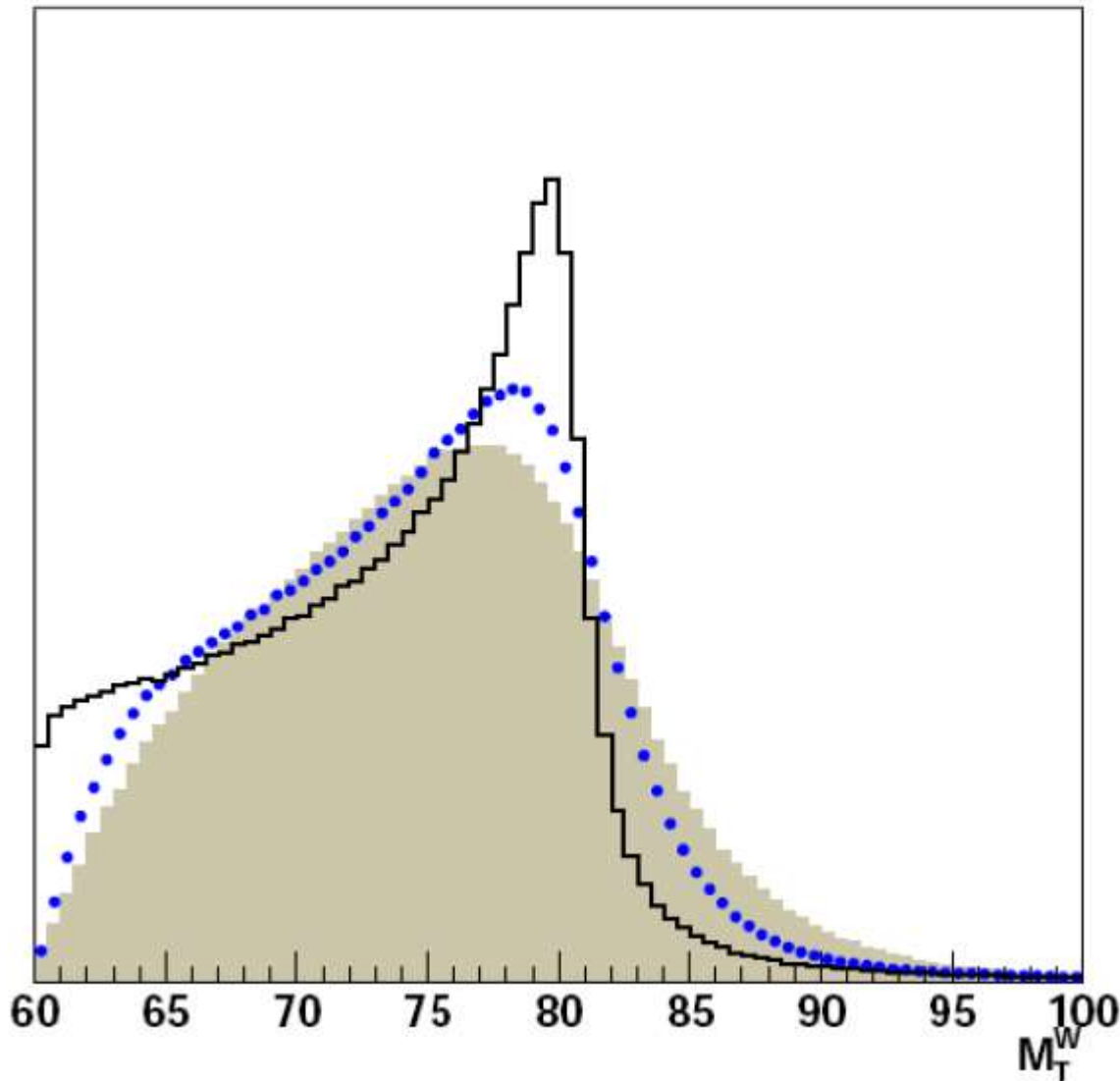- But measurement resolution on leptons is good

Black curve: truth level, no $p_T(W)$

Blue points: detector-level with lepton resolution and selection, But no $p_T(W)$

Shaded histogram: with $p_T(W)$

W mass measurement – decay kinematics

- Define "transverse mass" → approximately invariant under transverse boost

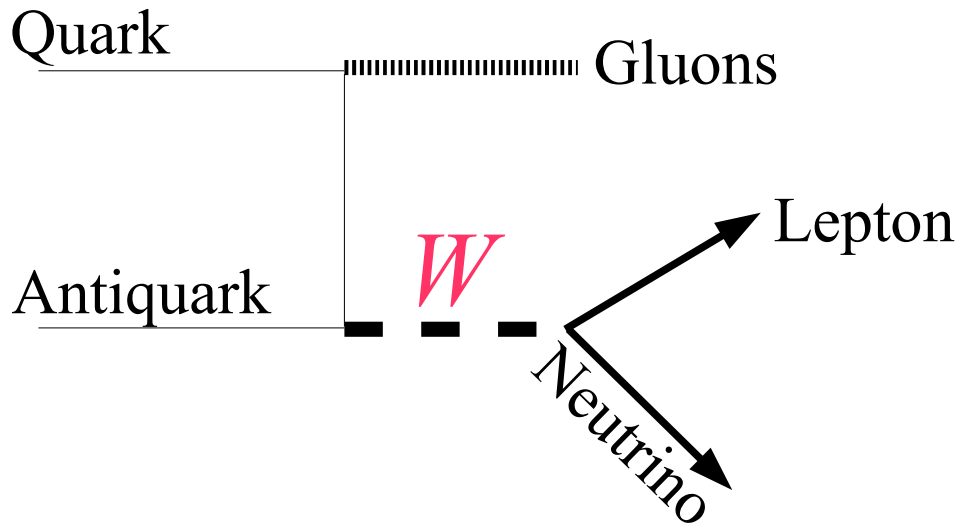- But measurement resolution of "neutrino" is not as good due to recoil

Black curve: truth level, no $p_T(W)$

Blue points: detector-level with lepton resolution and selection, But no $p_T(W)$

Shaded histogram: with $p_T(W)$

$$m_T = \sqrt{\left(E_T^l + E_T^\nu\right)^2 - \left(\overrightarrow{p}_T^{\,l} + \overrightarrow{p}_T^{\,\nu}\right)^2}$$
$$= \sqrt{2p_T^\mu p_T^\nu (1 - \cos\Delta\phi)}$$

W Boson Production at the Tevatron

Quark

Antiquark

Gluons

W

Lepton

Neutrino

Quark-antiquark annihilation
dominates (80%) @ Tevatron &
CP-symmetric initial state
Significant gluon, sea-quark, heavy flavor
@ LHC
Lepton p_T carries most of W mass
information, measured precisely (CDF achieved 0.004%)

QCD radiation is O(10 GeV), measure as soft 'hadronic recoil $\boldsymbol{u}$' in
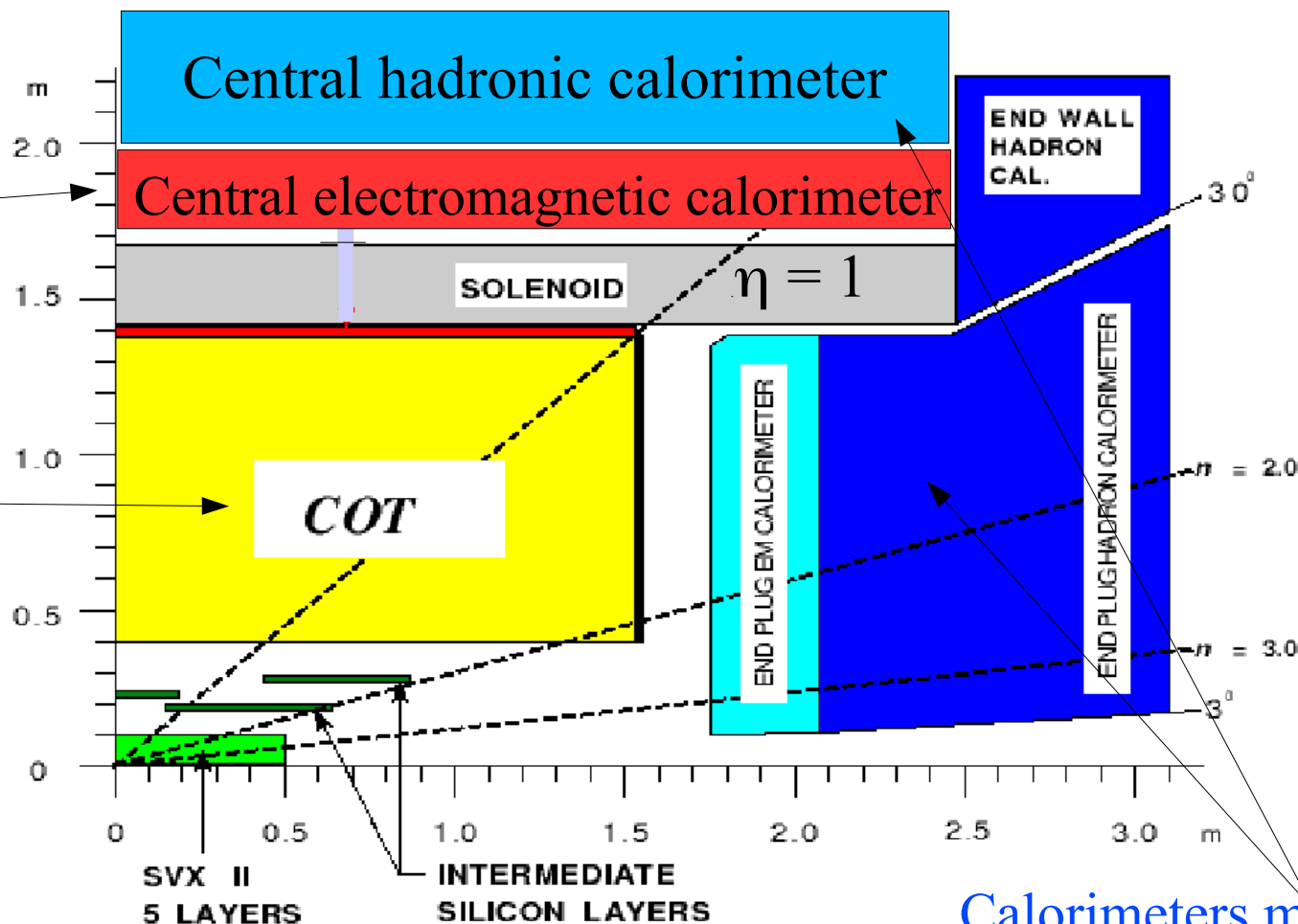calorimeter (calibrated to ~0.2%)
dilutes W mass information, fortunately for CDF $p_T(W) \ll M_W$
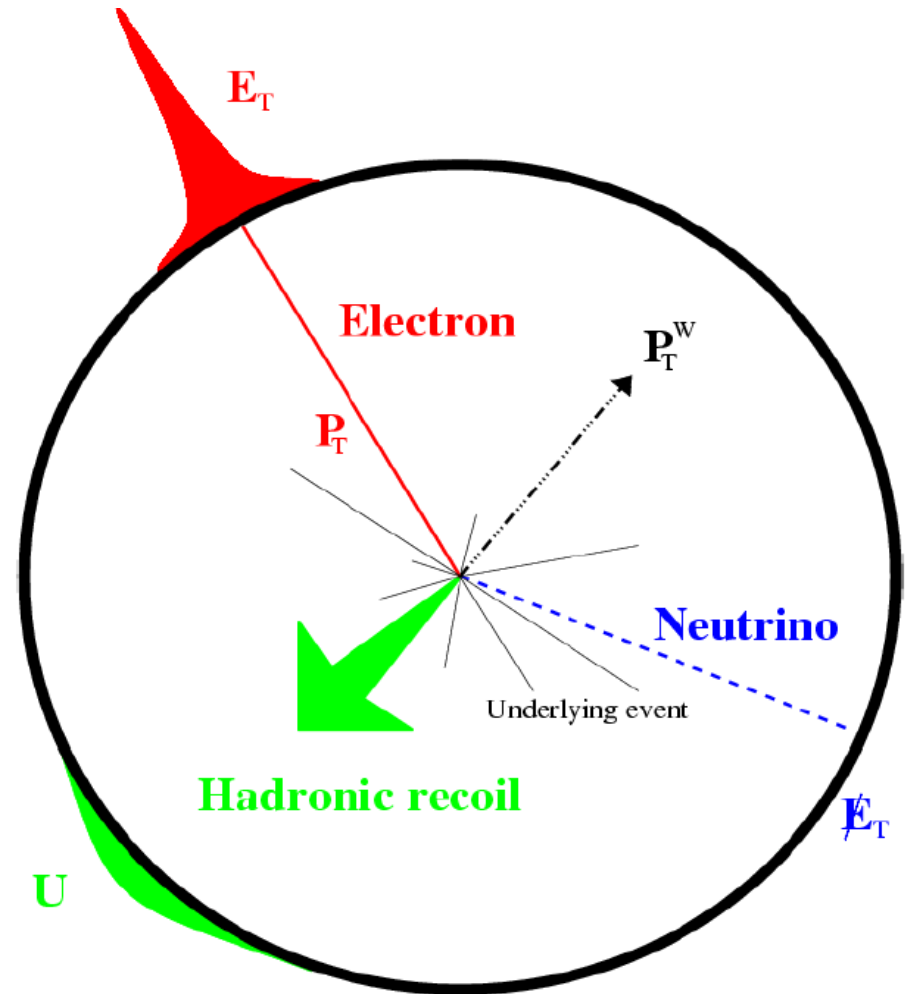
Quadrant of Collider Detector at Fermilab (CDF)

EM calorimeter provides precise electron energy measurement

COT provides precise lepton track momentum measurement

Central hadronic calorimeter

Central electromagnetic calorimeter

END WALL HADRON CAL.

SOLENOID

$\eta = 1$

30^0

COT

END PLUG EM CALORIMETER

END PLUG HADRON CALORIMETER

$\eta = 2.0$

$\eta = 3.0$

3^0

SVX II 5 LAYERS

INTERMEDIATE SILICON LAYERS

Calorimeters measure hadronic recoil particles

Event Selection

- Inclusive lepton triggers: loose lepton track and muon stub / calorimeter cluster requirements, with lepton $p_T > 18$ GeV

  - Kinematic efficiency of trigger ~100% for offline selection

- Offline selection requirements:

  - Electron cluster $E_T > 30$ GeV, track $p_T > 18$ GeV

  - Muon track $p_T > 30$ GeV

  - Loose identification requirements to minimize selection bias

- W boson event selection: one selected lepton, $|\boldsymbol{u}| < 15$ GeV & $p_T(\nu) > 30$ GeV

- ATLAS: similar lepton cuts but $|\boldsymbol{u}| < 30$ GeV

  - Admits more background

  - Much more QCD radiation

  - More efficiency-related corrections required

Analysis Strategy

Strategy

Maximize the number of internal constraints and cross-checks

Driven by three goals:

1) Robustness: constrain the same parameters in as many different ways as possible

2) Precision: combine independent measurements after showing consistency

3) minimize bias: blinded measurements of M_Z and M_W

Outline of Analysis

Energy scale measurements drive the W mass measurement

- Tracker Calibration

  - alignment of the COT (2,520 cells; 30,240 sense wires) using cosmic rays

  - COT momentum scale and tracker non-linearity constrained using $J/\psi \longrightarrow \mu\mu$ and $\Upsilon \longrightarrow \mu\mu$ mass fits

  - Confirmed using $Z \longrightarrow \mu\mu$ mass fit

- EM Calorimeter Calibration

  - COT momentum scale transferred to EM calorimeter using a fit to the peak of the E/p spectrum, around E/p ~ 1

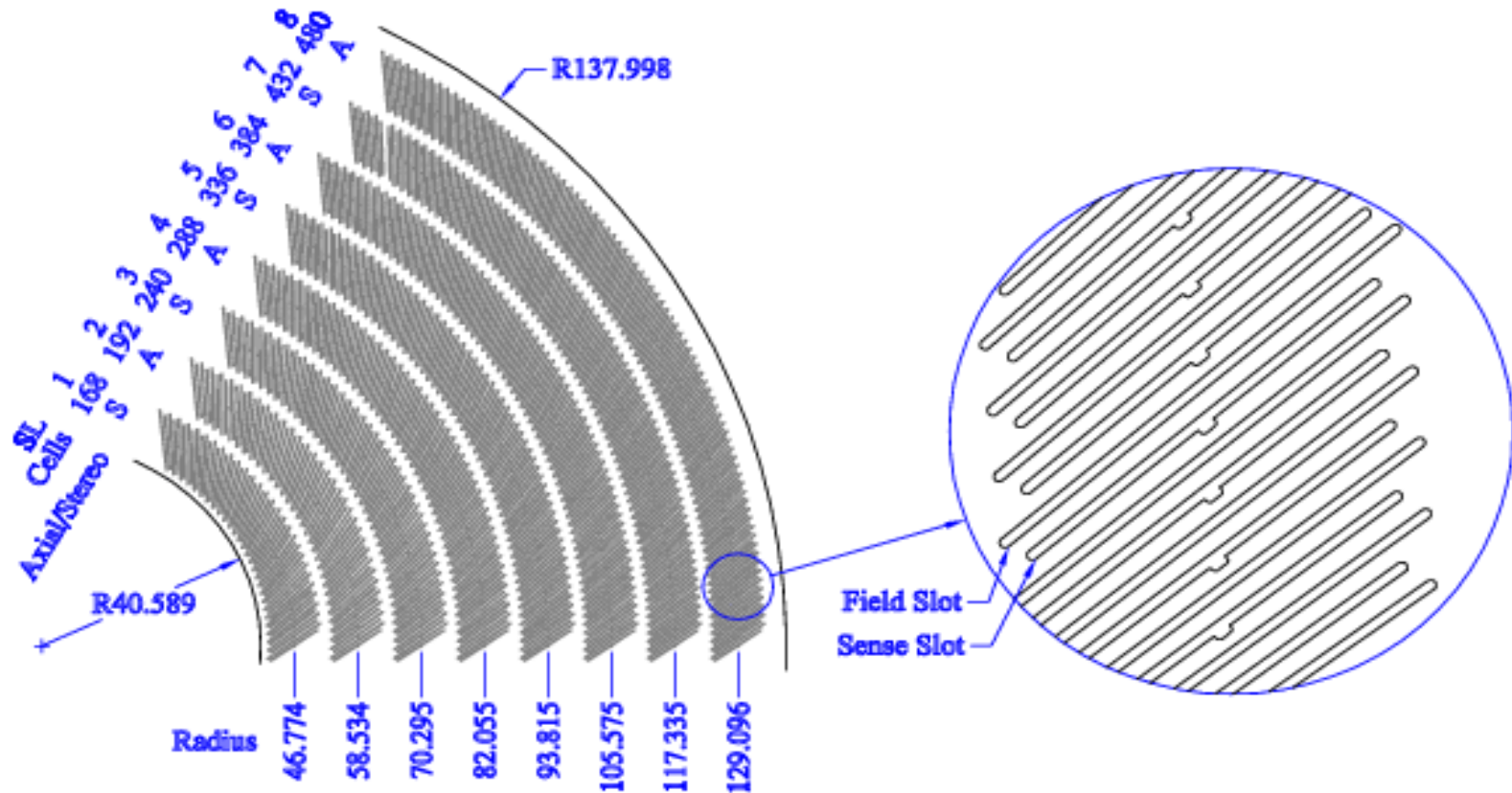 - Calorimeter energy scale confirmed using $Z \longrightarrow ee$ mass fit

- Tracker and EM Calorimeter resolutions

- Hadronic recoil modeling

  - Characterized using p_T-balance in $Z \longrightarrow ll$ events

Drift Chamber (COT) Alignment

COT endplate geometry

Only CDF demonstrates first-principles understanding and calibration of tracker

COT geometry guarantees analytic response as a function of track curvature
Because there are no gaps between sensors, which is not true for a silicon tracker

CDF Particle Tracking Chamber

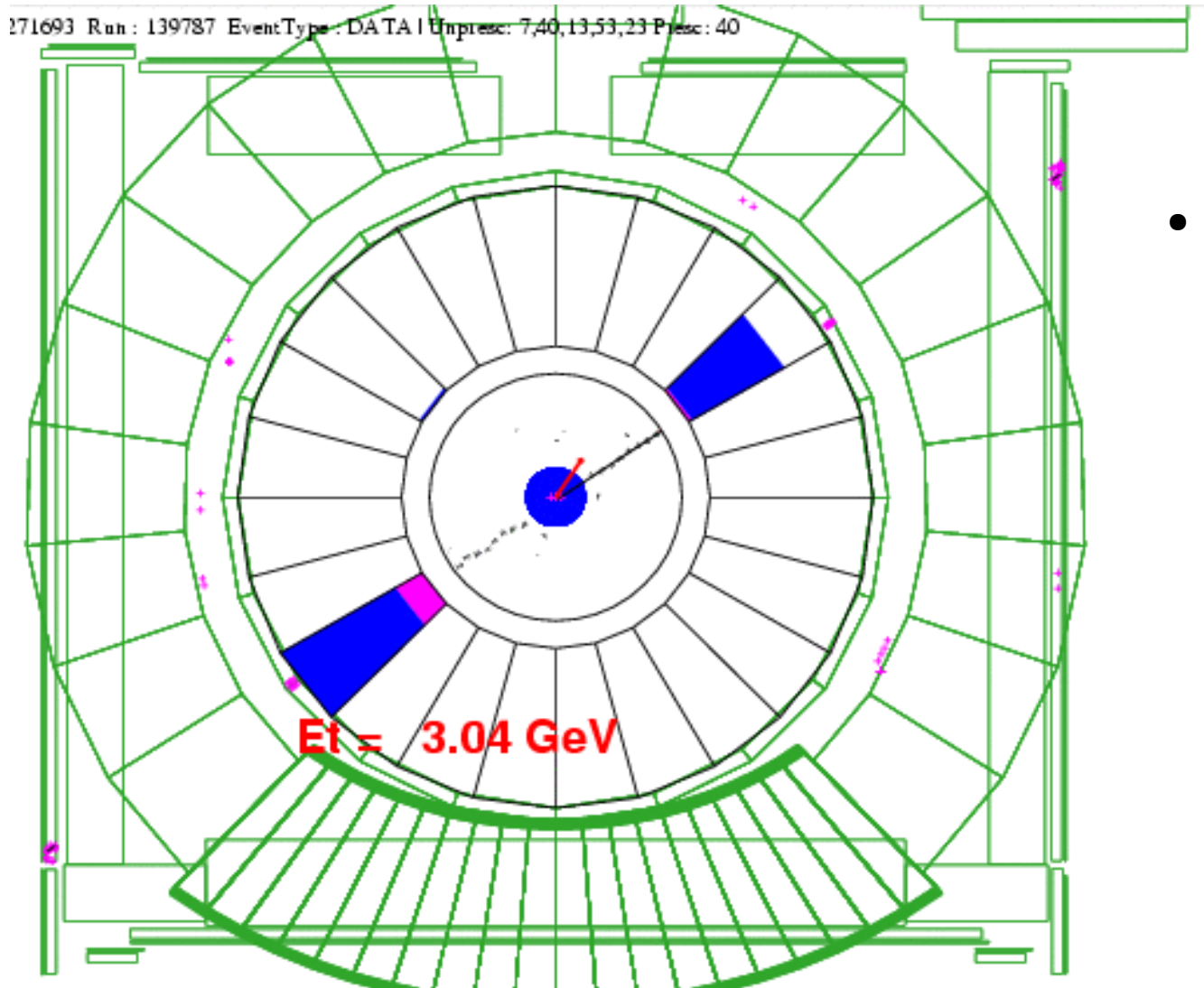Reconstruction of particle trajectories, calibration to ~1 μm accuracy:

A. Kotwal, H. Gerberich and C. Hays, NIM A506, 110 (2003)

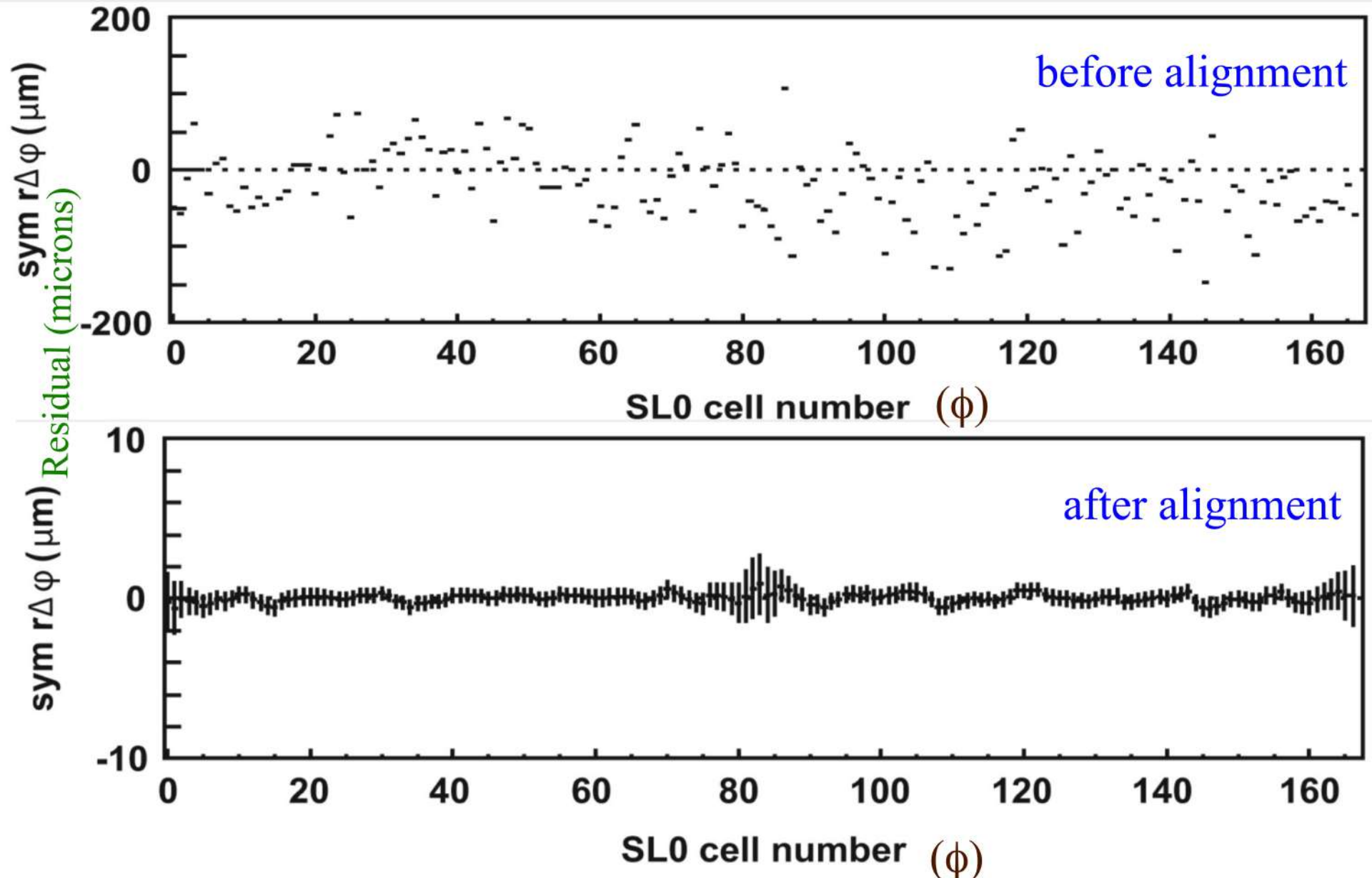C. Hays et al, NIM A538, 249 (2005)

Internal Alignment of COT

- Use a clean sample of ~480k cosmic rays for cell-by-cell internal alignment

- Fit COT hits on both sides simultaneously to a single helix (AVK, H. Gerberich and C. Hays, NIMA 506, 110 (2003))

  - Time of incidence is a floated parameter in this 'di-cosmic fit'
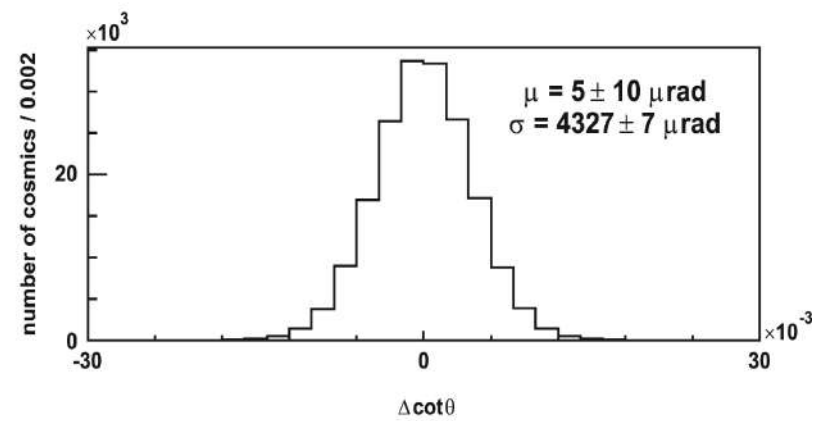
Residuals of COT cells after alignment

Final relative alignment of cells ~1 μm (initial alignment ~50 μm)

Consistency check of COT alignment procedure
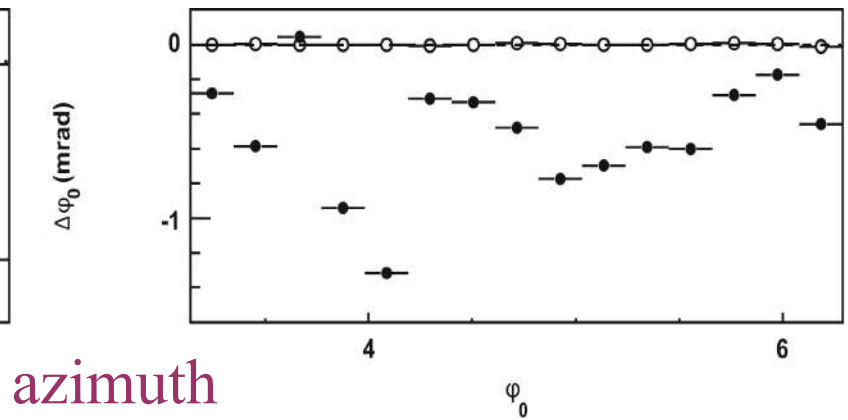
Fit separate helices to cosmic ray tracks

Compare track parameters of the two tracks: a measure of track parameter bias

$\mu = -3 \pm 4\ \text{PeV}^{-1}$
$\sigma = 1862 \pm 3\ \text{PeV}^{-1}$

$\mu = 0 \pm 2\ \mu\text{rad}$
$\sigma = 839 \pm 1\ \mu\text{rad}$

$\mu = -0.5 \pm 0.7\ \mu\text{m}$
$\sigma = 309.6 \pm 0.5\ \mu\text{m}$

$\mu = 5 \pm 10\ \mu\text{rad}$
$\sigma = 4327 \pm 7\ \mu\text{rad}$

$\mu = 3 \pm 9\ \mu\text{m}$
$\sigma = 3788 \pm 6\ \mu\text{m}$

$\mu = 8 \pm 1\ \text{ps}$
$\sigma = 432 \pm 1\ \text{ps}$

Consistency check of COT alignment procedure

track parameter
bias versus
azimuth

solid = before
alignment

open = after
alignment
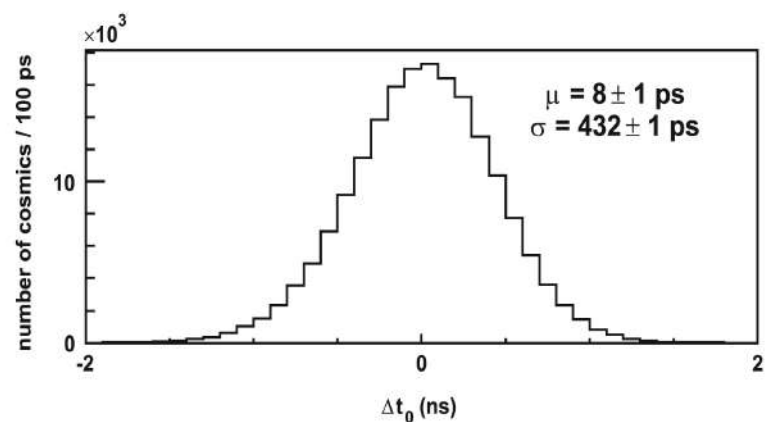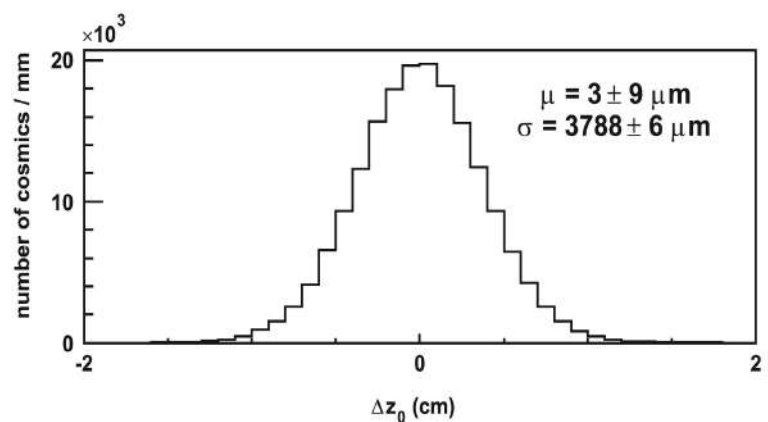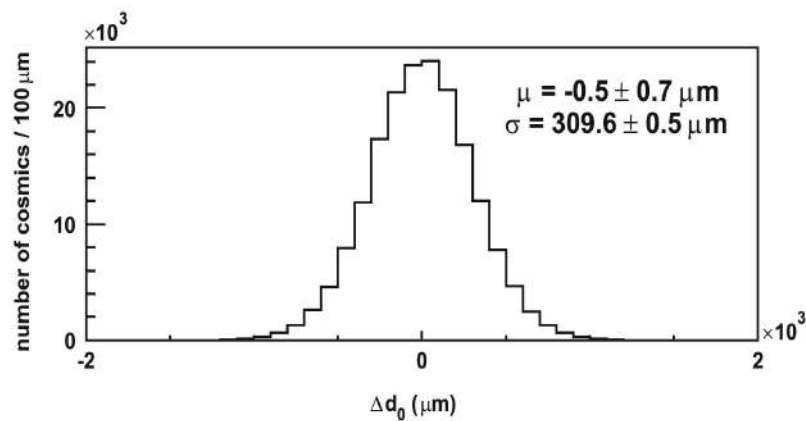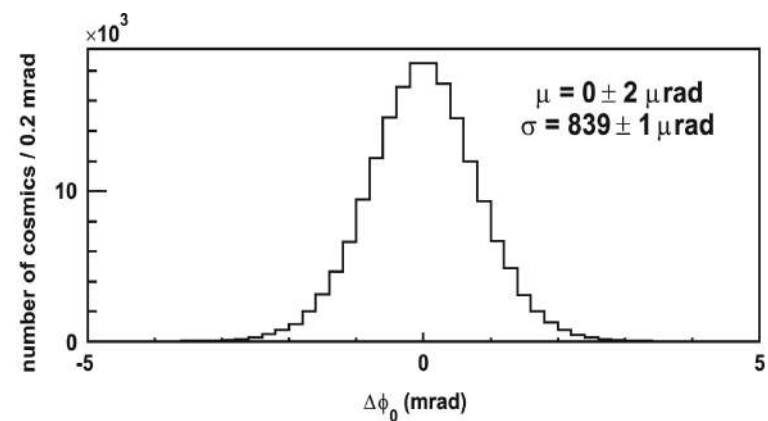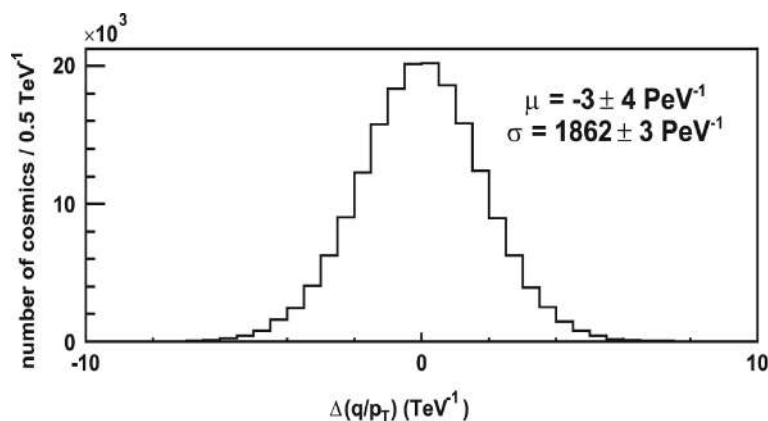
Consistency check of COT alignment procedure

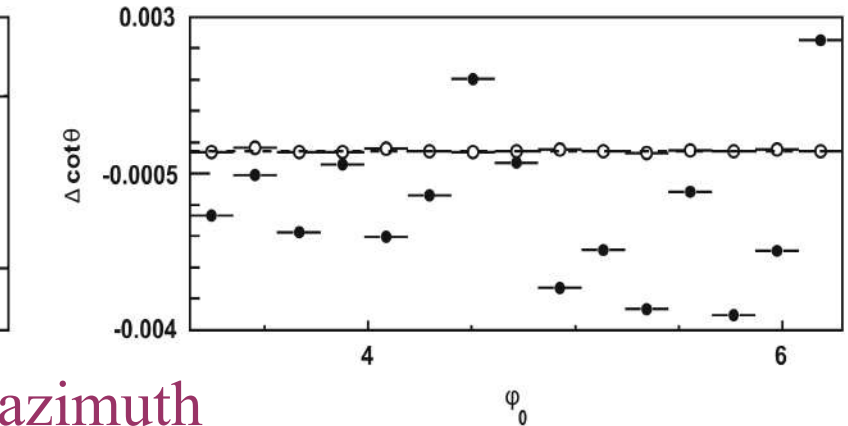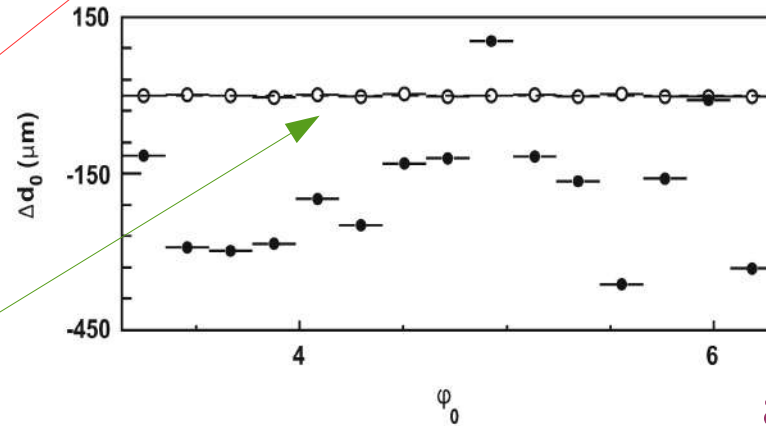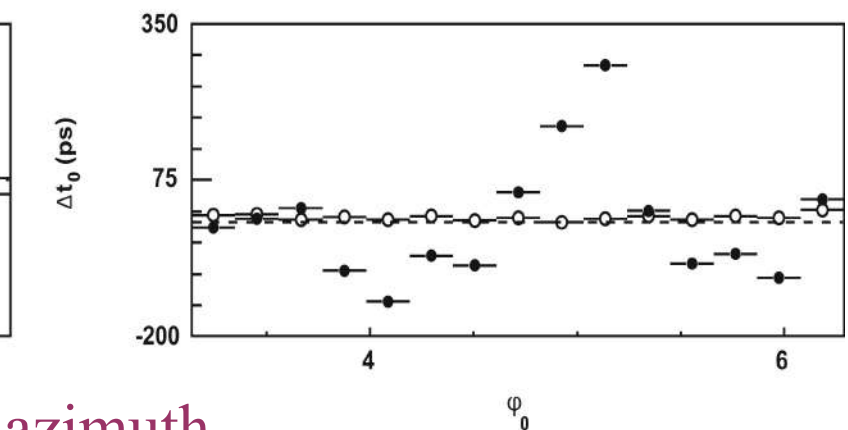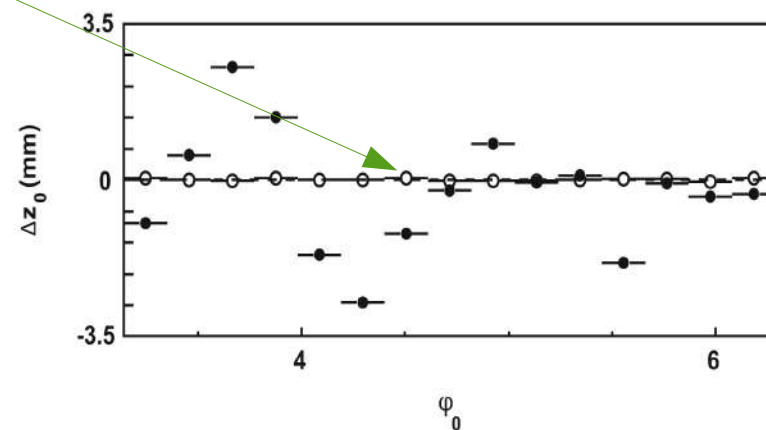(AVK & CH, *NIM A* 762 (2014) pp 85-99)

track parameter
bias versus
polar angle
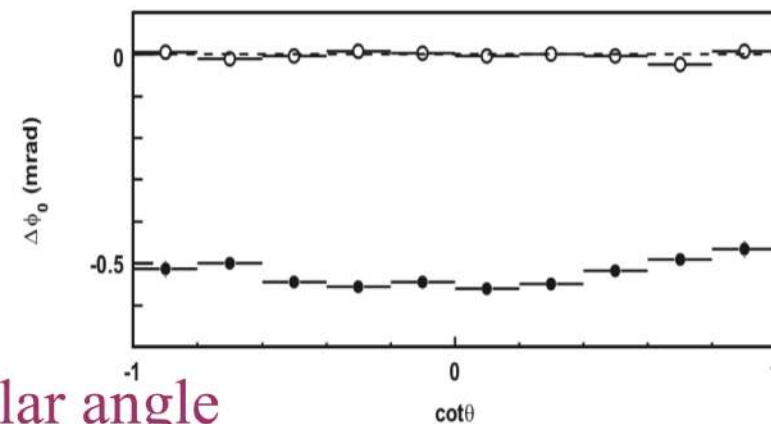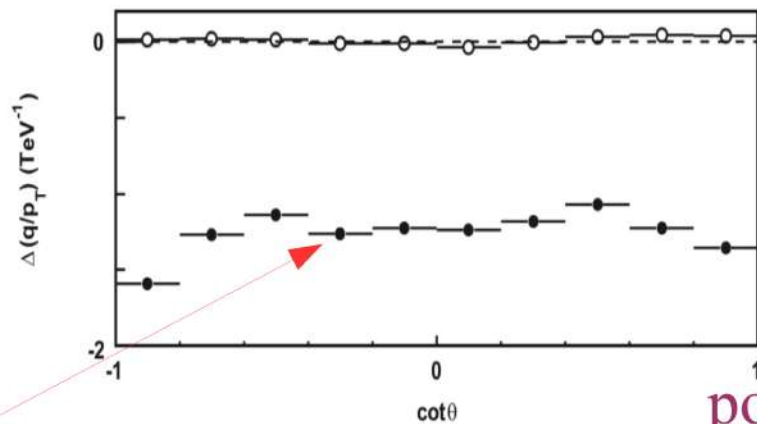
solid = before
alignment

open = after
alignment
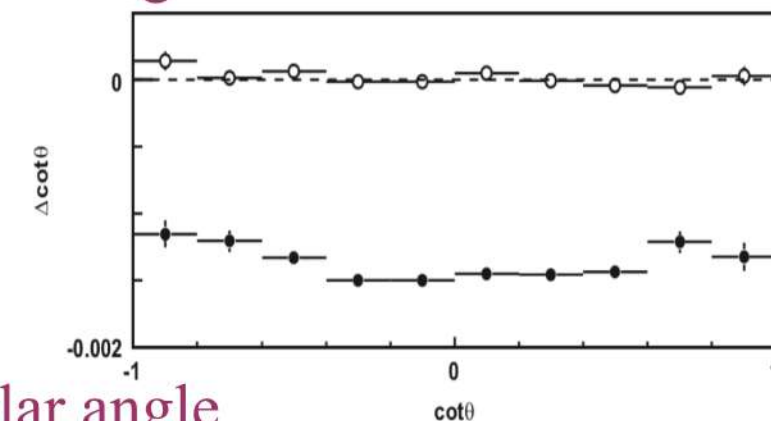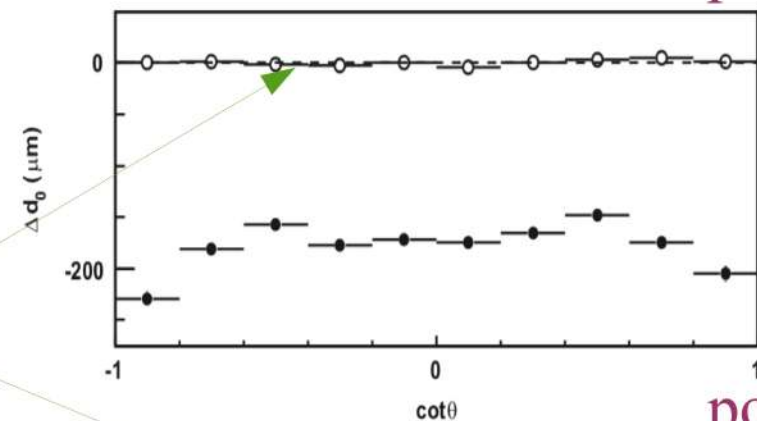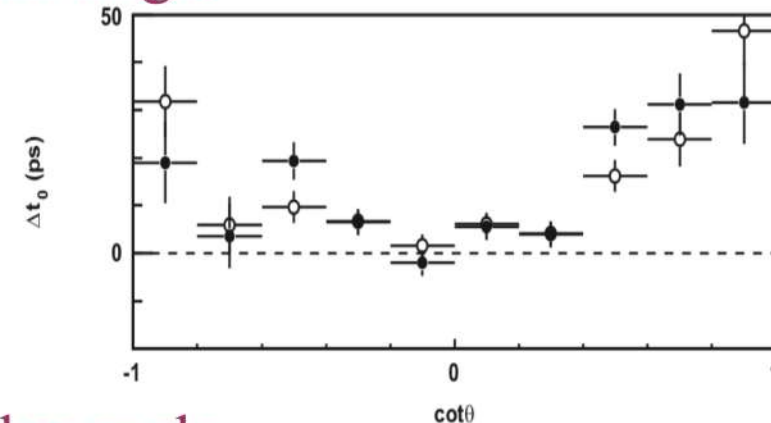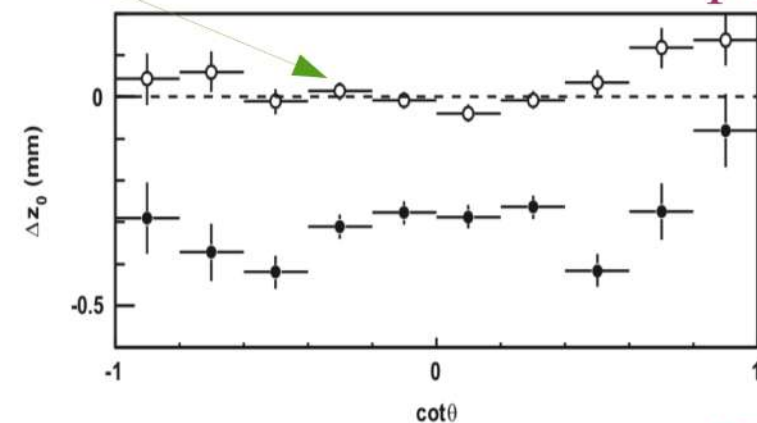
Cross-check of COT alignment

- Cosmic ray alignment removes most deformation degrees of freedom, but "weakly constrained modes" remain

- Final cross-check and correction to beam-constrained track curvature based on difference of <E/p> for positrons *vs* electrons

- Smooth ad-hoc curvature corrections as a function of polar and azimuthal angle: statistical errors => $\Delta M_W = 1$ MeV

q/p_T (measured) =

$c_0 + c_1\, q/p_T + c_2\, q/p_T^2$

$+ \ldots$

c_1 measures momentum scale
c_2 includes energy loss
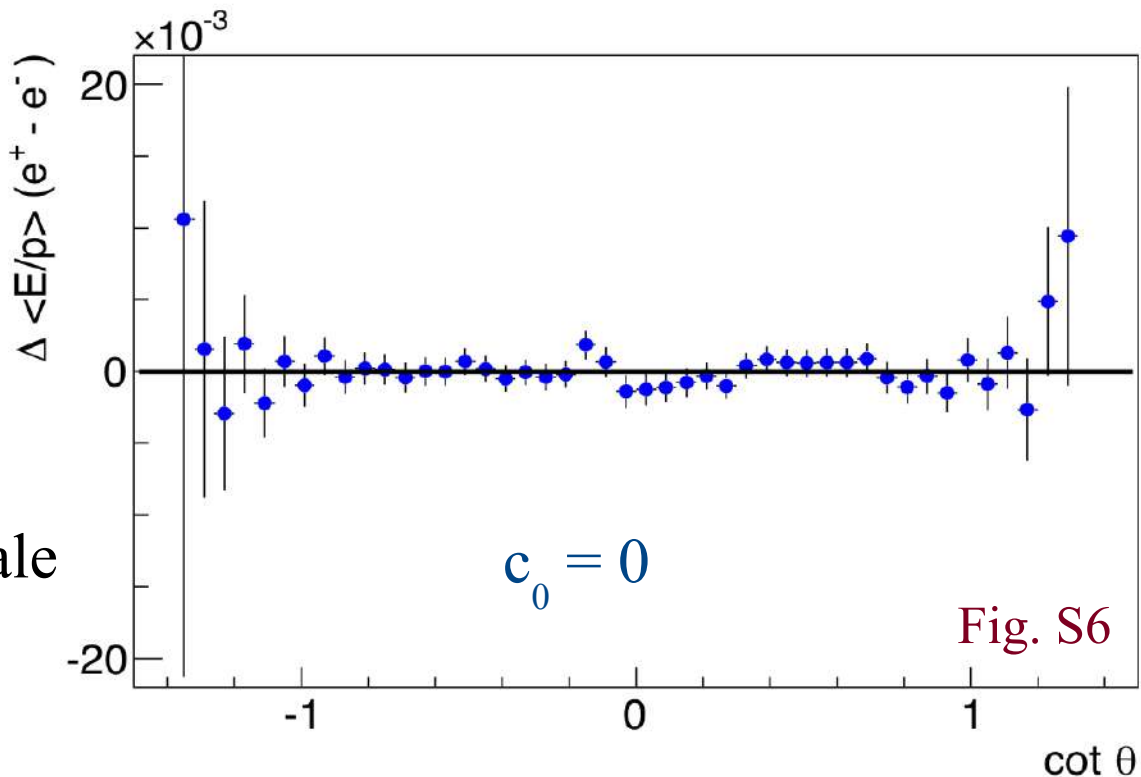
Fig. S6

$c_0 = 0$

Outline of Analysis

Energy scale measurements drive the W mass measurement

- **Tracker Calibration**

  - alignment of the COT (~2400 cells, ~30k sense wires) using cosmic rays

  → COT momentum scale and tracker non-linearity constrained using $J/\psi \longrightarrow \mu\mu$ and $\Upsilon \longrightarrow \mu\mu$ mass fits

  - Confirmed using $Z \longrightarrow \mu\mu$ mass fit

- **EM Calorimeter Calibration**

  - COT momentum scale transferred to EM calorimeter using a fit to the peak of the E/p spectrum, around E/p ~ 1

  - Calorimeter energy scale confirmed using $Z \longrightarrow ee$ mass fit

- **Tracker and EM Calorimeter resolutions**

- **Hadronic recoil modeling**

  - Characterized using p_T-balance in $Z \longrightarrow ll$ events

Custom Monte Carlo Detector Simulation

- A complete detector simulation of all quantities measured in the data

- First-principles simulation of tracking

  - Tracks and photons propagated through a high-resolution 3-D lookup table of material properties for silicon detector and COT
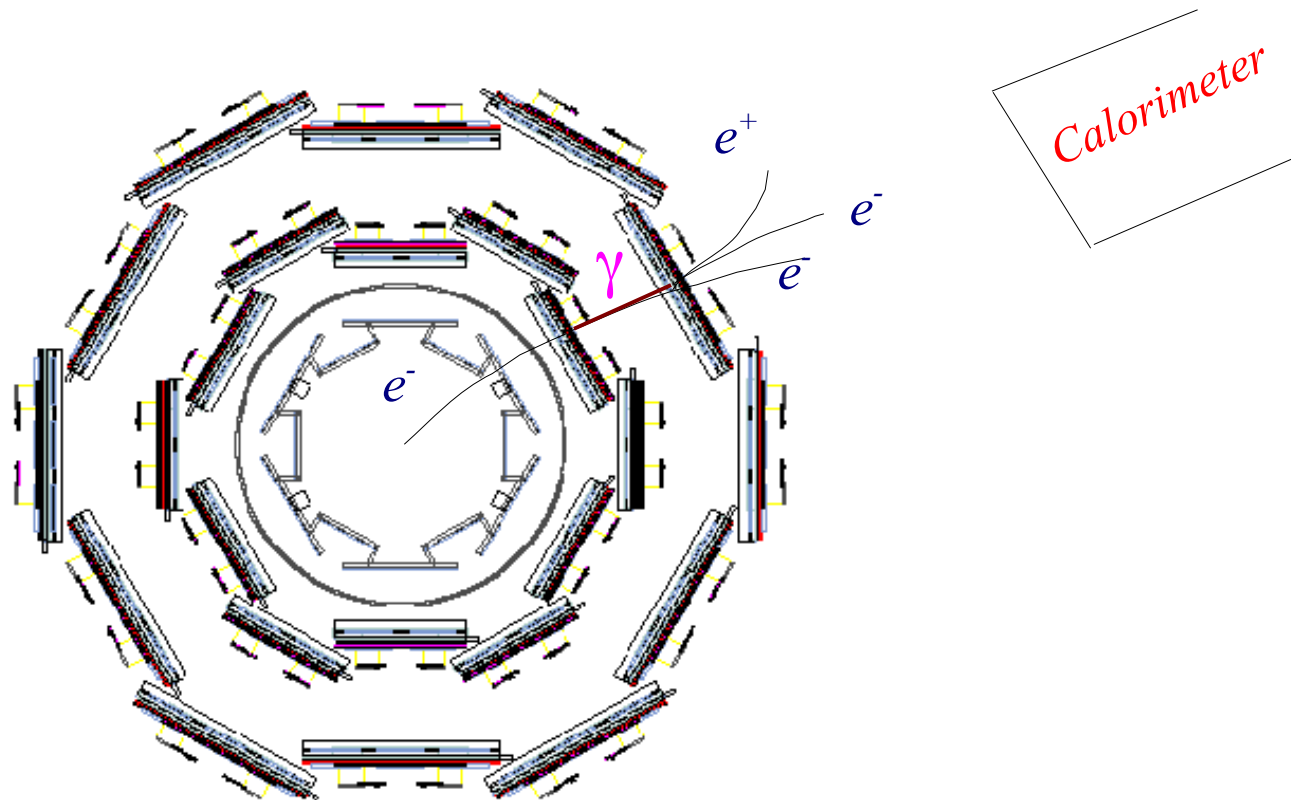
Tracking Momentum Scale

Tracking Momentum Scale

Set using J/ψ ⟶ μμ and ϒ ⟶ μμ resonance and Z ⟶ μμ masses

- Extracted by fitting J/ψ mass in bins of $1/p_T(\mu)$, after correcting for the measured ionization energy loss

- J/ψ ⟶ μμ mass independent of $p_T(\mu)$ after 2.6% tuning of energy loss

Fig. 2

Fig. S9

Tracking Momentum Scale

Υ ⟶ μμ resonance provides

- Momentum scale measurement at higher p_T

- Validation of beam-constaining procedure (upsilons are promptly produced)

- Cross-check of non-beam-constrained (NBC) and beam-constrained (BC) fits

Fig. S12
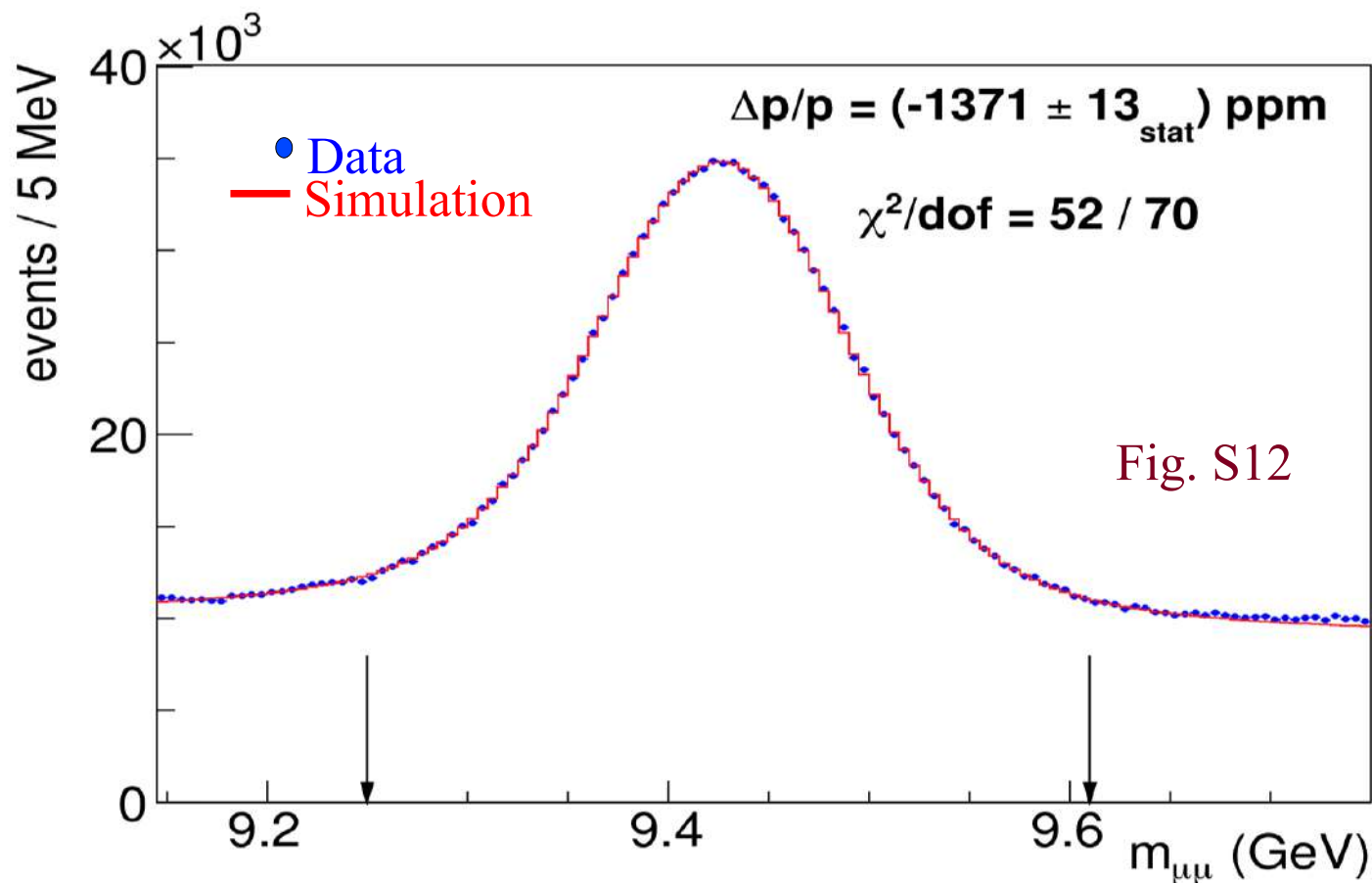
NBC Υ⟶μμ mass fit

Tracking Momentum Scale

$\Upsilon \longrightarrow \mu\mu$ resonance provides

- Cross-check of non-beam-constrained (NBC) and beam-constrained (BC) fits
- Consistent measurements after incorporating silicon detector passive energy loss in extrapolator code of track reconstruction

Fig. S12

BC $\Upsilon \longrightarrow \mu\mu$ mass fit

$\Delta p/p = (-1380 \pm 10_{stat})$ ppm

$\chi^2/dof = 82 / 70$

Tracking Momentum Scale Systematics

Systematic uncertainties on momentum scale (parts per million)

Source	J/ψ (ppm)	Υ (ppm)	Correlation (%)
QED	1	1	100
Magnetic field non-uniformity	13	13	100
Ionizing material correction	11	8	100
Resolution model	10	1	100
Background model	7	6	0
COT alignment correction	4	8	0
Trigger efficiency	18	9	100
Fit range	2	1	100
$\Delta p/p$ step size	2	2	0
World-average mass value	4	27	0
Total systematic	29	34	16 ppm
Statistical NBC (BC)	2	13(10)	0
Total	29	36	16 ppm

Table S2

$\Delta M_{W,Z} = 2$ MeV

Uncertainty dominated by magnetic field non-uniformity, passive material energy loss, low p_T modeling and Υ mass world average

$Z \rightarrow \mu\mu$ Mass Cross-check & Combination

- Using the J/ψ and Υ momentum scale, performed "blinded" measurement of *Z* boson mass

  – Z mass consistent with PDG value (91188 MeV) (0.7σ statistical)

  – $M_Z = 91192.0 \pm 6.4_{stat} \pm 2.3_{momentum} \pm 3.1_{QED} \pm 1_{alignment}$ MeV

Fig. 3
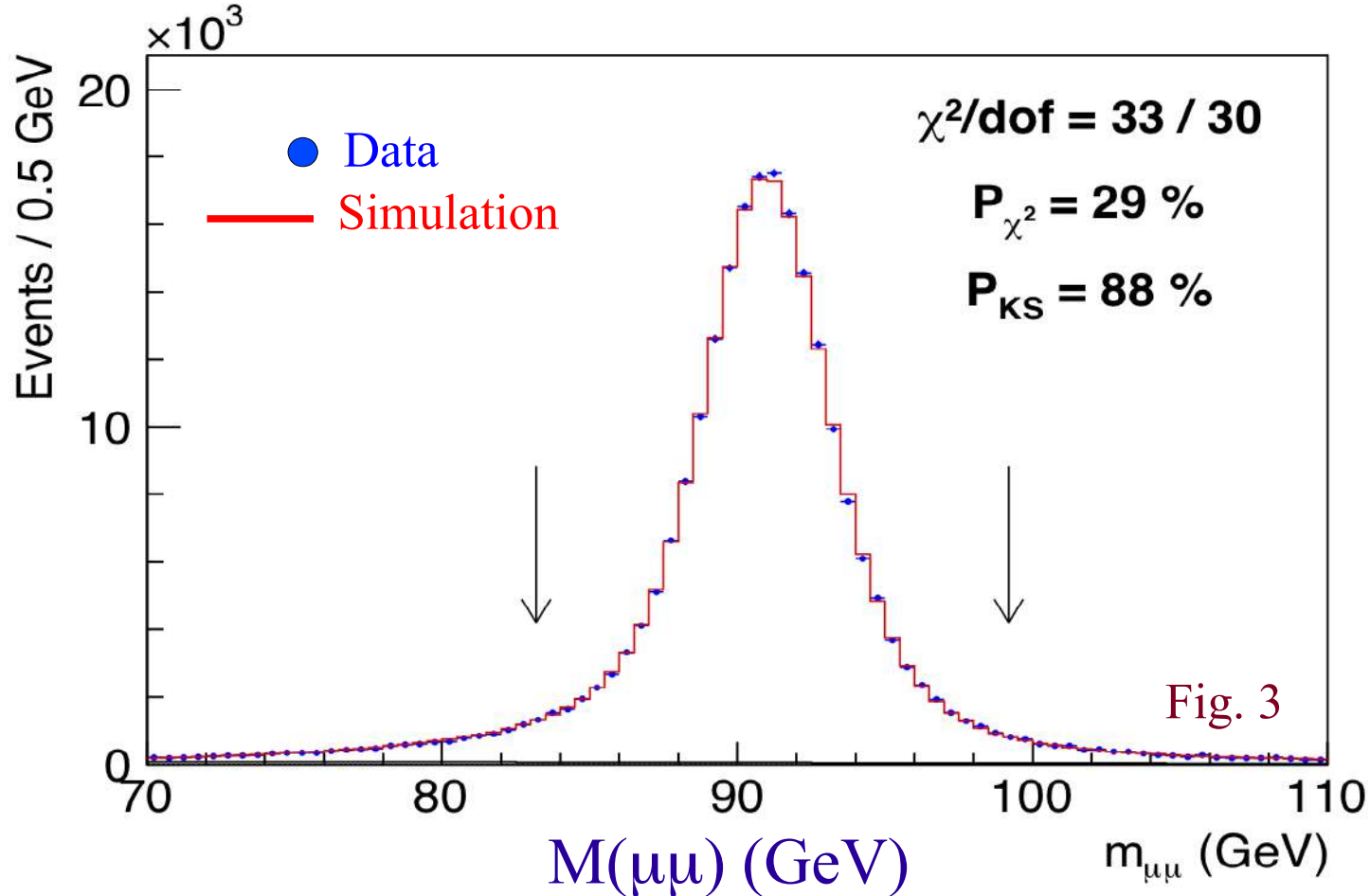
EM Calorimeter Response

Calorimeter Simulation for Electrons and Photons

- Distributions of lost energy calculated using detailed GEANT4 simulation of calorimeter, tuned on data

  - Leakage into hadronic calorimeter

  - Absorption in the coil

  - Dependence on incident angle and E_T

  (AVK & CH, *NIM A* 729 (2013) pp 25-35)
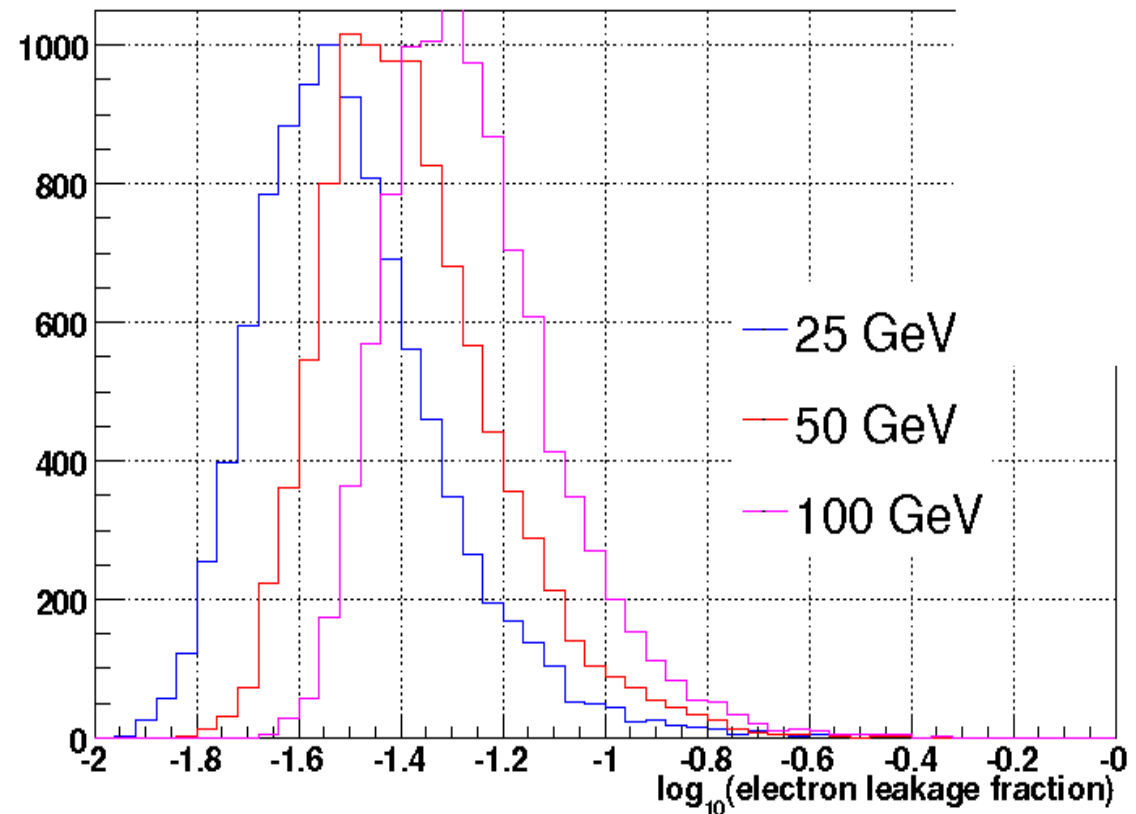
- Energy-dependent gain (non-linearity) parameterized and fit from data

- Energy resolution: fixed sampling term and tunable constant term

  - Constant terms are fit from the width of E/p peak and Z→ee mass peak

EM Calorimeter Scale

- E/p peak from $W \longrightarrow e\upsilon$ decays provides measurements of EM calorimeter scale and its (E_T-dependent) non-linearity

$$\Delta S_E = (43_{\text{stat}} \pm 30_{\text{non-linearity}} \pm 34_{\text{X0}} \pm 45_{\text{Tracker}}) \texttt{ parts per million}$$

Setting S_E to 1 using E/p calibration from combined $W \longrightarrow e\upsilon$ and $Z \longrightarrow ee$ samples

$\Delta M_W = 6$ MeV

$\Delta S_E = 12 \pm 43_{\text{stat}}$ ppm

$\chi^2/\text{dof} = 39 / 33$

$P_{\chi^2} = 21 \%$

$P_{KS} = 69 \%$

Data

Simulation

Low tail used for tuning calorimeter thickness

High tail of used for tuning model of radiative material

Fig. 2

45
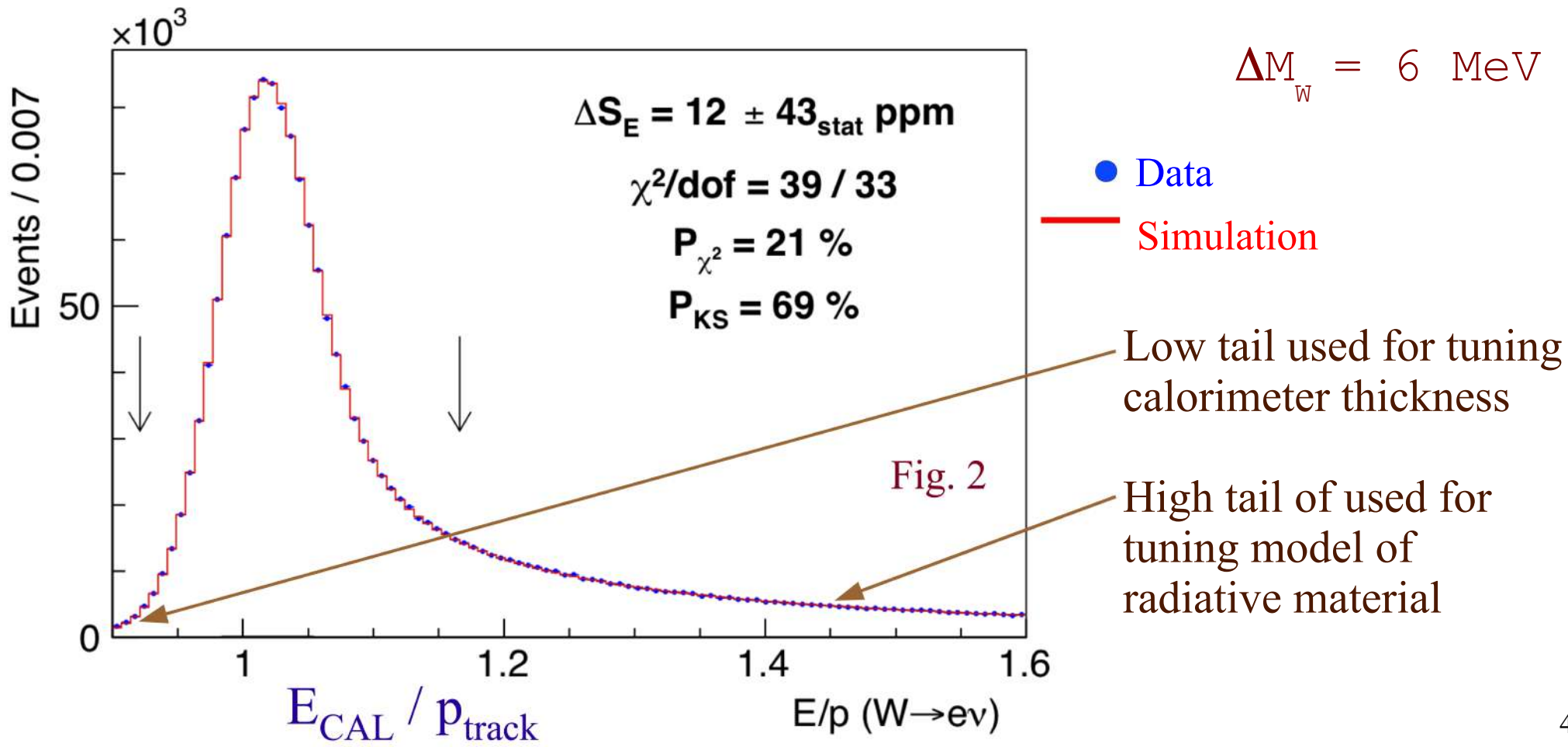
$Z \rightarrow ee$ Mass Cross-check and Combination

- Performed "blind" measurement of Z mass using E/p-based calibration

  - Consistent with PDG value (91188 MeV) within 0.5σ (statistical)

  - $M_Z = 91194.3 \pm 13.8_{stat} \pm 6.5_{calorimeter} \pm 2.3_{momentum} \pm 3.1_{QED} \pm 0.8_{alignment}$ MeV

- Combine E/p-based calibration with $Z \rightarrow ee$ mass for maximum precision
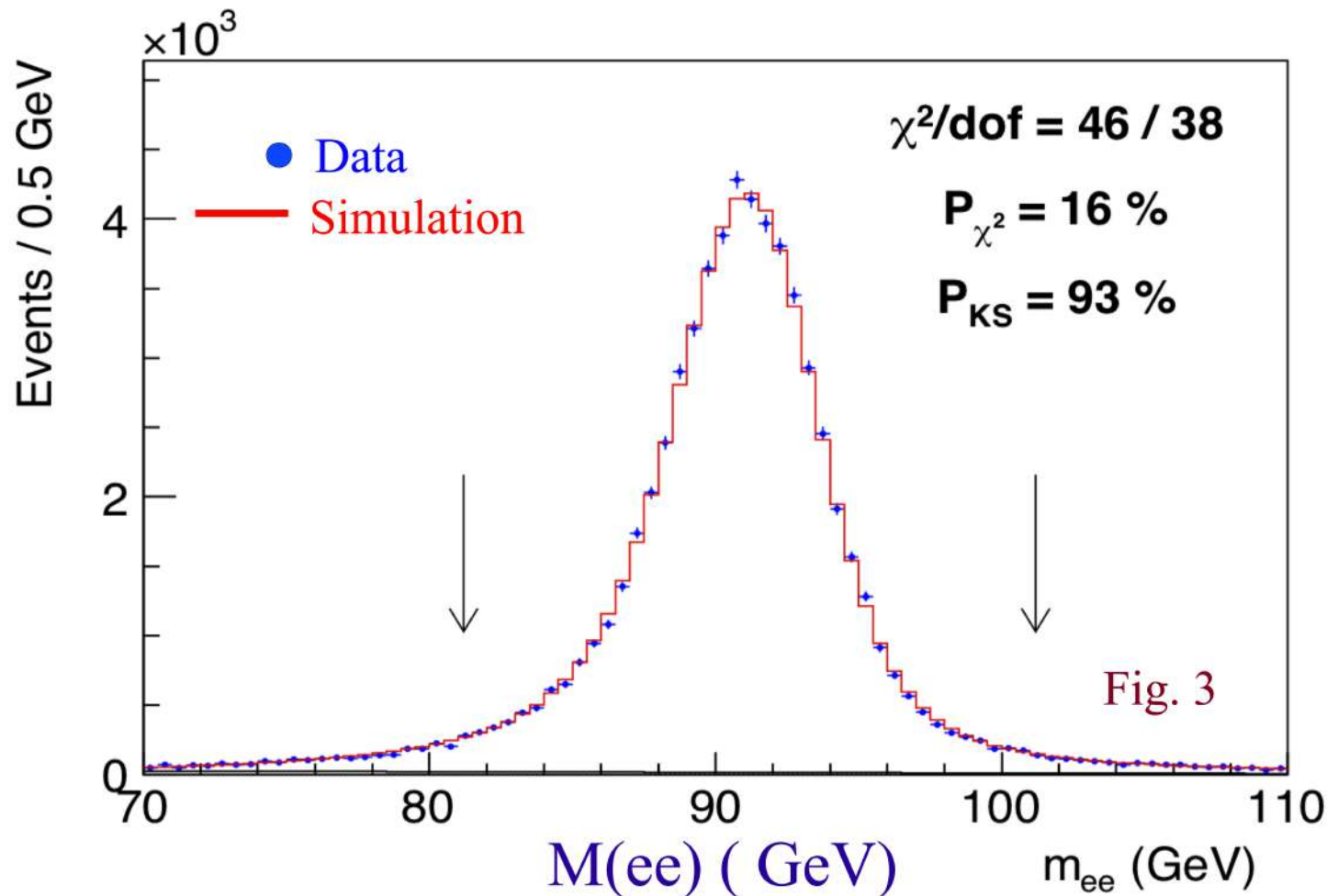
$\Delta M_W = 5.8$ MeV

$\Delta S_E = -14 \pm 72$ ppm

Fig. 3

Z → ee Mass Cross-check using Electron Tracks

- Performed "blind" measurement of Z mass using electron tracks, separately for radiative/non-radiative pairs

  - Consistent with PDG value

- Checks tracking for electrons vs muons, and model of radiative energy loss

$\chi^2/dof = 62 / 58$

$P_{\chi^2} = 31 \%$

$P_{KS} = 95 \%$

Fig. S16

● Data
— Simulation

$(E/p)_1 < 1.1$ &
$(E/p)_2 > 1.1$
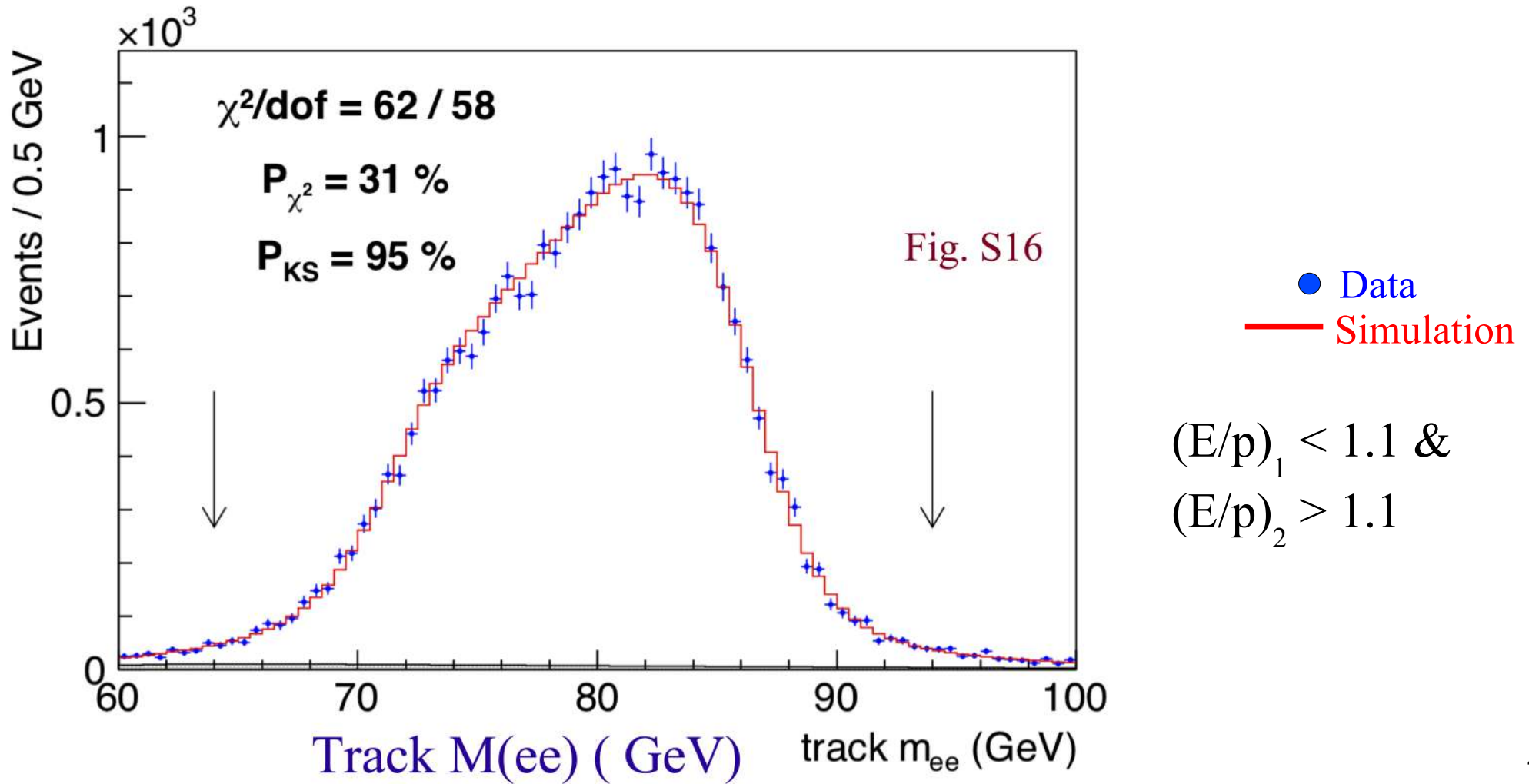
Compare & Contrast

CDF & ATLAS Calibration Strategies

- CDF calibration strategy built from "bottoms-up" understanding of detector concepts

  - First-principles alignment and calibration of drift chamber for track momentum

  - GEANT-based model of electromagnetic calorimeter

  - Handful of tuned parameters in detector response model based on "cause-and-effect" philosophy

- CDF demonstrates Z boson mass measurements as proof of calibrations

- ATLAS, LHCb & D0 jump directly to calibration on Z boson mass

  - First-principles studies of tracker and calorimeter not shown

  - In the 3+ decades of W boson mass measurements at hadron colliders, sole reliance on Z boson mass for calibration has never been "proven" to be as accurate as claimed

  - D0 has not analyzed latter 60% of Run 2 data due to tracker degradation (radiation damage), so calibration on Z-mass is not guaranteed to work

Hadronic Recoil Model

Constraining the Hadronic Recoil Model

Exploit similarity in production and decay of *W* and *Z* bosons

Detector response model for hadronic recoil tuned using p_T-balance in $Z \rightarrow ll$ events
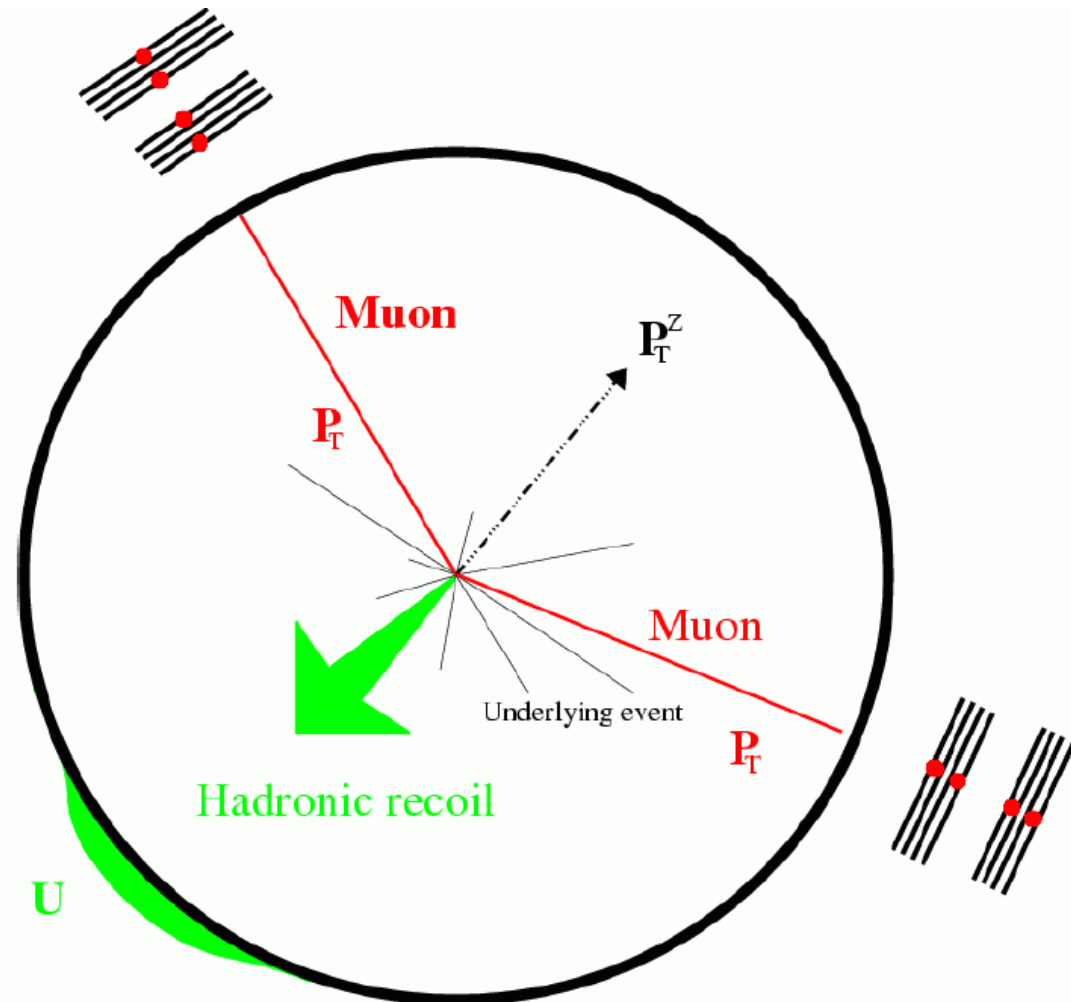
Transverse momentum of Hadronic recoil (***u***) calculated as 2-vector-sum over calorimeter towers

Lepton Tower Removal

- We remove the calorimeter towers containing lepton energy from the hadronic recoil calculation
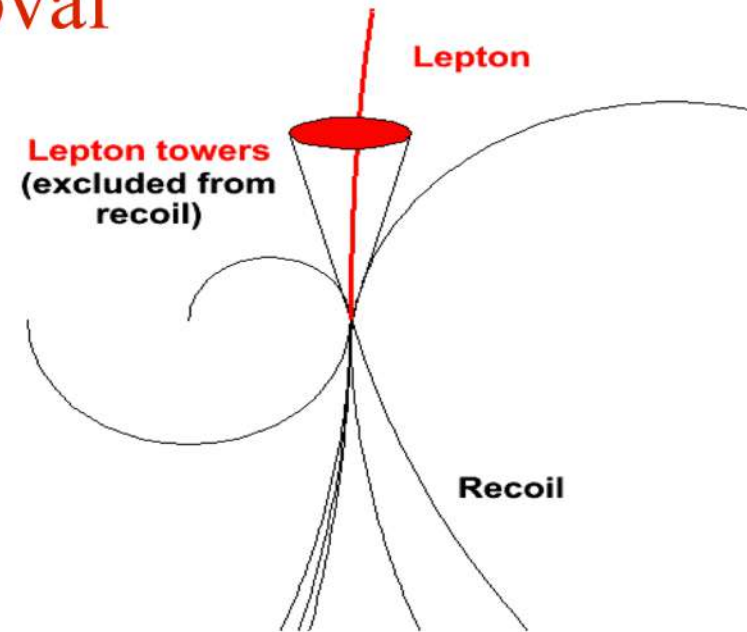
  – Lost underlying event energy is measured in φ-rotated windows in W boson data

$$\Delta M_W = 1 \text{ MeV}$$

Figs. S17 & S18

Electron Electromagnetic E_T (MeV)

Tower $\Delta\eta$						
3 — 61	61	62	63	62	61	61
2 — 62	61	62	69	64	62	61
1 — 63	63	66	1227	90	64	63
0 — 63	66	79	38534	176	68	64
-1 — 61	61	62	178	67	61	61
-2 — 61	61	61	63	62	61	61
-3 — 60	61	61	61	61	61	61

Tower $\Delta\phi$: -3, -2, -1, 0, 1, 2, 3

Muon Electromagnetic E_T (MeV)

Tower $\Delta\eta$						
3 — 60	60	60	61	60	60	60
2 — 59	59	60	62	61	59	59
1 — 61	61	62	82	66	61	61
0 — 61	61	63	378	70	62	61
-1 — 59	60	61	67	62	60	60
-2 — 59	59	60	61	61	60	59
-3 — 60	60	60	61	61	60	60

Tower $\Delta\phi$: -3, -2, -1, 0, 1, 2, 3
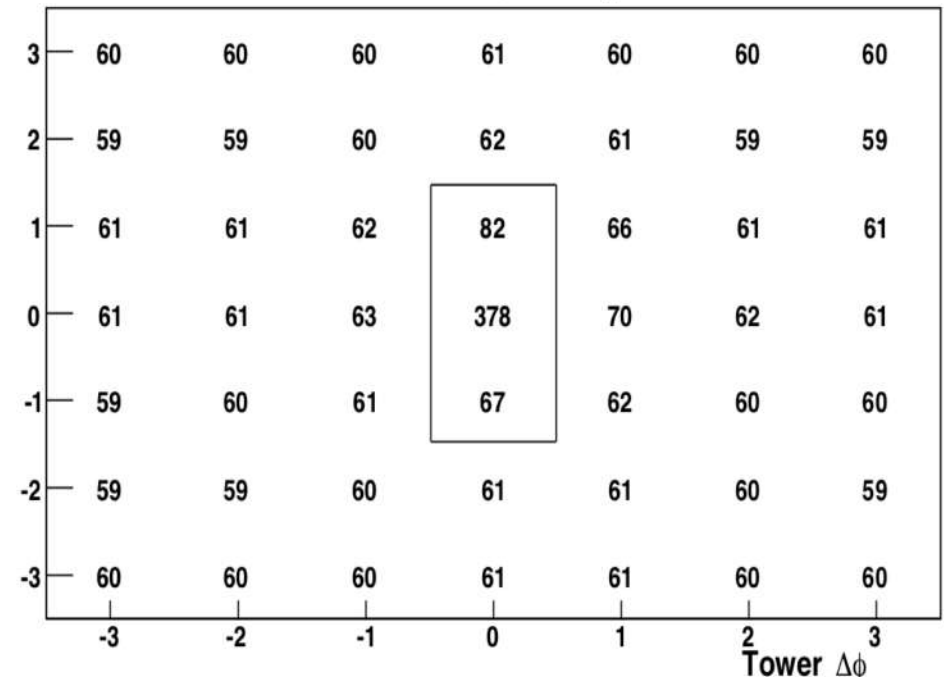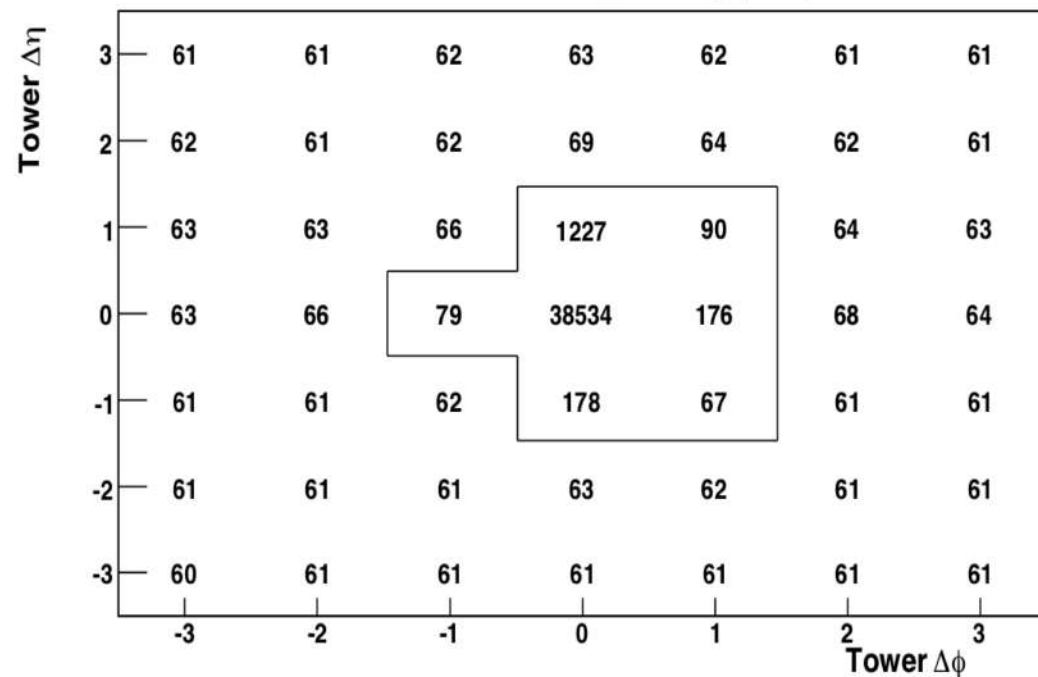
Lepton Tower Removal
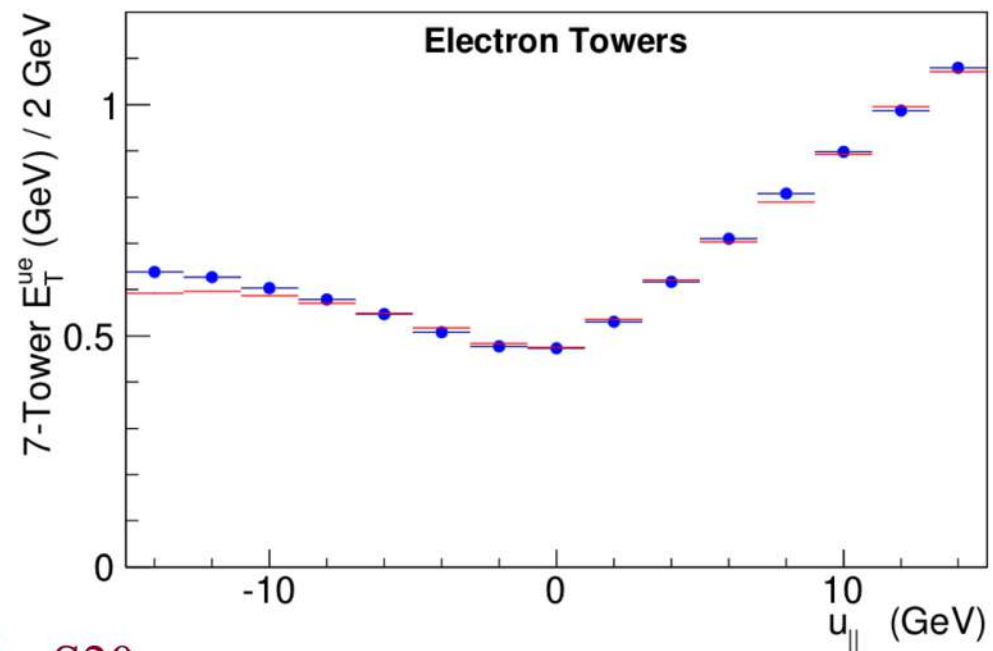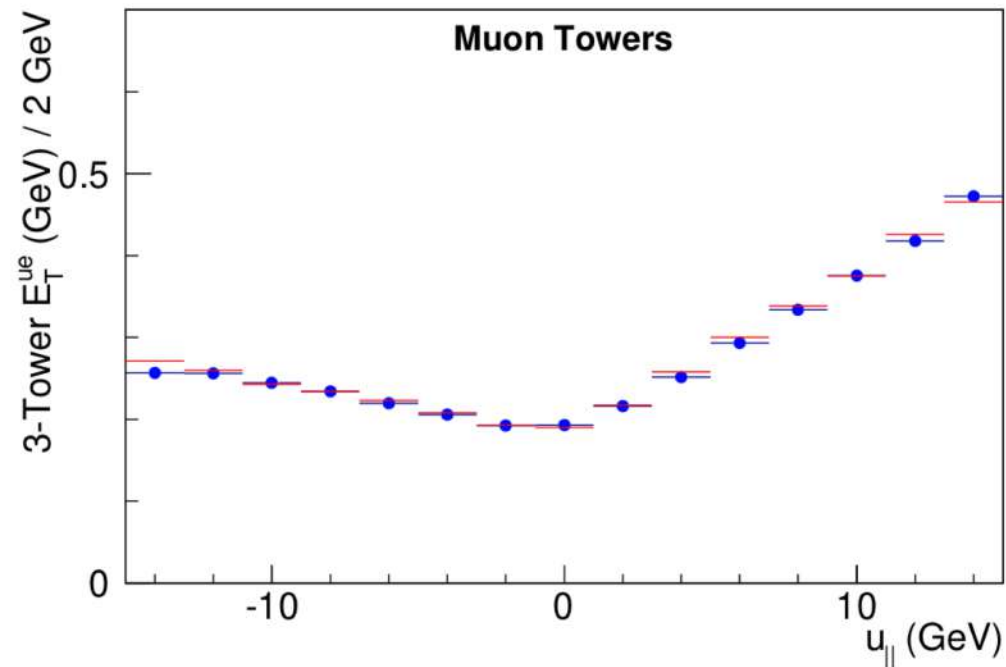
Fig. S20

Lepton Tower Removal

Fig. S20

No mention of this crucial detector aspect in the ATLAS paper

Testing Hadronic Recoil Model with *W* boson events

u(recoil)

l
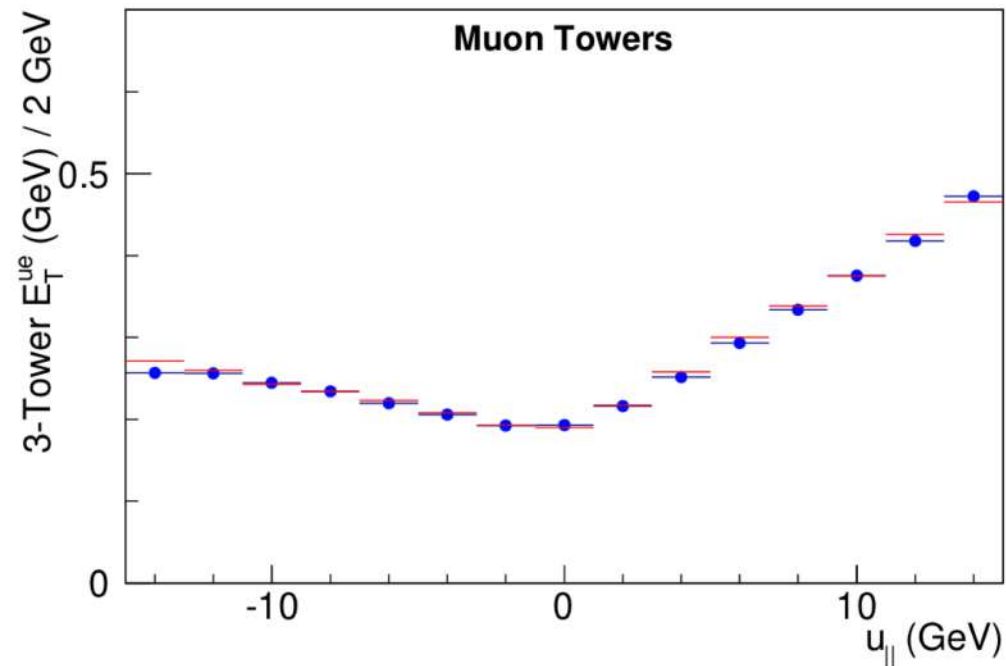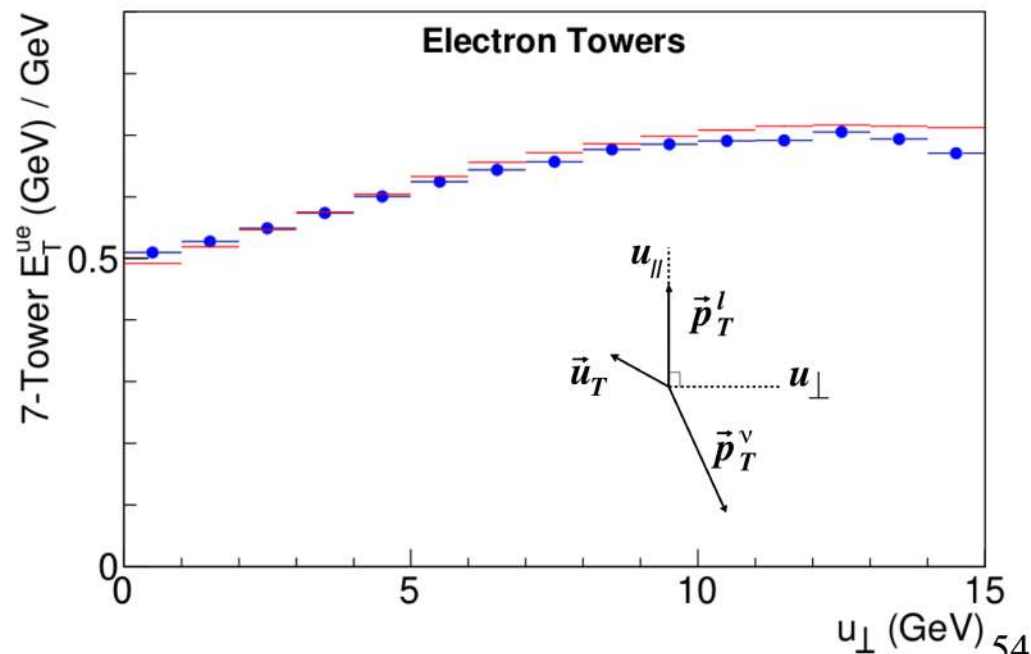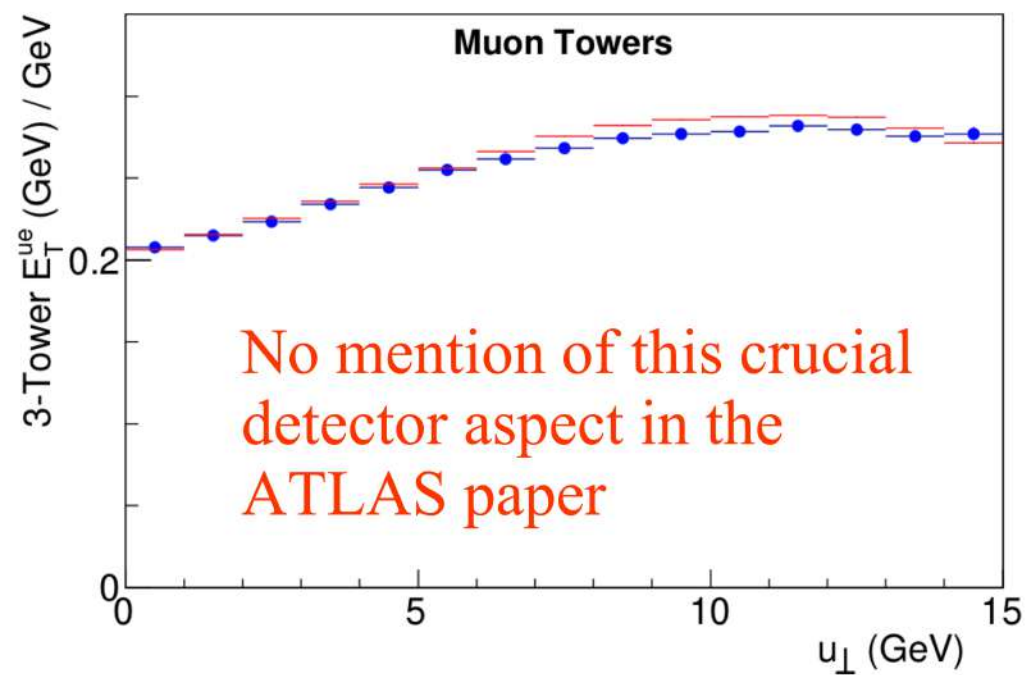
Recoil projection (GeV) on lepton direction
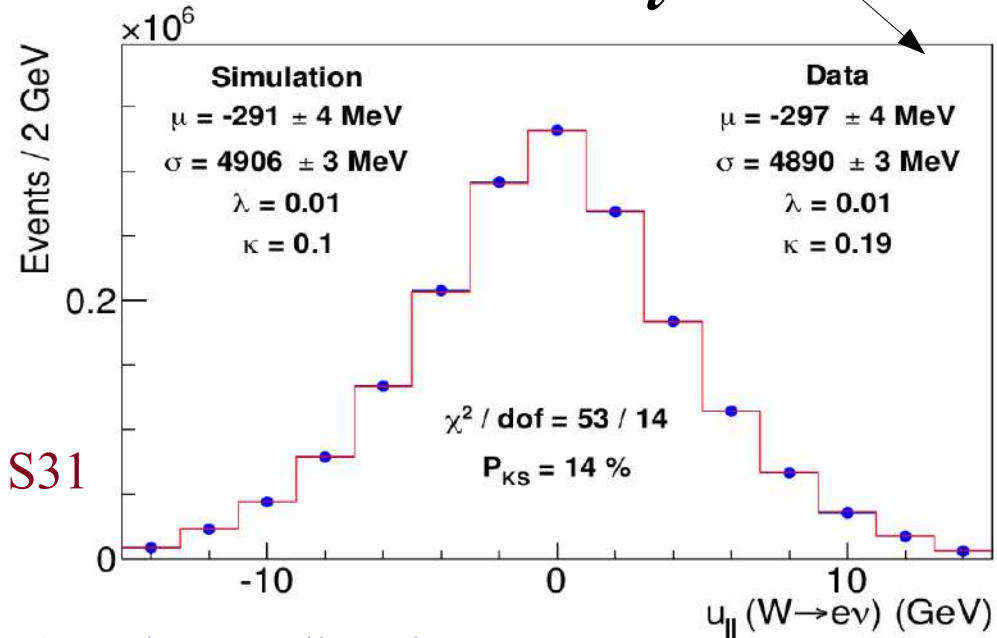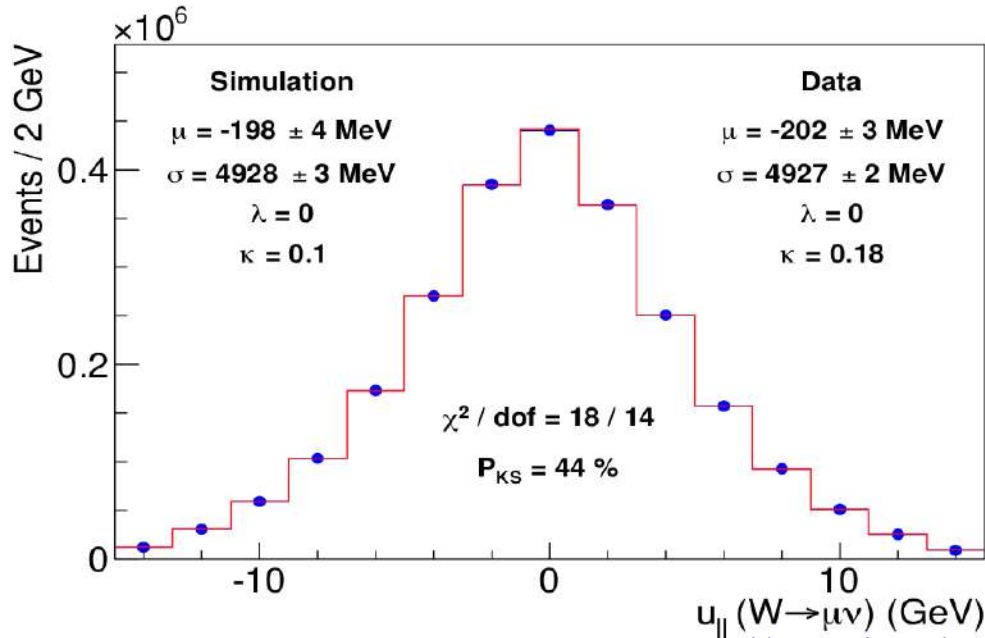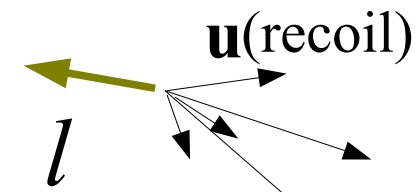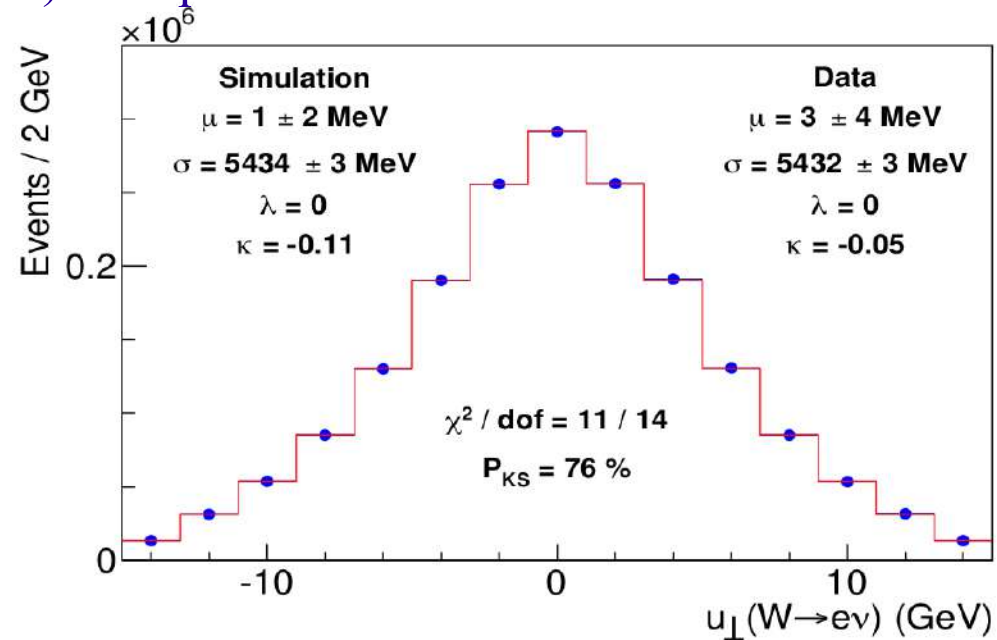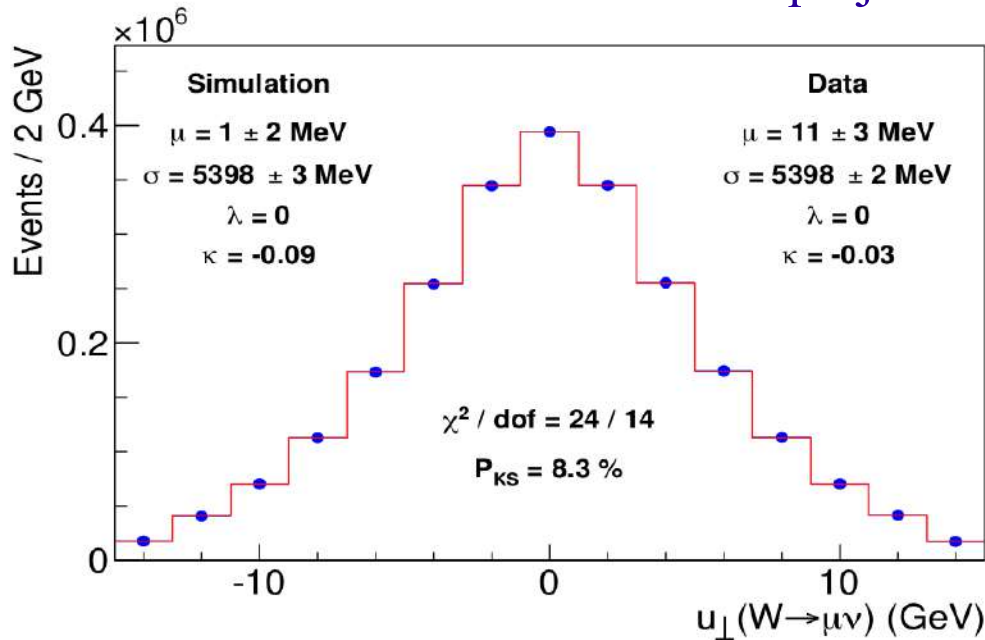
Fig. S31

Recoil projection (GeV) perpendicular to lepton

Testing Hadronic Recoil Model with *W* boson events

u(recoil)

l
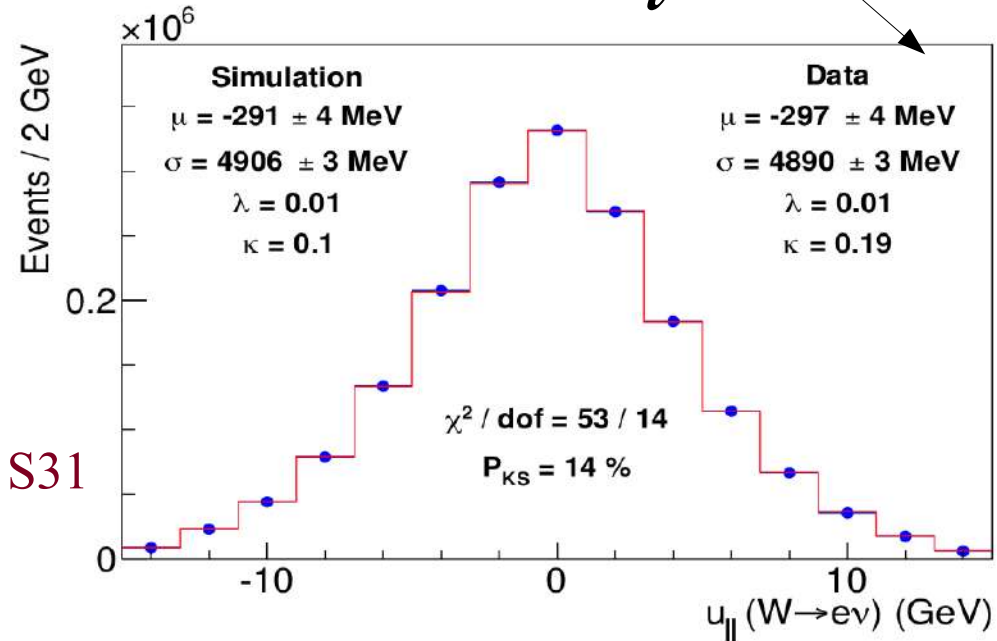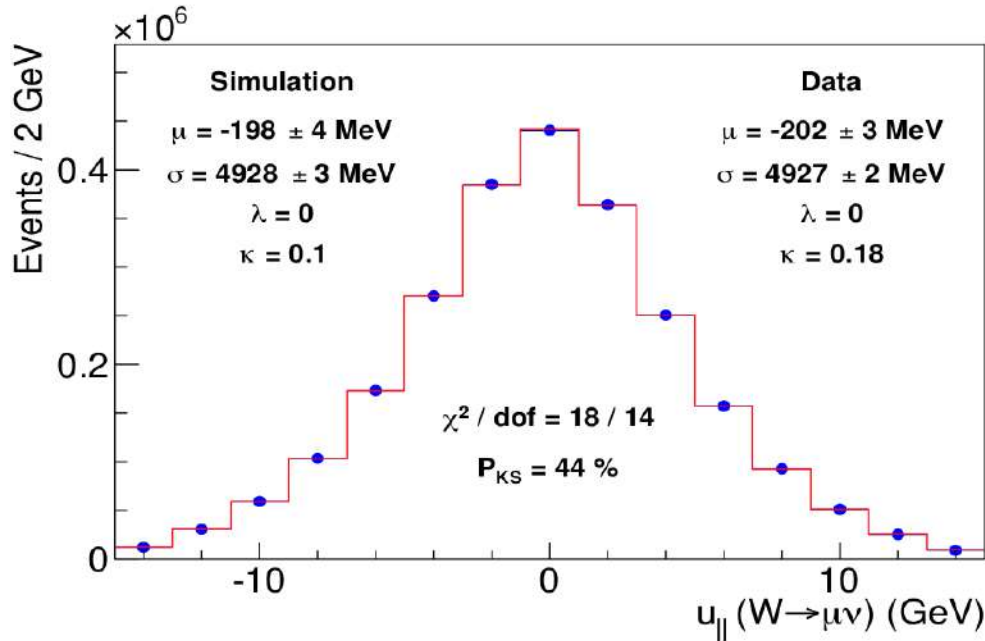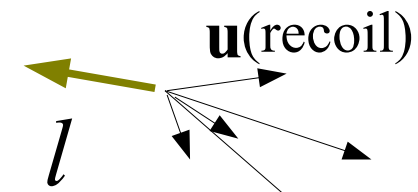
Fig. S31

Crucial cross-check plots not shown in ATLAS paper
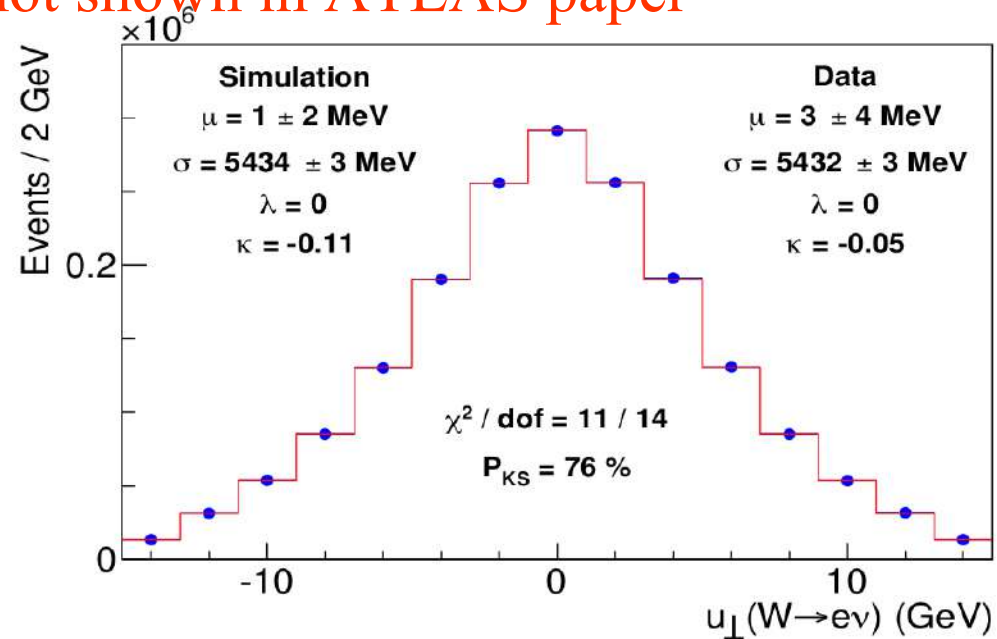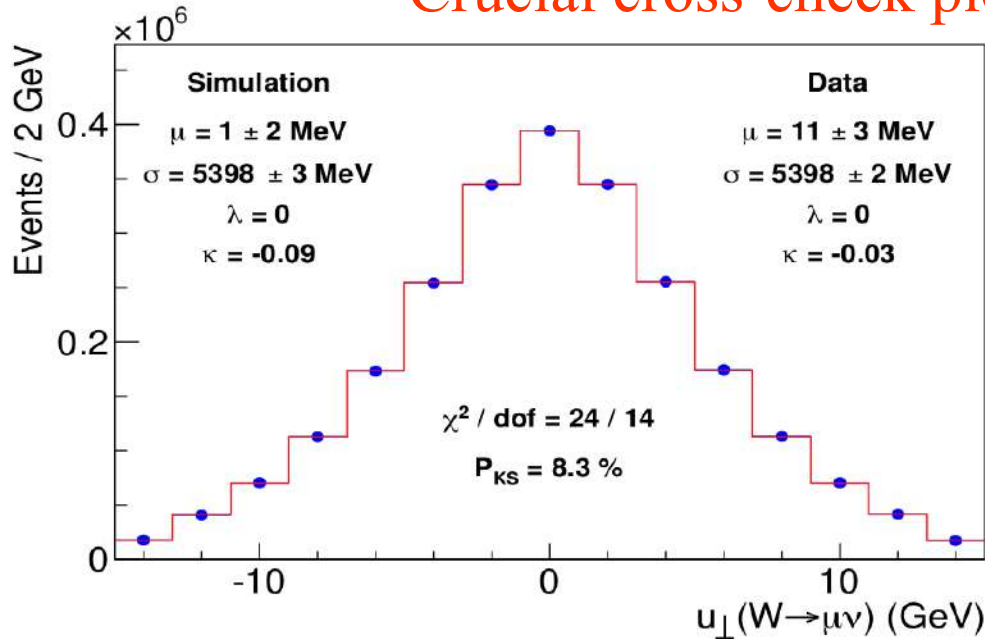
Recoil projection (GeV) perpendicular to lepton

Signal Simulation and Fitting

Parton Distribution Functions

- Affect W kinematic lineshapes through acceptance cuts

- In the rest frame, $p_T = m \sin \theta^* / 2$

- Longitudinal cuts on lepton in the lab frame sculpt the distribution of θ^*, hence biases the distribution of lepton p_T

  - Relationship between lab frame and rest frame depends on the boost of the W boson along the beam axis

- Parton distribution functions control the longitudinal boost

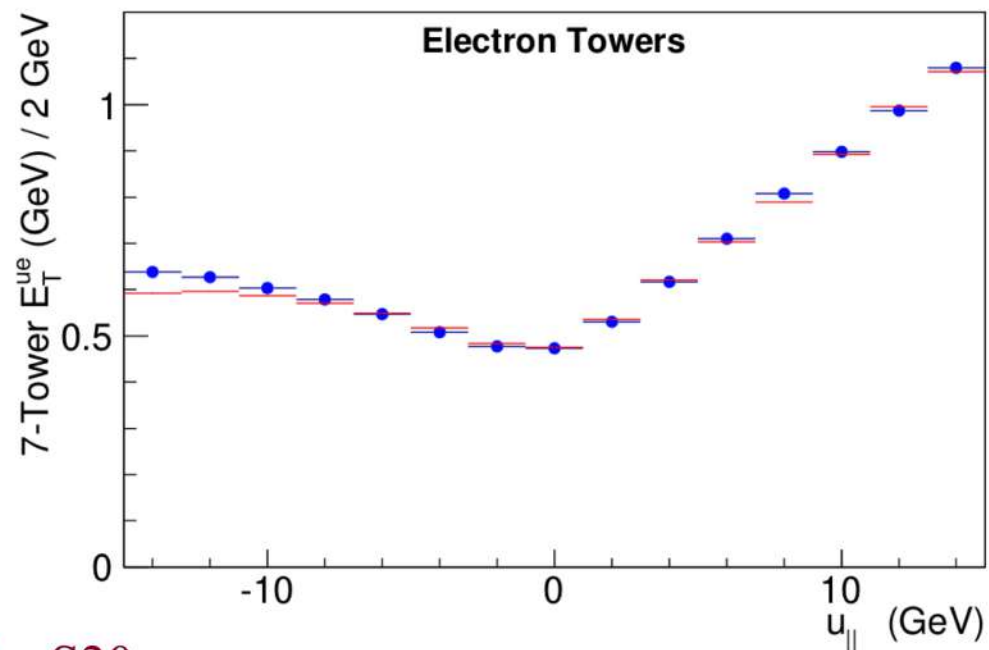- Uncertainty due to parton distribution functions evaluated by fitting pseudo-experiments (simulated samples with the same statistics and selection as data) with varied parton distribution functions

  - Current uncertainty 10 MeV

  - Largest source of systematic uncertainty

  - Expected to reduce with lepton and boson rapidity measurements at Tevatron and LHC

Generator-level Signal Simulation
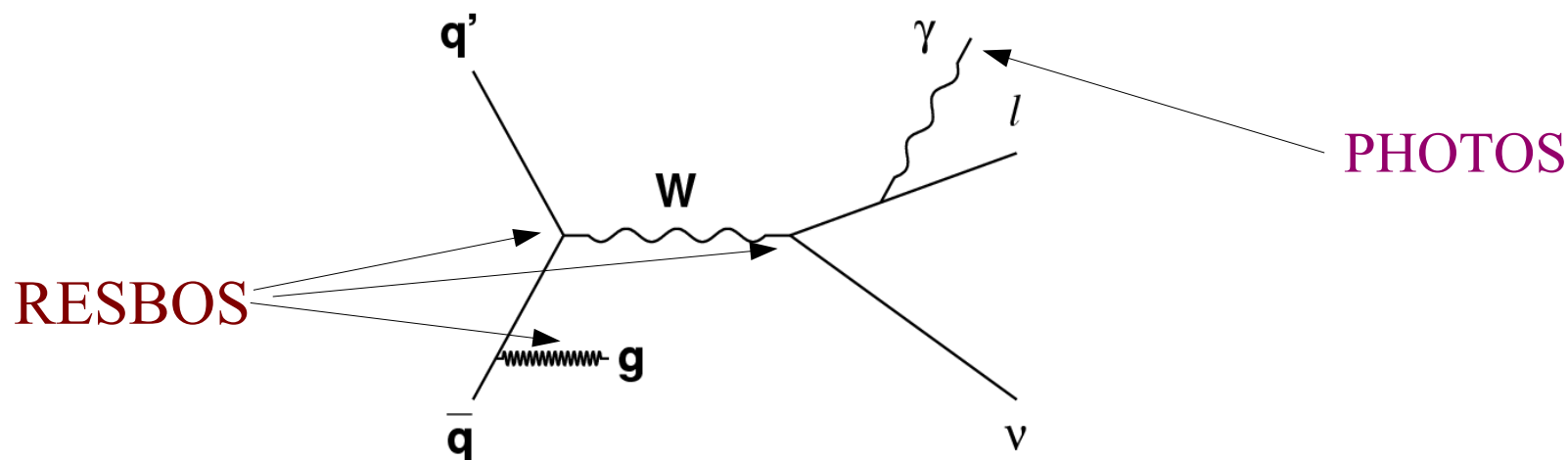
- Generator-level input for W & Z simulation provided by RESBOS
  (C. Balazs & C.-P. Yuan, PRD56, 5558 (1997) and references therein), which

    - Fully differential production and decay distributions

    - Benchmarked to RESBOS2 (J. Isaacson, Y. Fu & C.-P. Yuan, arXiv:2205.02788)

- Multiple radiative photons generated according to PHOTOS
  (P. Golonka and Z. Was, Eur. J. Phys. C 45, 97 (2006) and references therein)

    - Calibrated to HORACE (C.M. Carloni Calame, G. Montagna, O. Nicrosini
      and A. Vicini, JHEP 0710:109,2007)

Constraining Boson p_T Spectrum

- Fit the non-perturbative parameter g_2 and QCD coupling α_S in RESBOS to $p_T(ll)$ spectra:

$$\Delta M_W = 1.8 \text{ MeV}$$

Position of peak in boson p_T spectrum depends on g_2
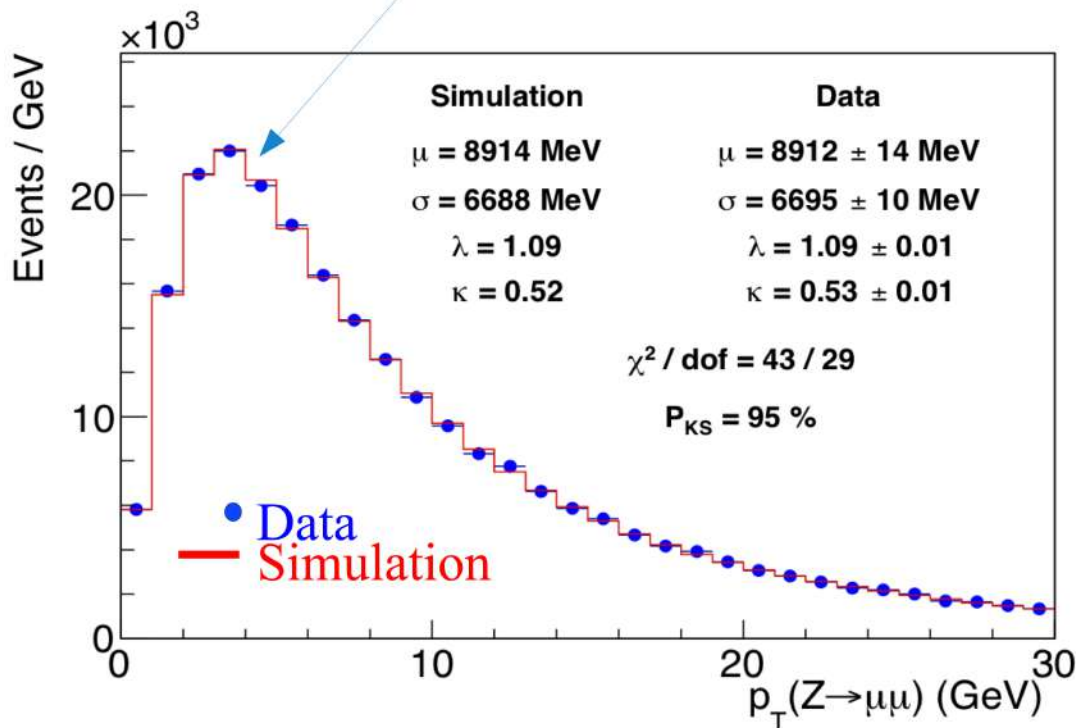
Tail to peak ratio depends on α_S

Simulation	Data
μ = 8914 MeV	μ = 8912 ± 14 MeV
σ = 6688 MeV	σ = 6695 ± 10 MeV
λ = 1.09	λ = 1.09 ± 0.01
κ = 0.52	κ = 0.53 ± 0.01

χ^2 / dof = 43 / 29

P_{KS} = 95 %

- Data
— Simulation

Simulation	Data
μ = 8940 MeV	μ = 8868 ± 26 MeV
σ = 6751 MeV	σ = 6715 ± 18 MeV
λ = 1.07	λ = 1.08 ± 0.01
κ = 0.46	κ = 0.51 ± 0.02

χ^2 / dof = 26 / 29

P_{KS} = 11 %

Fig. S2
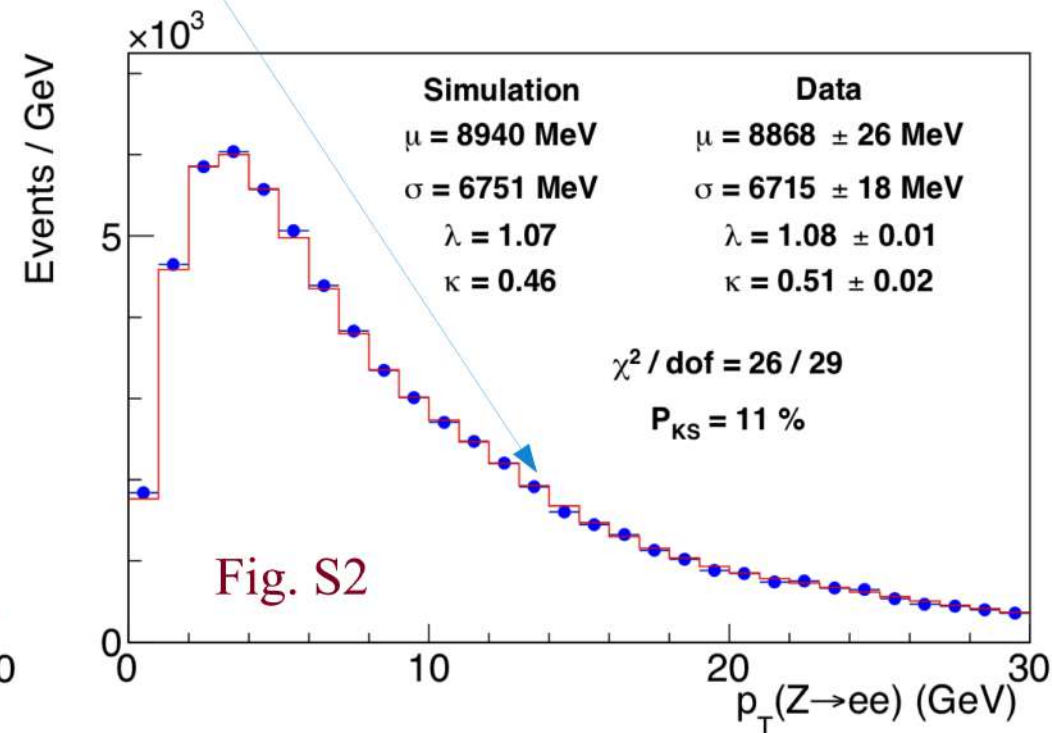
Additional Constraint on p$_T$(W) Model with *W* boson events

- NEW: In addition to the p$_T$(Z) data constrain on the boson p$_T$ spectrum, the ratio of the p$_T$(W) / p$_T$(Z) spectra is also constrained from the p$_T$(W) data

  - DyqT : triple-differential cross section calculation at NNLO-QCD used to model scale variation of ratio

  - p$_T$(W) data is used as constraint on ratio model

  - correlation with hadronic recoil model is taken into account

Fig. S32

p$_T$(W), muon channel

p$_T$(W), electron channel

• Data

— Simulation
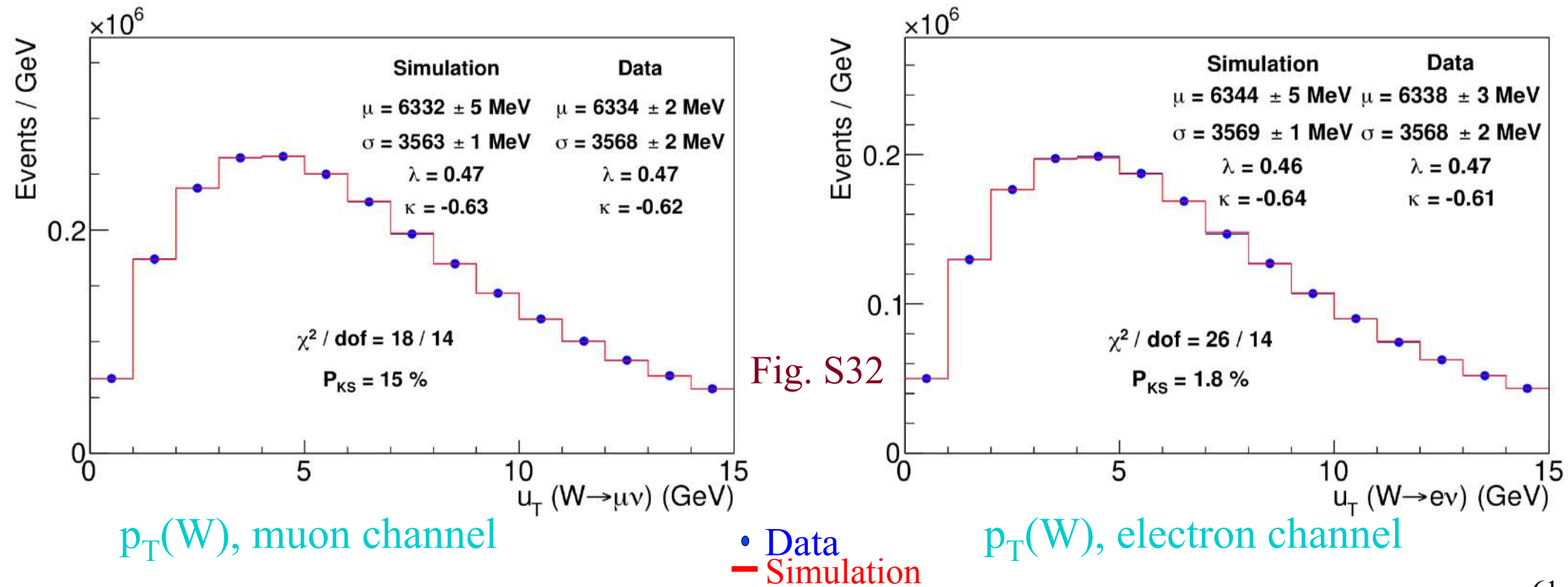
Compare & Contrast

Generator Usage and Tuning

- CDF uses RESBOS, corrected to RESBOS2

    - Small tuning on $p_T(Z)$ for non-perturbative parameter and α_S

    - No further tuning of $p_T(W)$ needed

    - DyqT used only to propagate constraint from data based on parameterized scale variation of $p_T(W)/p_T(Z)$

- ATLAS uses PYTHIA8

    - tuned on $p_T(Z)$

    - re-weighted rapidity distribution

    - No constraint on transference from $p_T(Z)$ to $p_T(W)$

    - Even though LHC measurement is more susceptible to QCD effects

    - $p_T(W) < 30$ GeV @LHC while $p_T(W) < 15$ GeV @ CDF

W Mass Fits

W Transverse Mass Fits

$\chi^2/\text{dof} = 50 / 48$

$P_{\chi^2} = 37\ \%$

$P_{KS} = 98\ \%$

muons

$\chi^2/\text{dof} = 39 / 48$

$P_{\chi^2} = 79\ \%$

$P_{KS} = 76\ \%$

electrons

Fig. 4

$W \to \mu\nu$

$W \to e\nu$
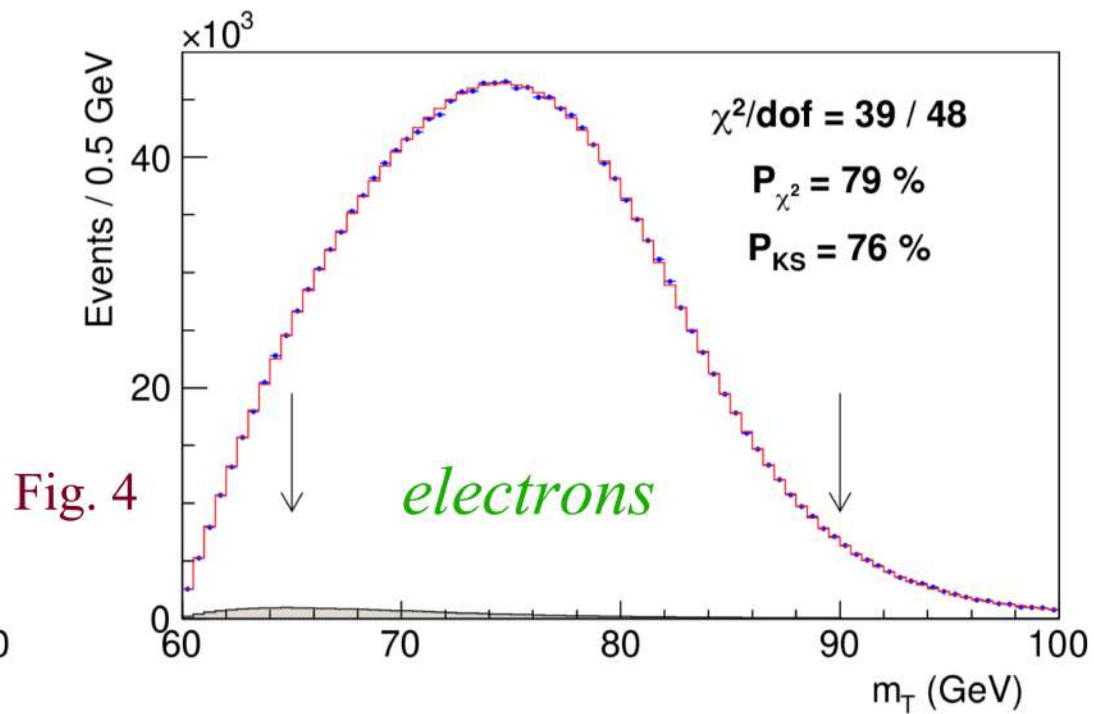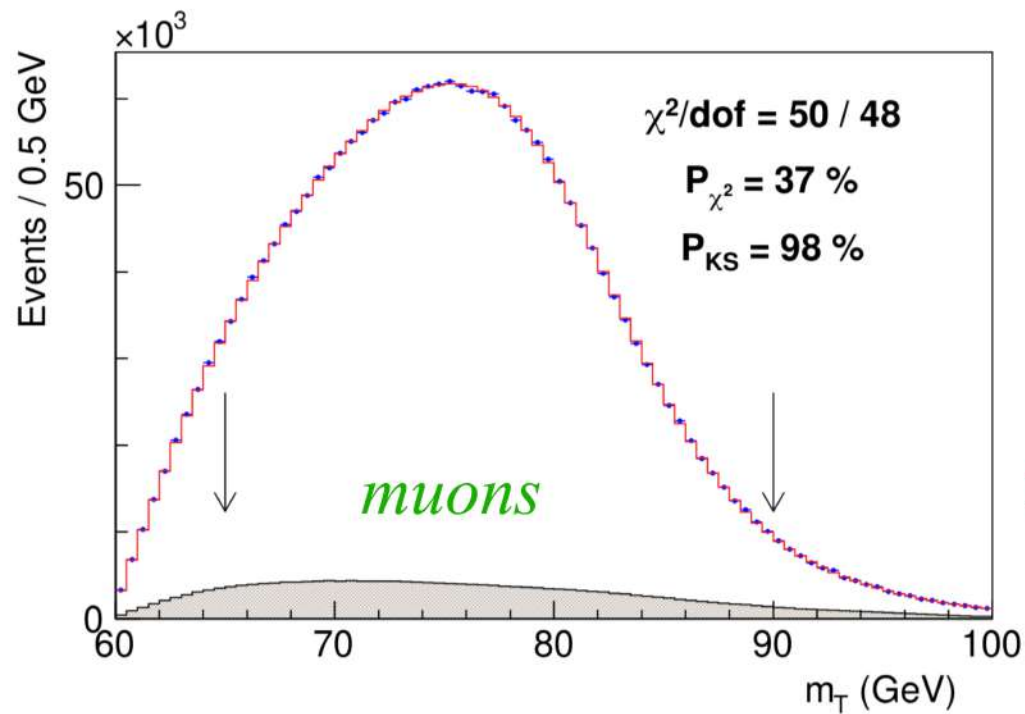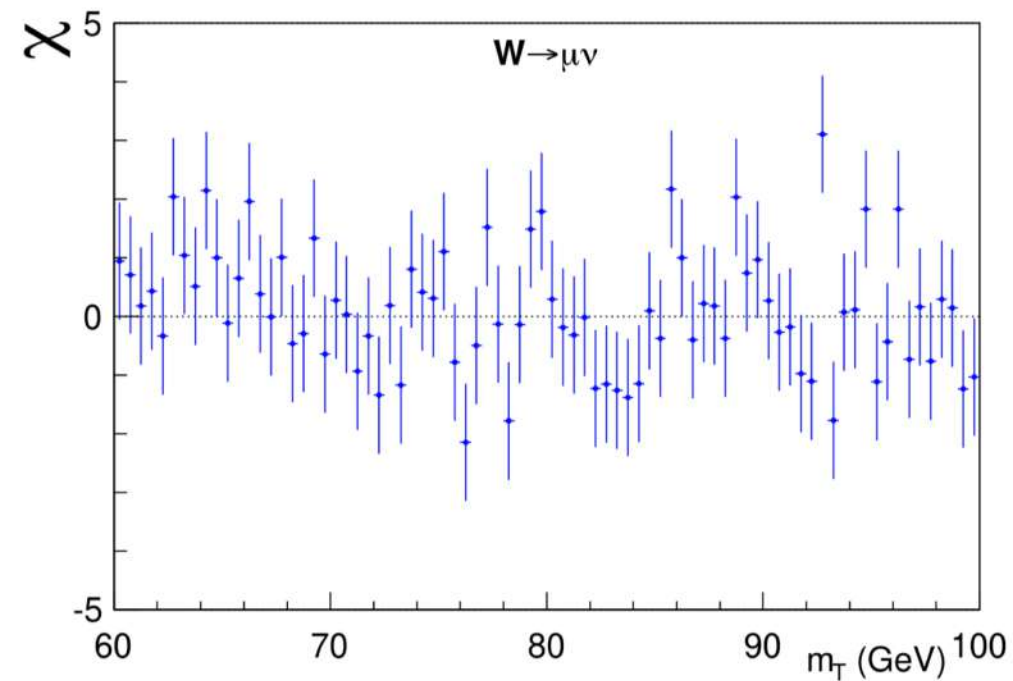
Fig. 36
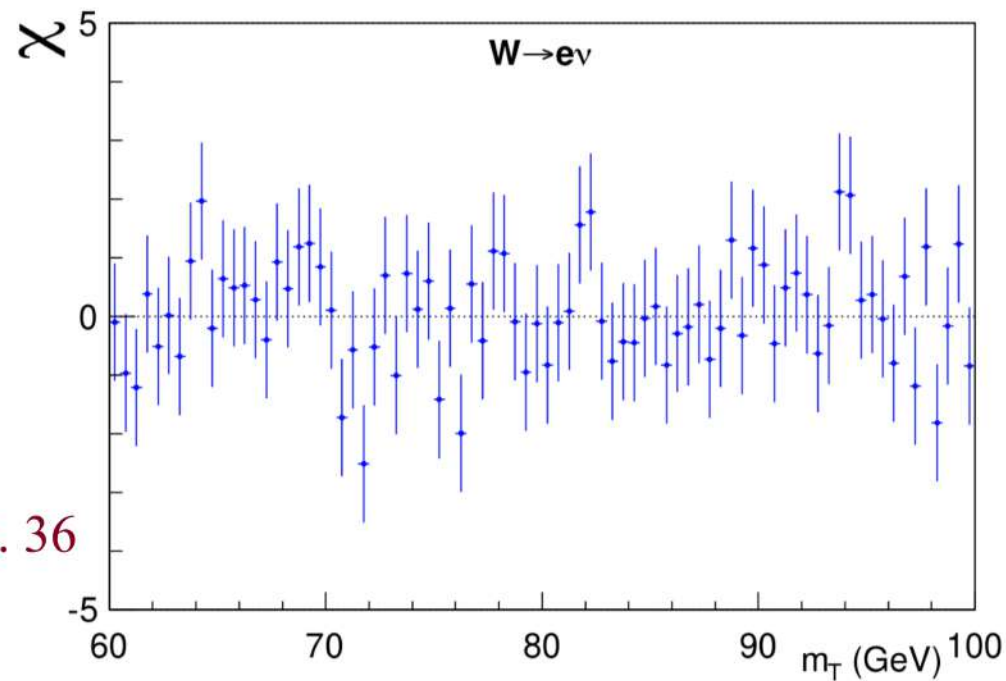
W Charged Lepton p$_T$ Fits
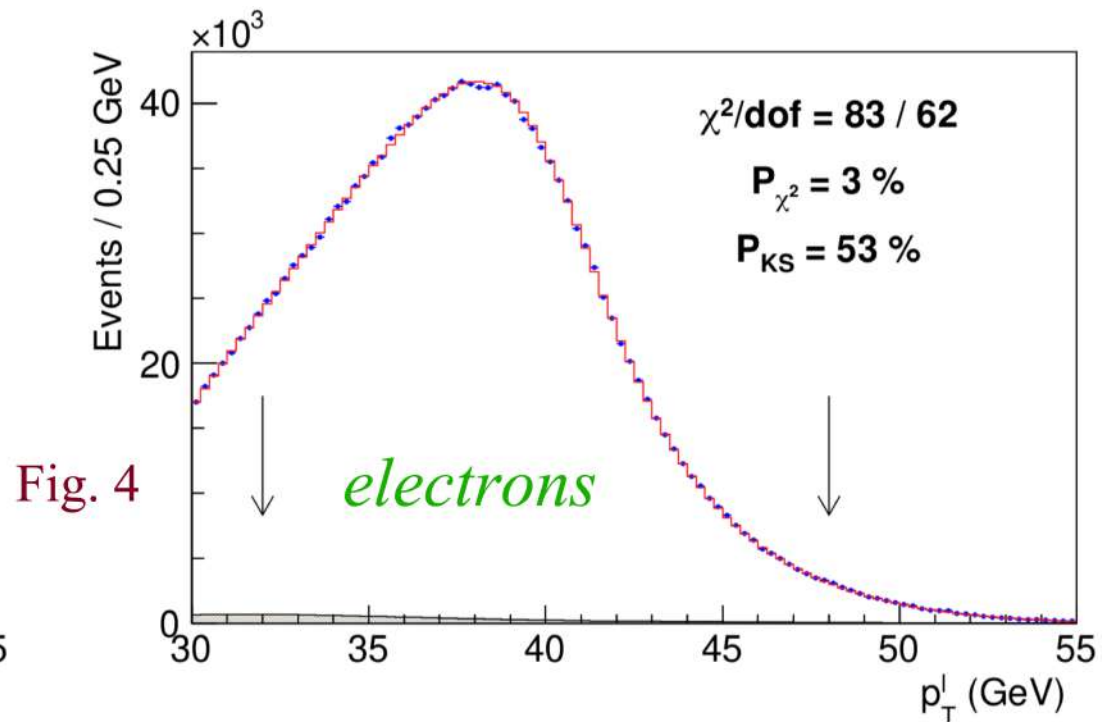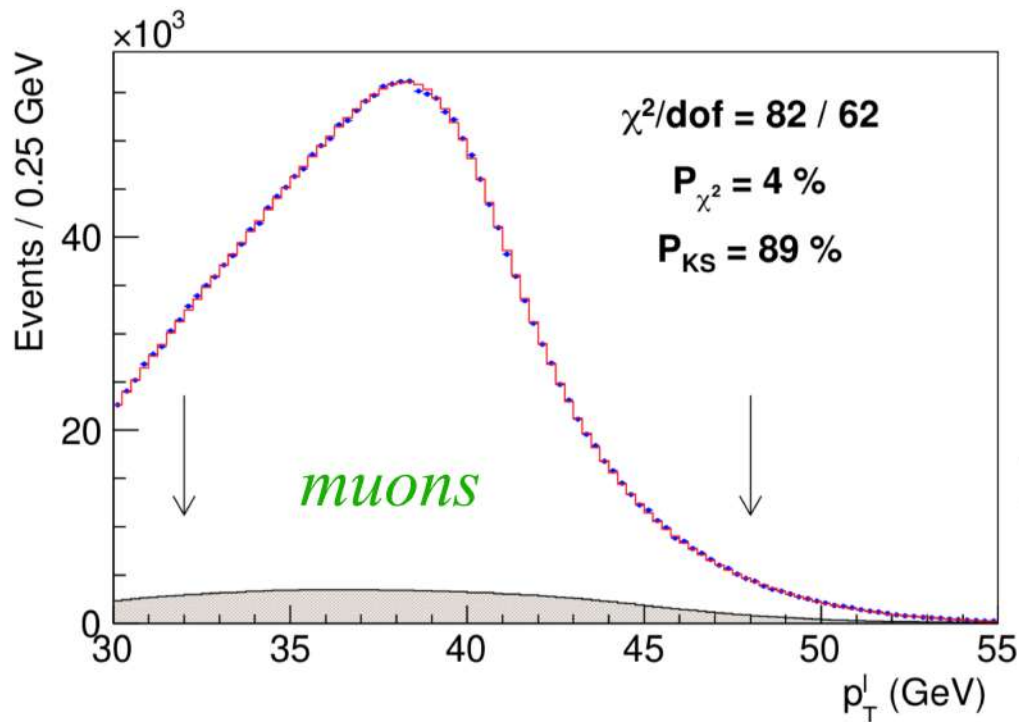
Fig. 4
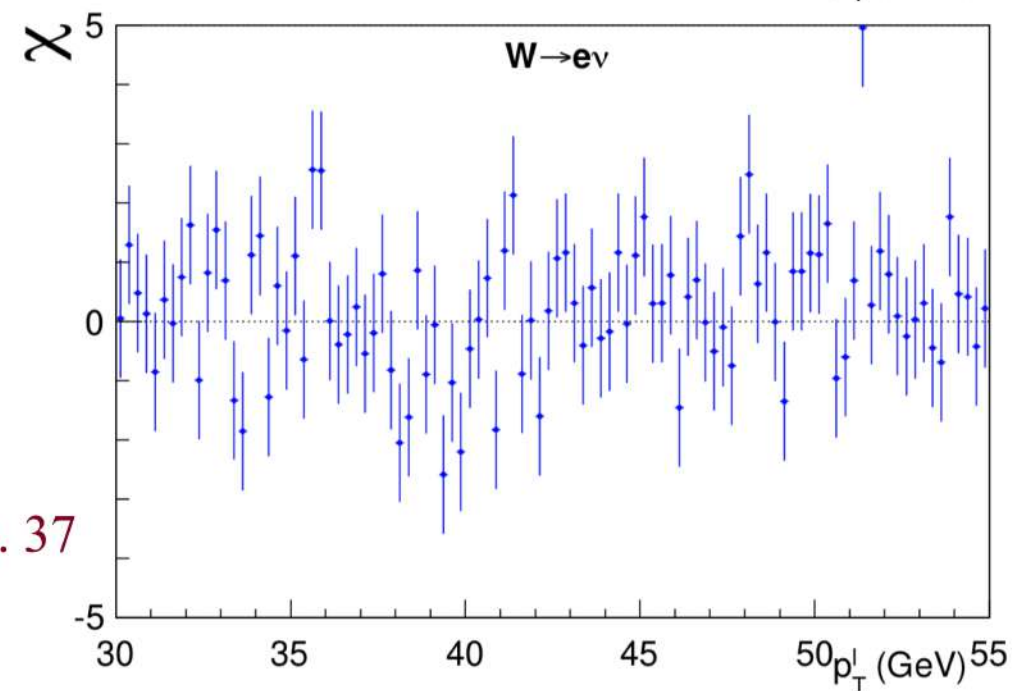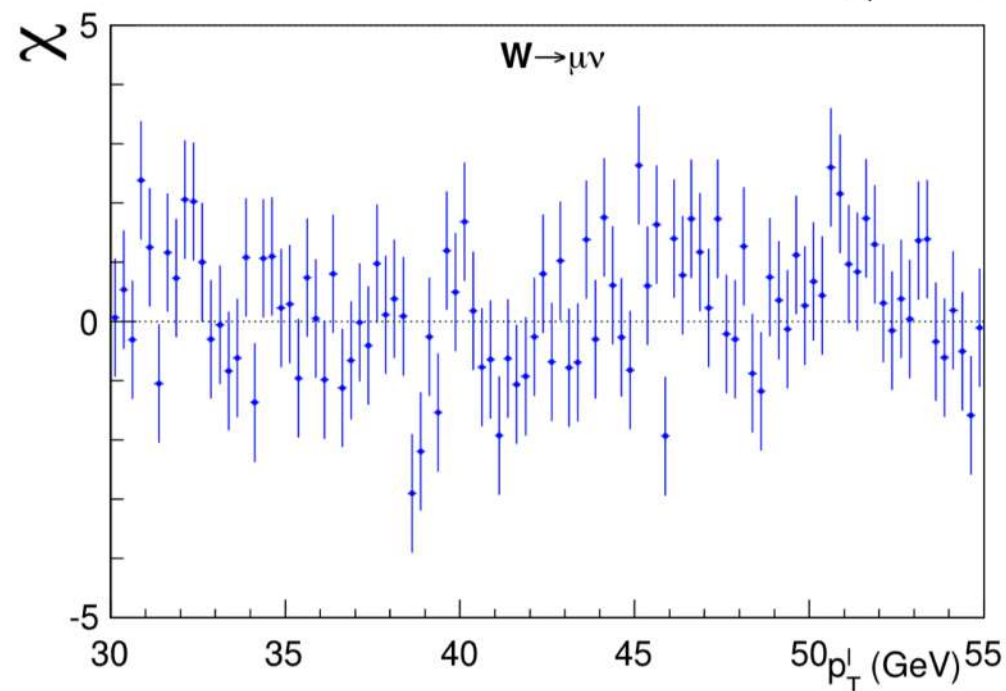
Fig. 37

W Neutrino p$_T$ Fits
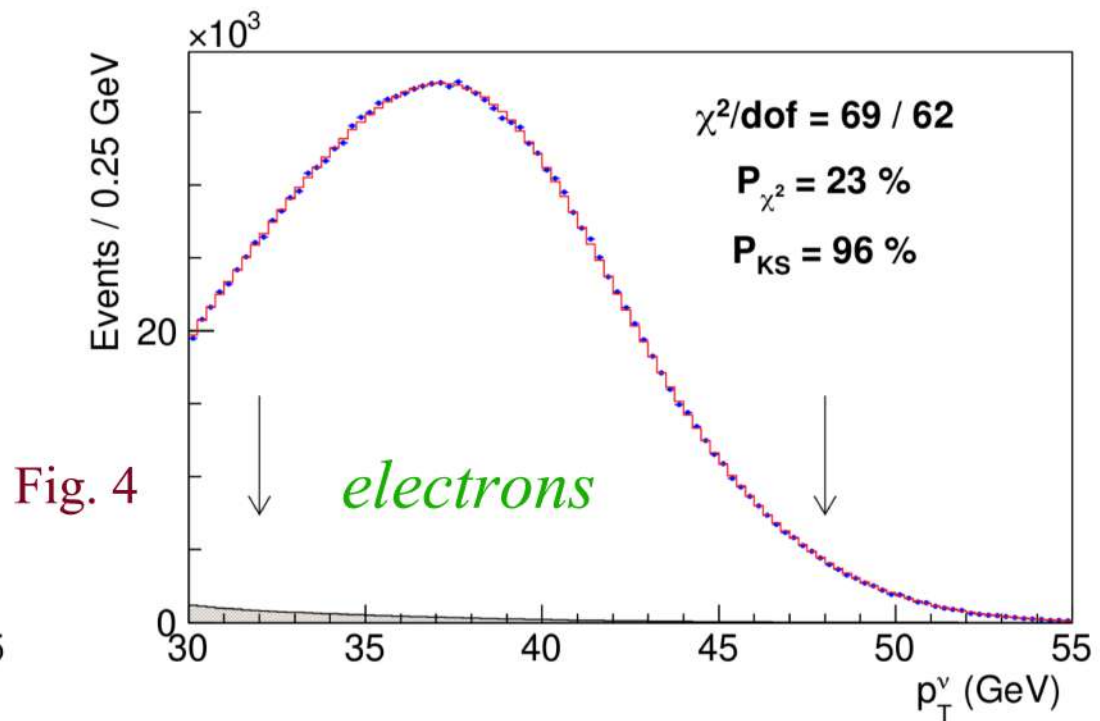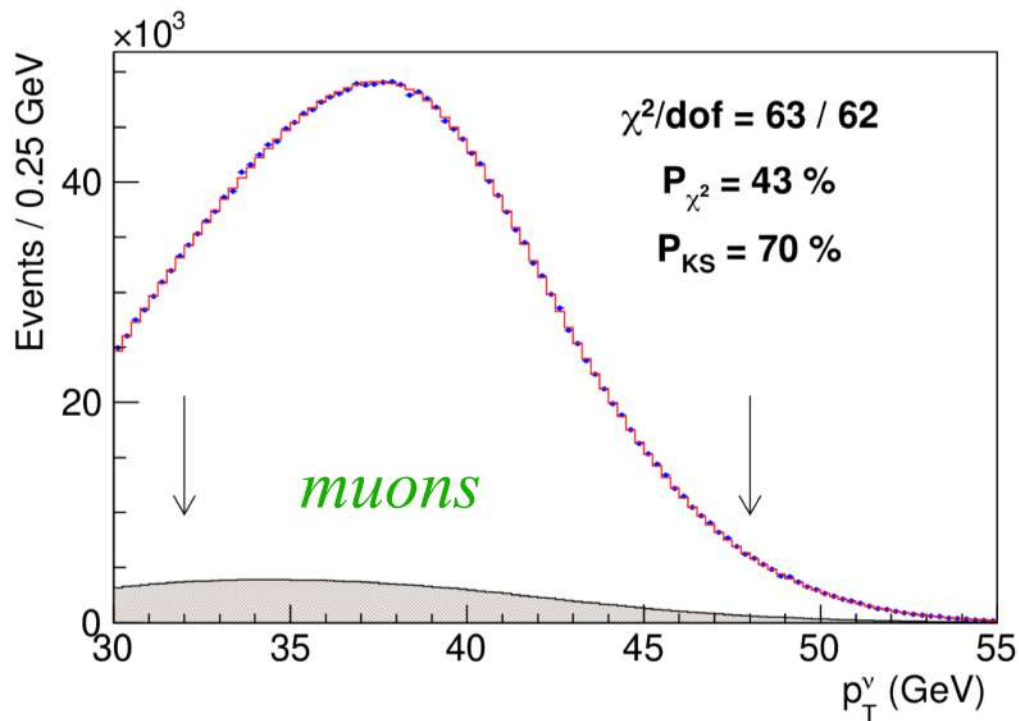
Fig. 4
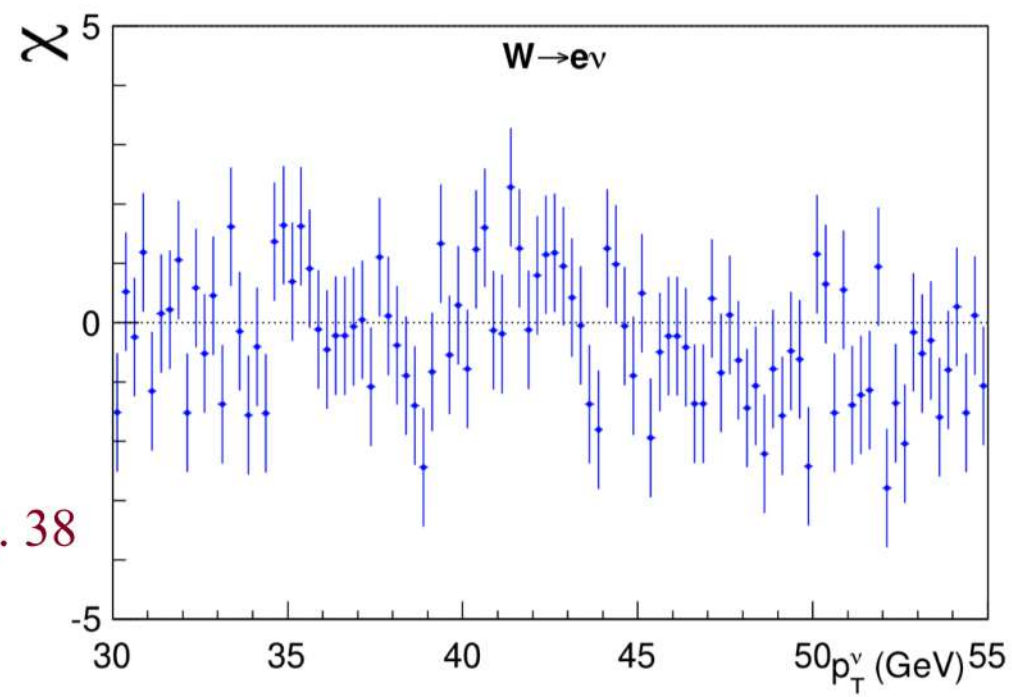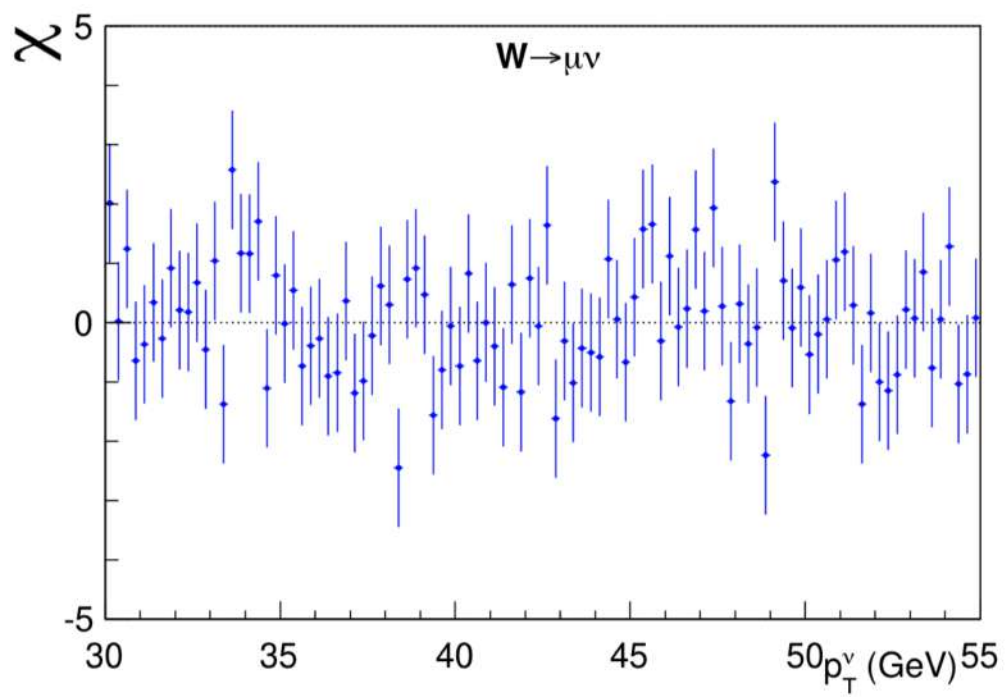
Fig. 38

Summary of *W* Mass Fits

Distribution	W-boson mass (MeV)	χ^2/dof
$m_T(e, \nu)$	$80\ 429.1 \pm 10.3_{\mathrm{stat}} \pm 8.5_{\mathrm{syst}}$	$39/48$
$p_T^{\ell}(e)$	$80\ 411.4 \pm 10.7_{\mathrm{stat}} \pm 11.8_{\mathrm{syst}}$	$83/62$
$p_T^{\nu}(e)$	$80\ 426.3 \pm 14.5_{\mathrm{stat}} \pm 11.7_{\mathrm{syst}}$	$69/62$
$m_T(\mu, \nu)$	$80\ 446.1 \pm 9.2_{\mathrm{stat}} \pm 7.3_{\mathrm{syst}}$	$50/48$
$p_T^{\ell}(\mu)$	$80\ 428.2 \pm 9.6_{\mathrm{stat}} \pm 10.3_{\mathrm{syst}}$	$82/62$
$p_T^{\nu}(\mu)$	$80\ 428.9 \pm 13.1_{\mathrm{stat}} \pm 10.9_{\mathrm{syst}}$	$63/62$
combination	$80\ 433.5 \pm 6.4_{\mathrm{stat}} \pm 6.9_{\mathrm{syst}}$	$7.4/5$

Table 1

Consistency between two channels and three kinematic fits

My Thoughts on Action Items

- CDF: Provide additional evidence of CDF tracker response

    - Check RESBOS and DyqT against another modern generator

    - Use pseudo-data to compare CDF's "causal" analysis procedures and ATLAS' simultaneous multi-parameter fitting procedures

- ATLAS: Discuss with ATLAS colleagues regarding independent constraints on nuisance parameters

    - Increase the explainability of analysis procedures

    - Understand how PDF uncertainty reduces from 28 MeV (pre-fit) to 6 MeV (post-fit)

    - Understand the transference from $p_T(Z)$ to $p_T(W)$ and associated uncertainty (could be 30 MeV)

    - Understand stability of multi-parameter fitting and Fisher information (eg. why re-analysis of 2018 publication caused 16 MeV shift)

Combinations of Fit Results

Combination	m_T fit Electrons	m_T fit Muons	p_T^ℓ fit Electrons	p_T^ℓ fit Muons	p_T^ν fit Electrons	p_T^ν fit Muons	Value (MeV)	χ^2/dof	Probability (%)
m_T	✓	✓					80 439.0 ± 9.8	1.2 / 1	28
p_T^ℓ			✓	✓			80 421.2 ± 11.9	0.9 / 1	36
p_T^ν					✓	✓	80 427.7 ± 13.8	0.0 / 1	91
m_T & p_T^ℓ	✓	✓	✓	✓			80 435.4 ± 9.5	4.8 / 3	19
m_T & p_T^ν	✓	✓			✓	✓	80 437.9 ± 9.7	2.2 / 3	53
p_T^ℓ & p_T^ν			✓	✓	✓	✓	80 424.1 ± 10.1	1.1 / 3	78
Electrons	✓		✓		✓		80 424.6 ± 13.2	3.3 / 2	19
Muons		✓		✓		✓	80 437.9 ± 11.0	3.6 / 2	17
All	✓	✓	✓	✓	✓	✓	80 433.5 ± 9.4	7.4 / 5	20

Table S9

- Combined electrons (3 fits): M_W = 80424.6 ± 13.2 MeV, $P(\chi^2)$ = 19%

- Combined muons (3 fits): M_W = 80437.9 ± 11.0 MeV, $P(\chi^2)$ = 17%

- All combined (6 fits): M_W = 80433.5 ± 9.4 MeV, $P(\chi^2)$ = 20%

Compare & Contrast

M_W Fit Consistency

- CDF: transverse mass, charged-lepton p_T and neutrino p_T fits contribute 64%, 26% and 10% weight respectively to final answer

    - Provide powerful cross-check on hadronic recoil modeling

- ATLAS: charged-lepton p_T fit contributes 95% weight to final answer

    - No cross-check on hadronic recoil modeling

Fitting Methodology

- CDF: constrains all nuisance parameters on independent control samples

  - Only M_W floated when fitting m_T and lepton p_T distributions

  - Robust and interpretable fitting method

- ATLAS: In addition to M_W, 1000 nuisance parameters (pruned to 200) also floated when fitting m_T and lepton p_T distributions

  - Interpretation of post-fit M_W and uncertainties is opaque

    - Loss of causal interpretation of nuisance parameters if reduced to "smoothing knobs"

  - Pre-fit uncertainties due to nuisance parameters not quoted

  - Is M_W getting tuned to eliminate all internal inconsistencies?

  - Possibility of "random walk" of M_W by $\sqrt{200}\,\delta$

W Boson Mass Measurements from Different Experiments
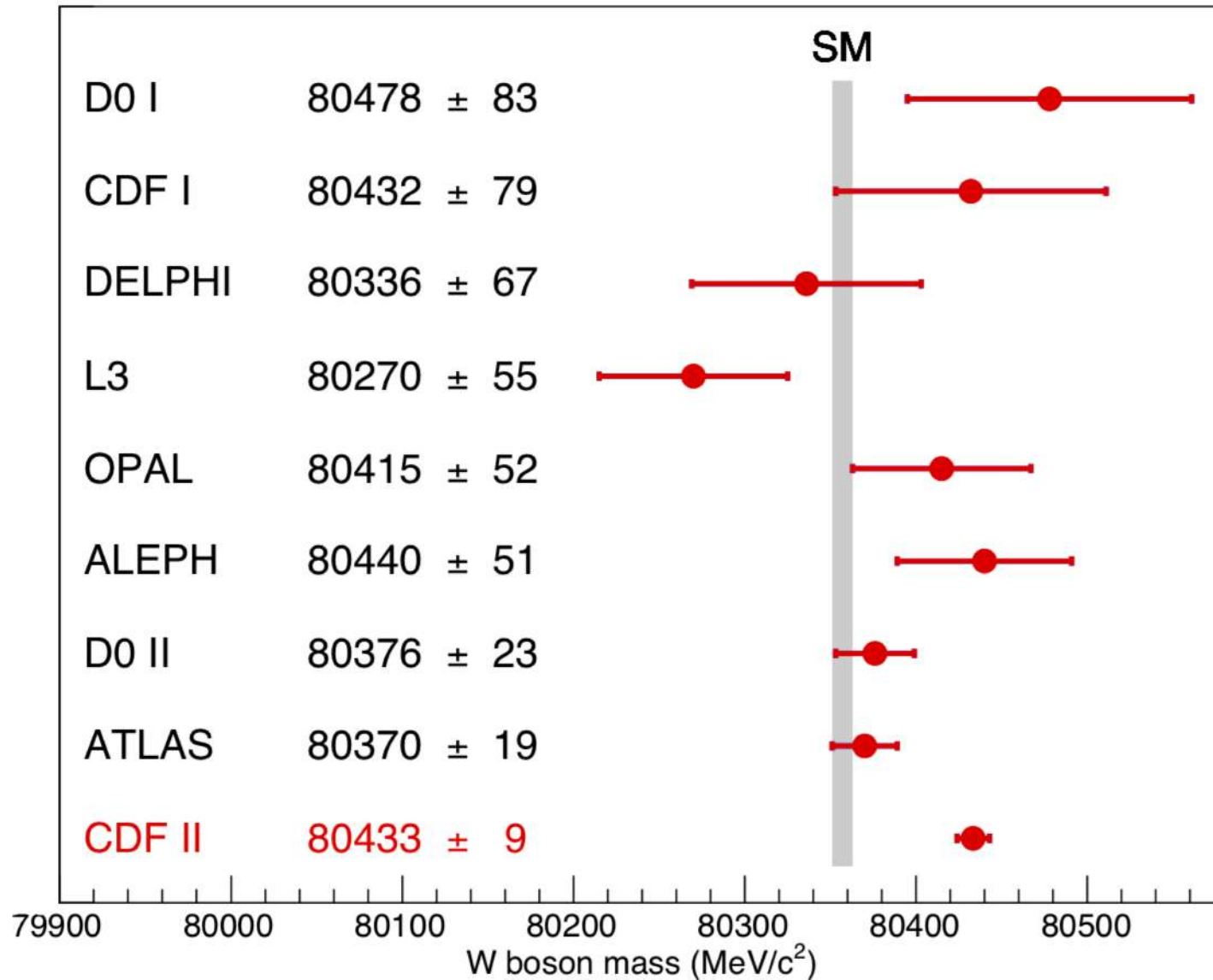
Fig. 5

SM expectation: $M_W = 80,357 \pm 4_{inputs} \pm 4_{theory}$ (PDG 2020)

LHCb measurement : $M_W = 80,354 \pm 23_{stat} \pm 10_{exp} \pm 17_{theory} \pm 9_{PDF}$ *[JHEP **2022**, 36 (2022)]*

My Thoughts on Action Items

- CDF: Provide additional evidence of CDF tracker response

  - Check RESBOS and DyqT against another modern generator
  - Use pseudo-data to compare CDF's "causal" analysis procedures and ATLAS' simultaneous multi-parameter fitting procedures

- ATLAS: Discuss with ATLAS colleagues regarding independent constraints on nuisance parameters

  - Increase the explainability of analysis procedures
  - Understand how PDF uncertainty reduces from 28 MeV (pre-fit) to 6 MeV (post-fit)
  - Understand the transference from $p_T(Z)$ to $p_T(W)$ and associated uncertainty (could be 30 MeV)
  - Understand stability of multi-parameter fitting and Fisher information (eg. why re-analysis of 2018 publication caused 16 MeV shift)

Summary

- The *W* boson mass is a very interesting parameter to measure with increasing precision

- New CDF result is twice as precise as previous measurements:

  - $M_W = 80433.5 \pm 6.4_{stat} \pm 6.9_{syst}$ MeV
    $= 80433.5 \pm 9.4$ MeV

- Difference from SM expectation of $M_W = 80,357 \pm 6$ MeV

  - significance of 7.0σ

  - suggests the possibility of improvements to the SM calculation or of extensions to the SM

Thank you for your attention !

Backup slides

M$_W$ *Status in 2003*

Standard Model Indirect Prediction

UA2 (1992)	M$_W$ = 80.36 ± 0.37
D0	M$_W$ = 80.483 ± 0.084
CDF	M$_W$ = 80.433 ± 0.079
Hadron Collider Avg	M$_W$ = 80.454 ± 0.059
preliminary LEP2 Avg	M$_W$ = 80.447 ± 0.042
preliminary World Avg	M$_W$ = 80.450 ± 0.034

M$_W$ (GeV)
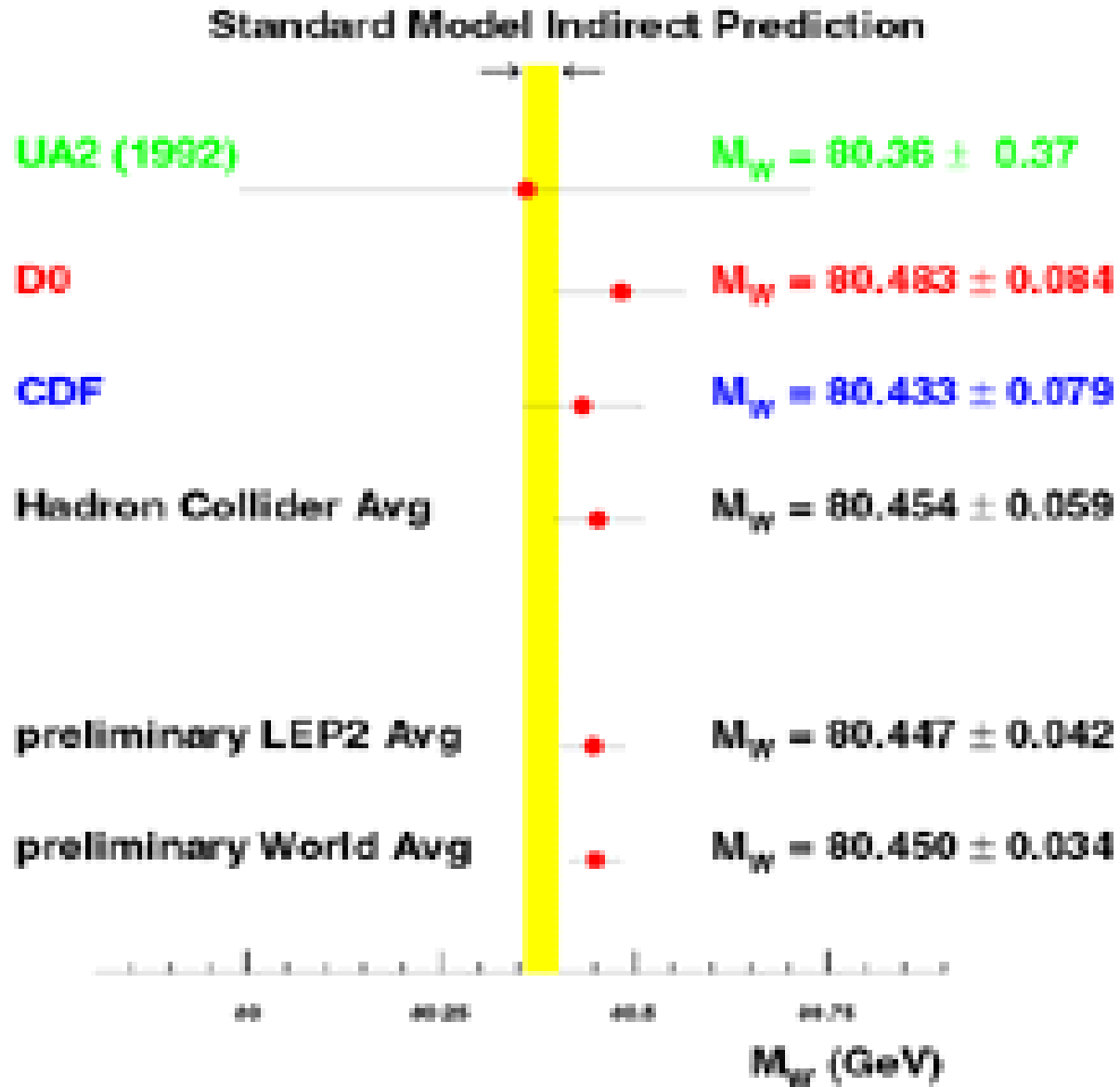
MW has historically been high relative to SM prediction

CDF M_W vs m_{top}
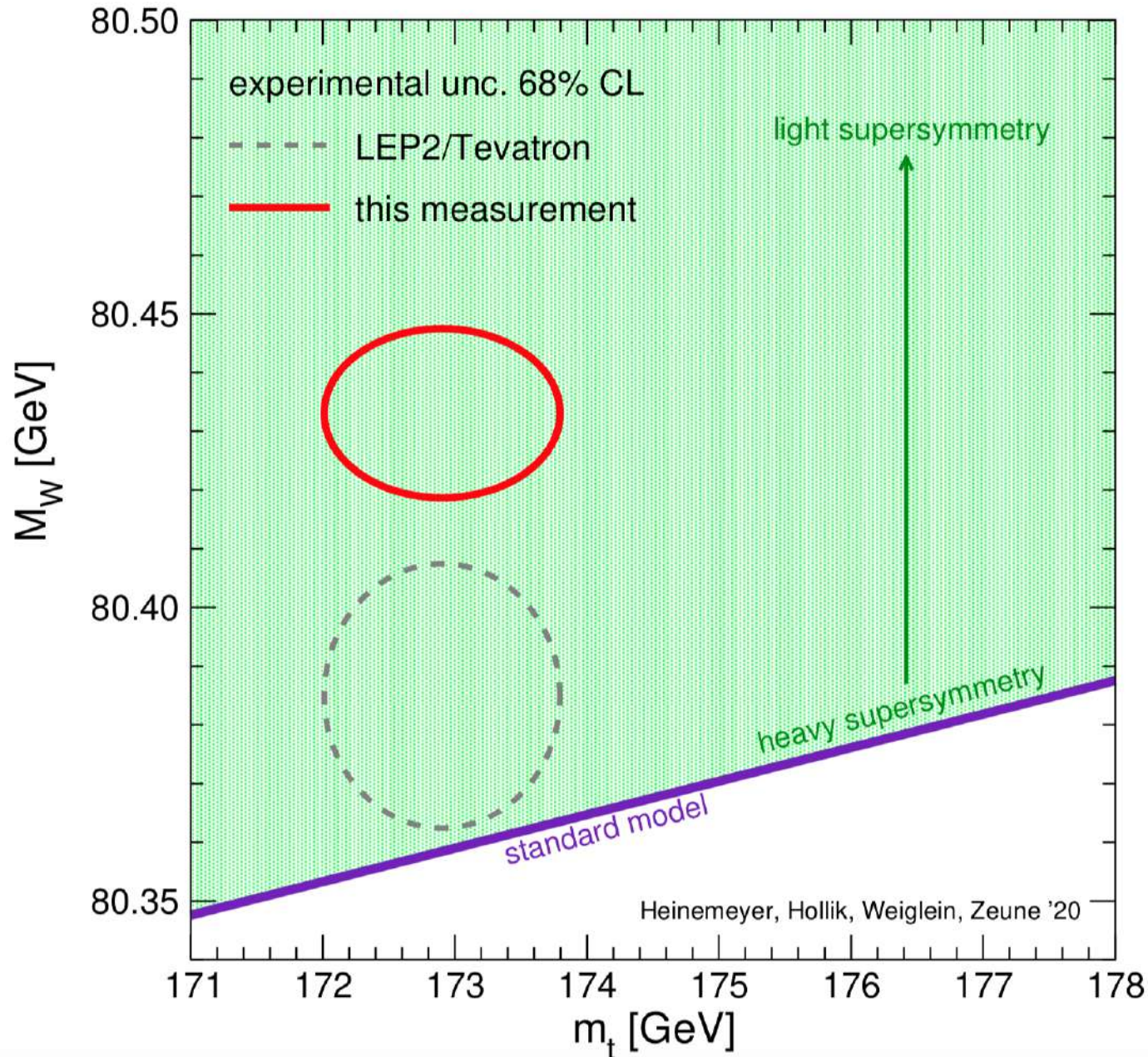
Fig. 1

Understanding Tevatron-LHC correlations and combination with ATLAS in progress

W Mass Fit Window Variation, m$_T$ Fit
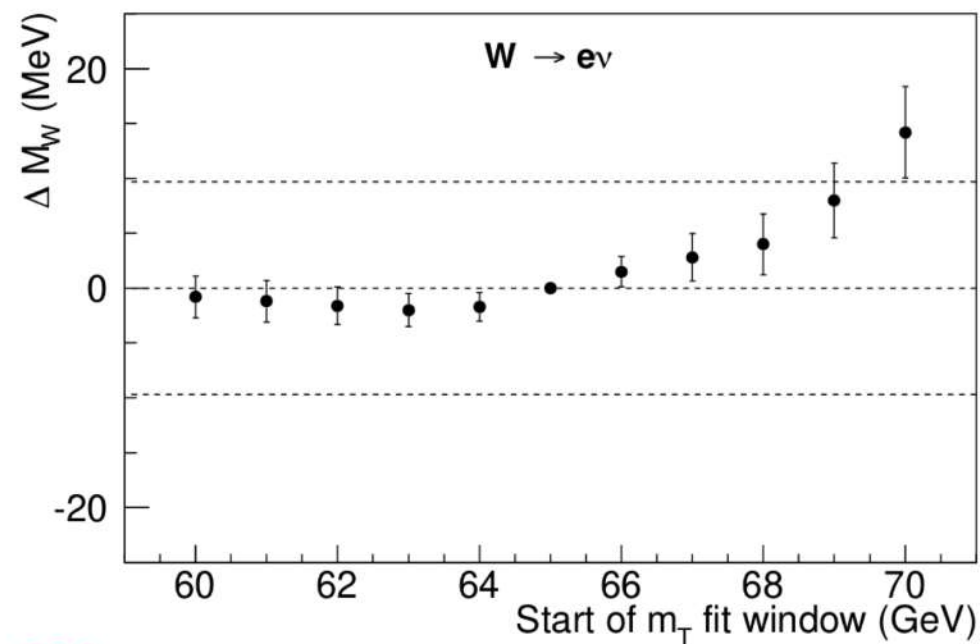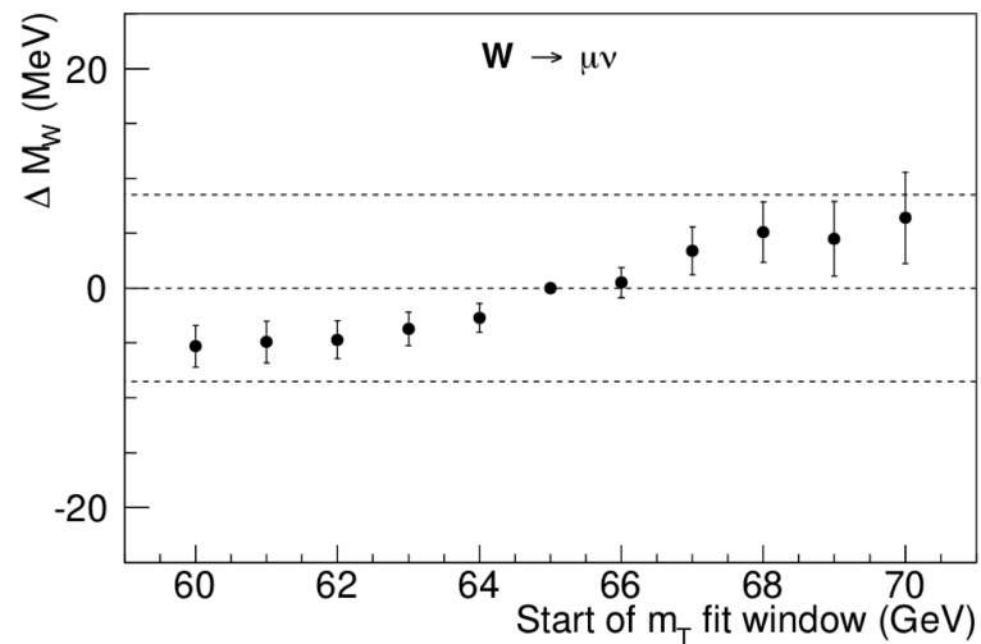
Fig. S39
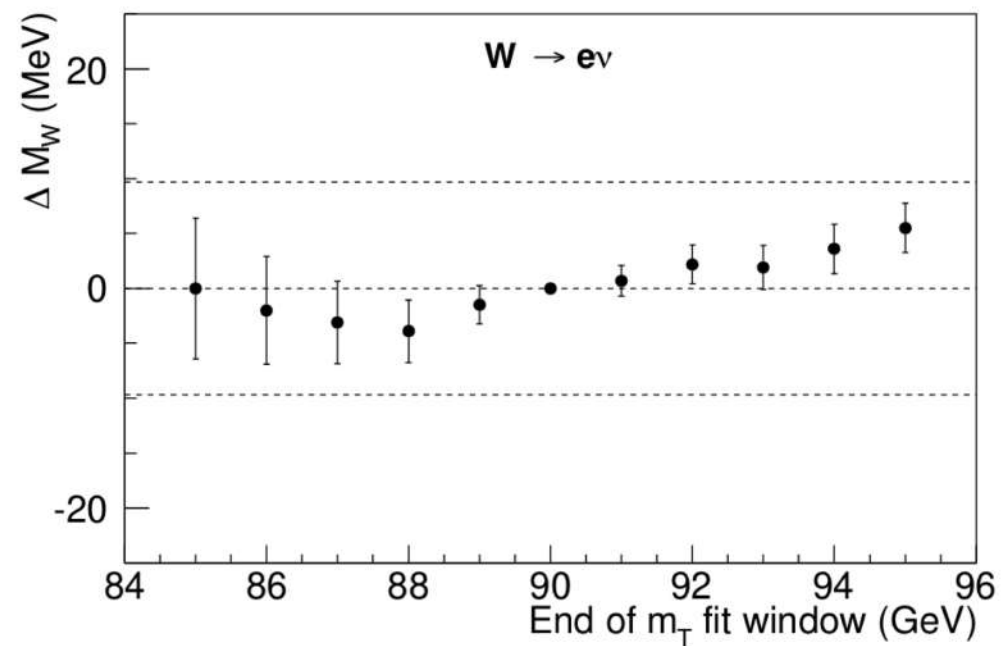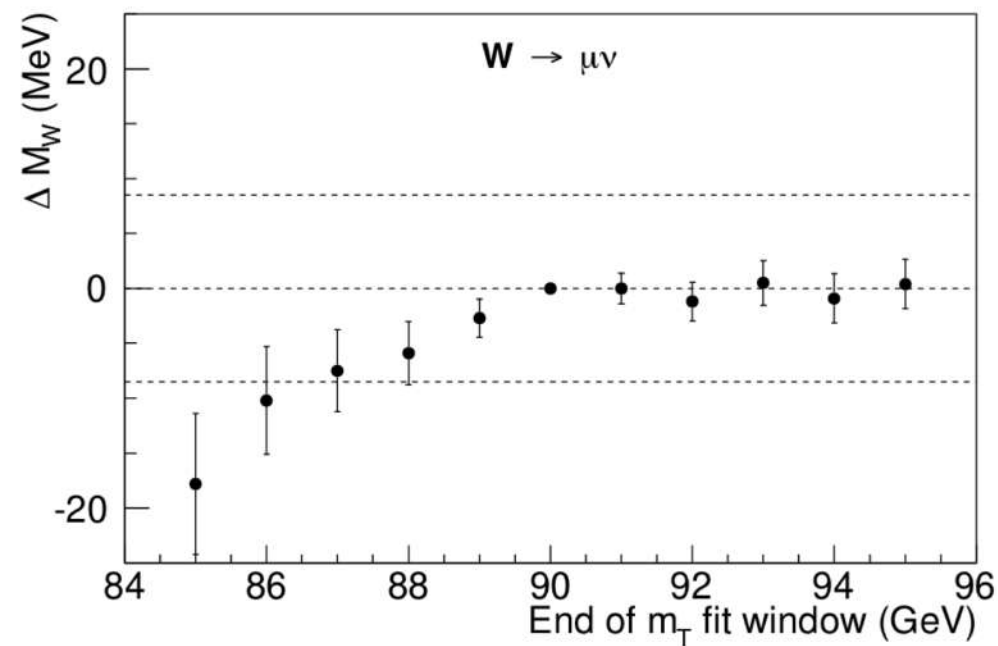
W Mass Fit Window Variation, $p_T(l)$ Fit
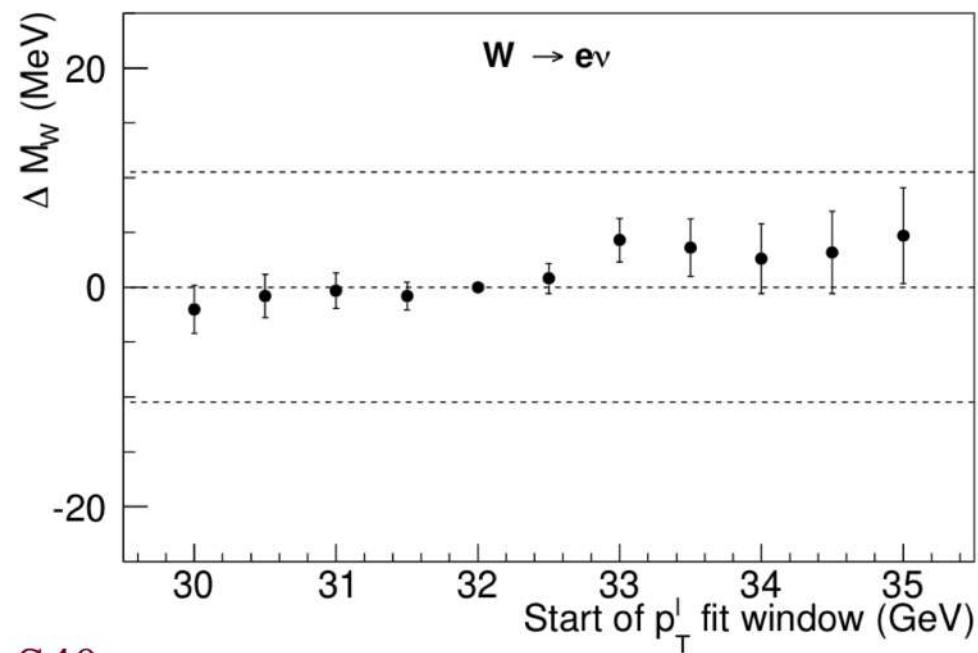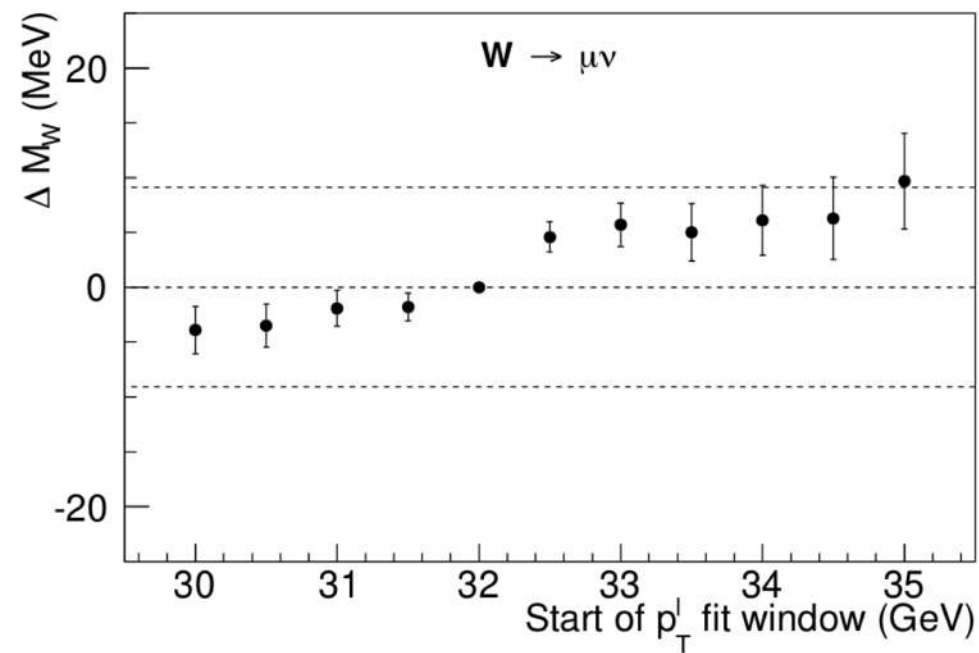
Fig. S40
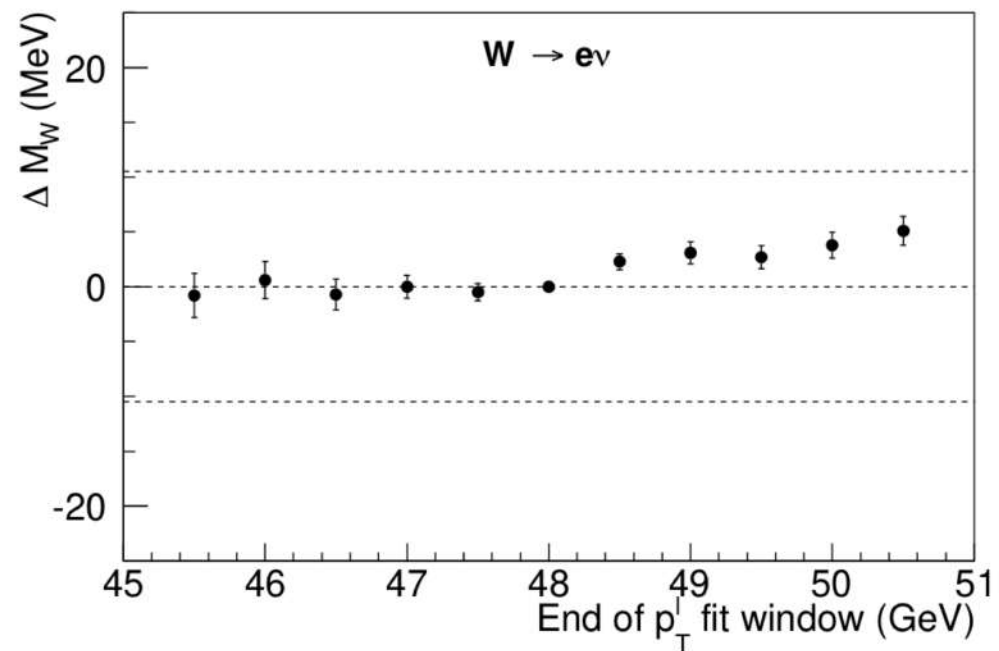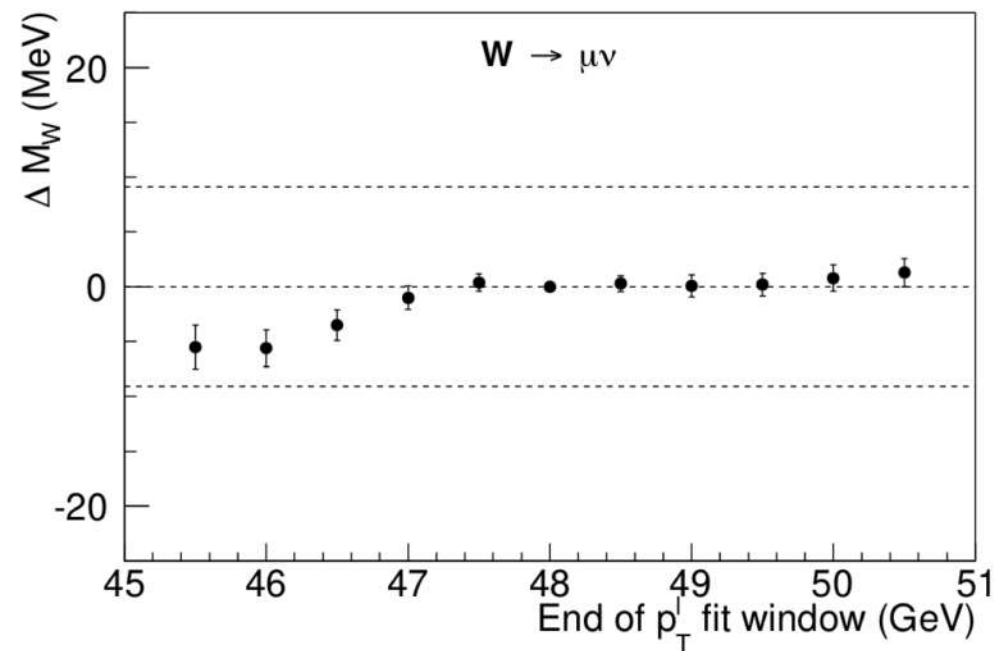
W Mass Fit Window Variation, $p_T(v)$ Fit
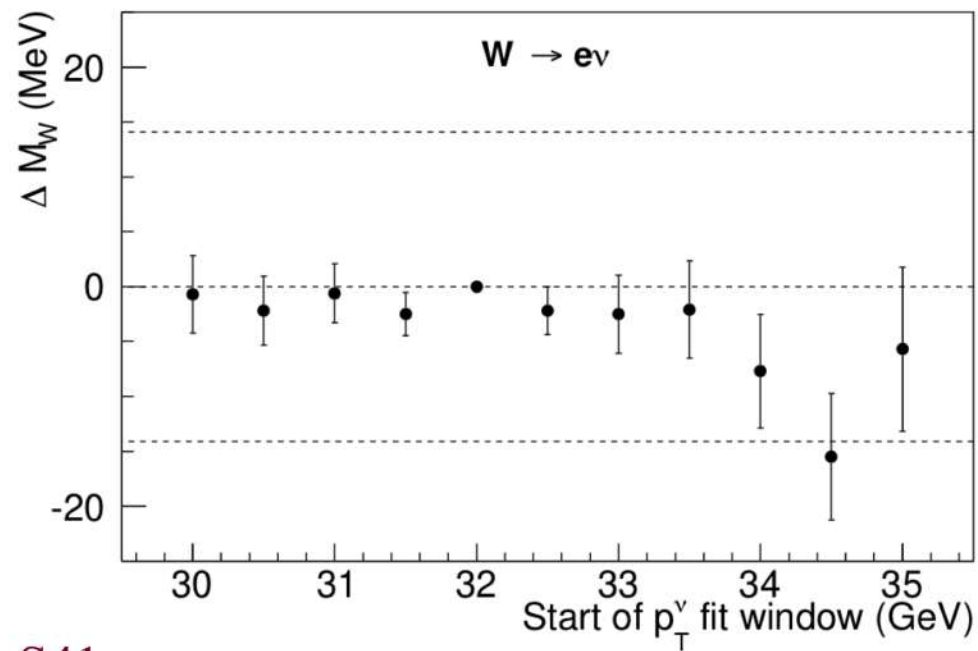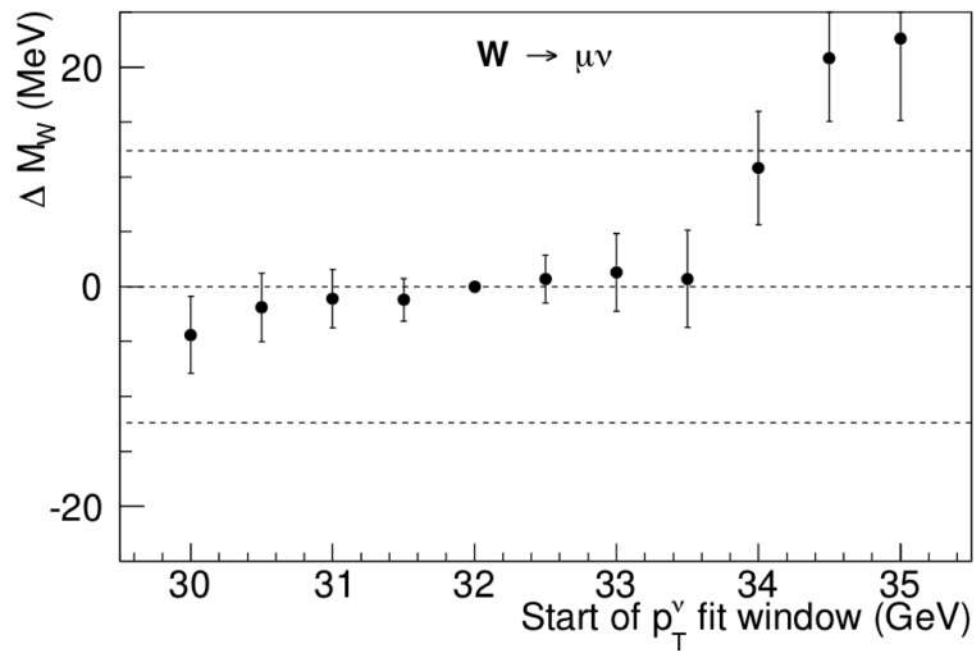
Fig. S41
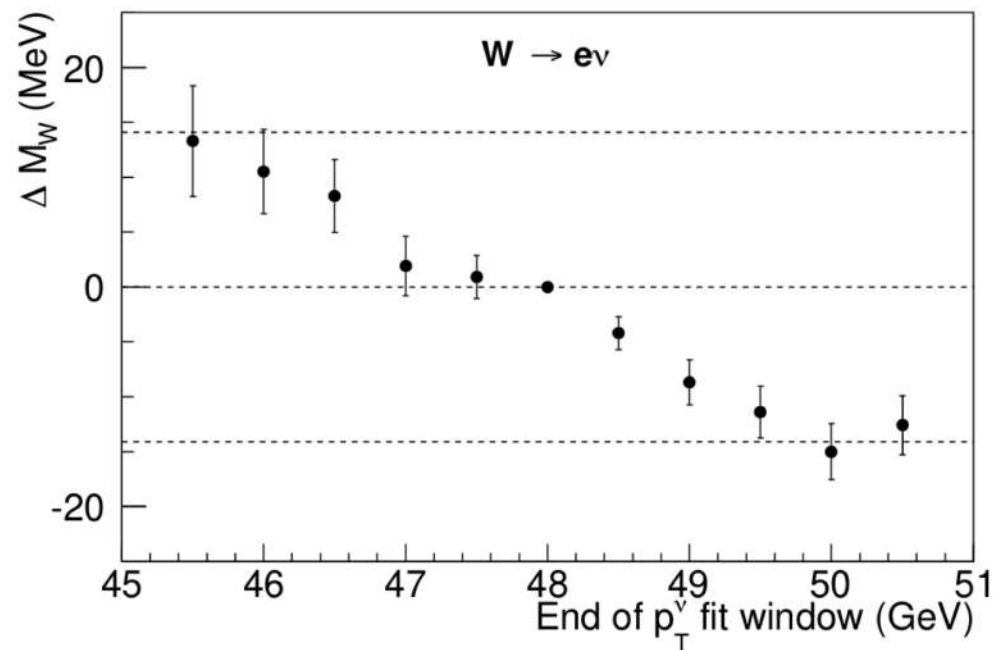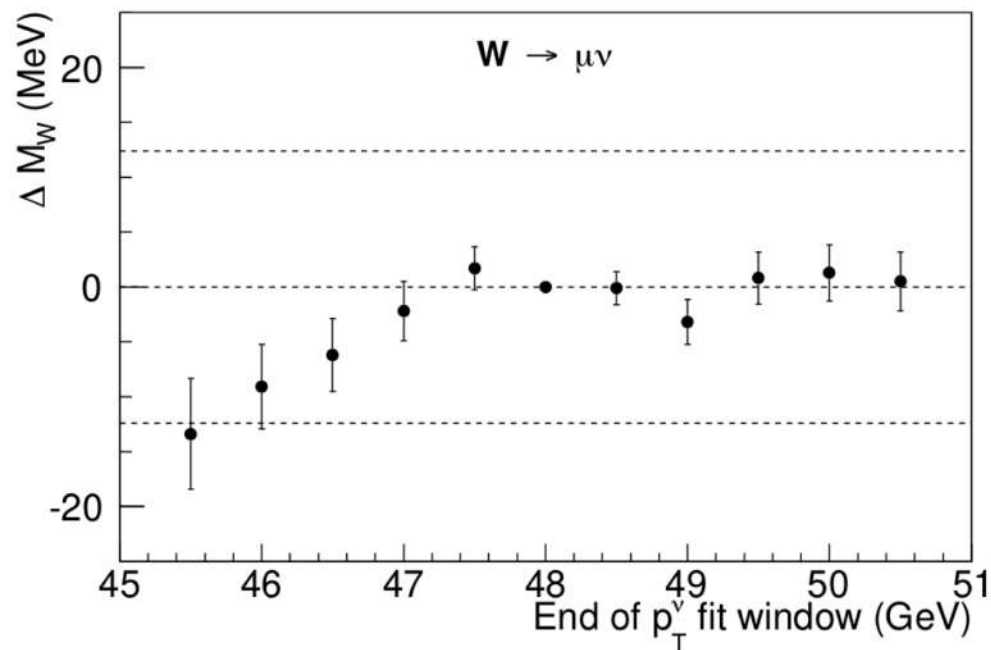
Backgrounds in the *W* boson sample

Muon channel

Source	Fraction (%)	δM_W (MeV) m_T fit	p_T^μ fit	p_T^ν fit
$Z/\gamma^* \to \mu\mu$	7.37 ± 0.10	1.6 (0.7)	3.6 (0.3)	0.1 (1.5)
$W \to \tau\nu$	0.880 ± 0.004	0.1 (0.0)	0.1 (0.0)	0.1 (0.0)
Hadronic jets	0.01 ± 0.04	0.1 (0.8)	-0.6 (0.8)	2.4 (0.5)
Decays in flight	0.20 ± 0.14	1.3 (3.1)	1.3 (5.0)	-5.2 (3.2)
Cosmic rays	0.01 ± 0.01	0.3 (0.0)	0.5 (0.0)	0.3 (0.3)
Total	8.47 ± 0.18	2.1 (3.3)	3.9 (5.1)	5.7 (3.6)

Electron channel

Source	Fraction (%)	δM_W (MeV) m_T fit	p_T^e fit	p_T^ν fit
$Z/\gamma^* \to ee$	0.134 ± 0.003	0.2 (0.3)	0.3 (0.0)	0.0 (0.6)
$W \to \tau\nu$	0.94 ± 0.01	0.6 (0.0)	0.6 (0.0)	0.6 (0.0)
Hadronic jets	0.34 ± 0.08	2.2 (1.2)	0.9 (6.5)	6.2 (-1.1)
Total	1.41 ± 0.08	2.3 (1.2)	1.1 (6.5)	6.2 (1.3)

Backgrounds are small (except Z ⟶ μμ with a forward muon)

Previous CDF Result (2.2 fb^{-1})
Transverse Mass Fit Uncertainties (MeV)

	electrons	muons	common
W statistics	19	16	0
Lepton energy scale	10	7	5
Lepton resolution	4	1	0
Recoil energy scale	5	5	5
Recoil energy resolution	7	7	7
Selection bias	0	0	0
Lepton removal	3	2	2
Backgrounds	4	3	0
pT(W) model	3	3	3
Parton dist. Functions	10	10	10
QED rad. Corrections	4	4	4
Total systematic	18	16	15
Total	26	23	

Systematic uncertainties shown in green: statistics-limited by control data samples

New CDF Result (8.8 fb^{-1})
Transverse Mass Fit Uncertainties (MeV)

	electrons	muons	common
W statistics	10.3	9.2	0
Lepton energy scale	5.8	2.1	1.8
Lepton resolution	0.9	0.3	-0.3
Recoil energy scale	1.8	1.8	1.8
Recoil energy resolution	1.8	1.8	1.8
Selection bias	0.5	0.5	0
Lepton removal	1	1.7	0
Backgrounds	2.6	3.9	0
pT(Z) & pT(W) model	1.1	1.1	1.1
Parton dist. Functions	3.9	3.9	3.9
QED rad. Corrections	2.7	2.7	2.7
Total systematic	8.7	7.4	5.8
Total	13.5	11.8	5.8

Improvements over 2012 Analysis (Table S1 of Paper)

Method or technique	impact	section of paper
Detailed treatment of parton distribution functions	+3.5 MeV	IV A
Resolved beam-constraining bias in CDF reconstruction	+10 MeV	VI C
Improved COT alignment and drift model [65]	uniformity	VI
Improved modeling of calorimeter tower resolution	uniformity	III
Temporal uniformity calibration of CEM towers	uniformity	VII A
Lepton removal procedure corrected for luminosity	uniformity	VIII A
Higher-order calculation of QED radiation in J/ψ and Υ decays	accuracy	VI A & B
Modeling kurtosis of hadronic recoil energy resolution	accuracy	VIII B 2
Improved modeling of hadronic recoil angular resolution	accuracy	VIII B 3
Modeling dijet contribution to recoil resolution	accuracy	VIII B 4
Explicit luminosity matching of pileup	accuracy	VIII B 5
Modeling kurtosis of pileup resolution	accuracy	VIII B 5
Theory model of p_T^W/p_T^Z spectrum ratio	accuracy	IV B
Constraint from p_T^W data spectrum	robustness	VIII B 6
Cross-check of p_T^Z tuning	robustness	IV B

Table S1

Quantified shifts in 2012 result due to updates in PDF and track reconstruction

Improvements over 2012 Analysis

- The statistical precision of the measurement from the four times larger sample is improved by almost a factor of 2

- To achieve a commensurate reduction in systematic uncertainties, a number of analysis improvements have been incorporated

- These improvements are based on using cosmic-ray and collider data in ways not employed previously to improve

    - the COT alignment and drift model and the uniformity of the EM calorimeter response

    - the accuracy and robustness of the detector response and resolution model in the simulation

    - theoretical inputs to the analysis have been updated

- Upon incorporating the improved understanding of PDFs and track reconstruction, our previous measurement is increased by 13.5 MeV to 80,400.5 MeV

    - consistency of the latter with the new measurement is at the percent probability level

Updates to 2012 Result (2.2 fb^{-1})

- Shift from CTEQ6 to NNPDF3.1 PDF used for central value = +3.5 MeV

- In the 2.2 fb^{-1} analysis, an additional systematic uncertainty was quoted to cover an inconsistency between the NBC and BC Y $\rightarrow$ $\mu\mu$ mass fits.

- In this analysis we resolve the inconsistency caused by the beam-constraining procedure, eliminating the additional systematic uncertainty and increasing the measured M$_W$ value by $\approx$ 10 MeV.

- The beam-constraining procedure in the CDF track reconstruction software extrapolates the tracks found in the COT inward to the transverse position of the beamline. This extrapolation can and should take into account the energy loss in the material inside the inner radius of the COT (the beampipe, the silicon vertex detector and its services) to infer and update the track parameters at the beam position before applying the beam constraint.

- This update had been deactivated in the reconstruction software used for the previous analysis. By activating this updating feature of the extrapolator, the flaw in the BC Y $\rightarrow$ $\mu\mu$ mass is corrected, which changes the momentum scale derived from it.

Subsample Fit Stability

TABLE S10: Differences (in MeV) between W-mass p_T^ℓ-fit results and Z-mass fit results obtained from subsamples of our data with equal statistics. For the spatial and time dependence of the electron channel fit result, we show the dependence with (without) the corresponding cluster energy calibration using the subsample E/p fit.

Fit difference	Muon channel	Electron channel
$M_W(\ell^+) - M_W(\ell^-)$	$-7.8 \pm 18.5_{\text{stat}} \pm 12.7_{\text{COT}}$	$14.7 \pm 21.3_{\text{stat}} \pm 7.7^{\text{E/p}}_{\text{stat}}\ (0.4 \pm 21.3_{\text{stat}})$
$M_W(\phi_\ell > 0) - M_W(\phi_\ell < 0)$	$24.4 \pm 18.5_{\text{stat}}$	$9.9 \pm 21.3_{\text{stat}} \pm 7.5^{\text{E/p}}_{\text{stat}}\ (-0.8 \pm 21.3_{\text{stat}})$
$M_Z(\text{run} > 271100) - M_Z(\text{run} < 271100)$	$5.2 \pm 12.2_{\text{stat}}$	$63.2 \pm 29.9_{\text{stat}} \pm 8.2^{\text{E/p}}_{\text{stat}}\ (-16.0 \pm 29.9_{\text{stat}})$

$\Upsilon \to \mu\mu$ mass fit – stability w.r.t. time and instantaneous luminosity

Table S2. The BC $\Upsilon \to \mu\mu$ sample is divided into two equal size sub-samples to check the stability of the momentum scale versus time and versus instantaneous luminosity. The momentum scales are consistent within the statistical uncertainty; the difference between the later and earlier datasets is $(\frac{\Delta p}{p})_{\text{later}} - (\frac{\Delta p}{p})_{\text{earlier}} = (23 \pm 22_{\text{stat}})$ ppm and the difference between the higher and lower instantaneous-luminosity datasets is $(\frac{\Delta p}{p})_{\text{higher}} - (\frac{\Delta p}{p})_{\text{lower}} = (22 \pm 22_{\text{stat}})$ ppm (the later dataset has a higher average instantaneous luminosity).

- The use of a single ``constant term'' for the EM calorimeter resolution is improved in this analysis by making the constant term a linear function of the absolute value of pseudorapidity. This modification takes into account the observed degradation of the EM calorimeter resolution with pseudorapidity

  - The measured width of the $Z{\to}ee$ peak is found to be consistent with this resolution mode. In the past, there was an inconsistency which had to be resolved by introducing another resolution parameter with an additional systematic uncertainty.

- Uniformity of the COT calibration is significantly enhanced by an alignment of the COT wire-positions using cosmic-ray data. A number of improvements were incorporated in the latest (separately published) alignment procedure compared to the procedure presented in the previous analysis

  - Residual biases that were not resolved in the previous iteration of the alignment were eliminated in this iteration.

- A temporal uniformity calibration of the EM calorimeter is introduced in this analysis. The calorimeter response in each longitudinal tower is studied as functions of experiment operational time, and the time-dependence is corrected for.
  - In the previous analysis the time dependence of the EM response was not studied or corrected for, beyond the standard uniformity calibration applied globally within CDF.

- The procedure of tuning the recoil angular smearing model on the distributions of the azimuthal angle difference between the recoil vector and the dilepton p_T vector in $Z \to ll$ data is a new feature that incorporates additional information from the data compared to the previous analysis.

- The procedure of tuning the kurtosis of the recoil energy resolution on the distributions of p_T-balance in the $Z \to l\,l$ data is a new feature that incorporates additional information compared to the previous analysis.
  - Higher moments of the recoil resolution (beyond the first two moments) were not considered in past analyses
  - This enhancement of the analysis is incorporated independently for the parallel and the perpendicular components of the recoil.

- As another refinement to the previous analysis, which only considered the first two moments of the fluctuations of energy flow from multiple interactions, we also examine the skewness and excess kurtosis of the fluctuations as functions of $\sqrt{\Sigma E_T}$
  - To better model the resolution function arising from multiple interactions, we include these measurements as functions of $\sqrt{\Sigma E_T}$ in the simulation

Description of Analysis Changes since 2012 (Table S1 of Paper)

- The fluctuations in the energy flow from spectator parton interactions and additional proton-antiproton collisions contribute to the recoil resolution. These fluctuations are measured from zero-bias data; the luminosity profile of these data must be matched to the triggered data

  - In the past, this matching was performed ``by hand'', and a single distribution was used for both the electron and muon channels

- The new procedure for matching the luminosity profiles uses a 2D histogram look-up technique which performs the matching by construction, separately for each channel

  - This automated procedure is more robust than the ``by hand'' matching of the previous analysis

- Confirmed by comparing the data and simulated distributions of $\sqrt{\Sigma E_T}$ for the W and Z boson data in each channel. This comparison was not shown in the previous analysis

- The use of a theoretical calculation of the p_T^W / p_T^Z spectrum ratio to study its QCD scale variation is a new feature of this analysis compared to the previous analysis.
  - We use the **DYqT** program for this purpose.

- The constraint from the p_T^W data spectrum is another new feature that incorporates additional information compared to the previous analysis.
  - In the past, only the p_T^Z data spectrum was used to constrain the production model. In the new analysis we use both spectra.

- Comparisons between the recoil distributions of the W- and Z-boson data and simulation were shown in the past, but the shapes were not compared, only the first two moments were compared.
  - In this analysis we quantify the quality of the shape comparisons and we also compare the values of the first four moments.

The Future of the M$_W$ Measurement

- The experiments at the LHC have collected and are collecting a lot of data.
  - While W bosons are produced slightly differently at the LHC (pp collider) than the Tevatron ($p\bar{p}$ collider), the LHC experiments have the opportunity to make this measurement.

- If built, a new electron-positron collider can also measure the W boson mass very precisely.

- The LHC as well as smaller, specialized experiments are sensitive to the kinds of new particles and interactions that can influence the W boson mass.
  - If there is new physics which could explain the tension of our result with the SM expectation, this new physics could show up directly in these experiments.

- CDF has analyzed and published on the full dataset. We have incorporated a lot of new ideas in this round of analysis. If we get more ideas, we will pursue them systematically.